

ALMA MATER STUDIORUM - UNIVERSITÀ DI BOLOGNA

---

FACOLTÀ DI INGEGNERIA  
DOTTORATO DI RICERCA IN INGEGNERIA ELETTRTECNICA  
XXIV CICLO

Tesi di Dottorato

**General effective medium model for the  
complex permittivity extraction with an  
open-ended coaxial probe in presence of  
a multilayer material under test**

Dott. Mauricio David Perez

Tutore:

Chiar.mo Prof.

UGO REGGIANI

Coordinatore Dottorato:

Chiar.mo Prof.

DOMENICO CASADEI

---

Bologna, Italia, Marzo 2012



ALMA MATER STUDIORUM - UNIVERSITÀ DI BOLOGNA

---

FACOLTÀ DI INGEGNERIA  
DOTTORATO DI RICERCA IN INGEGNERIA ELETTROTECNICA  
XXIV CICLO

Tesi di Dottorato

**General effective medium model for the  
complex permittivity extraction with an  
open-ended coaxial probe in presence of  
a multilayer material under test**

Dott. Mauricio David Perez

Tutore:

Chiar.mo Prof.

UGO REGGIANI

Coordinatore Dottorato:

Chiar.mo Prof.

DOMENICO CASADEI

Settore scientifico disciplinare di afferenza: ING-IND/31

---

Bologna, Italia, Marzo 2012

*Many people helped and supported me during the realization of this Thesis. I want to express gratitude to all of them.*

*The first thought goes to my supervisors Ugo Reggiani and Leonardo Sandrolini. They taught not only the beauty of the research but, more important, to become a better professional and person.*

*The following thoughts to all the Ph.D student and graduated, particularly to Fabio Roveda, Gabrielle Neretti, Marco Casali, G. Azcrraga., Nemo the american, Jeco and Sanjin. A big big thanks to their help during these years. My best thoughts to my great-grandfather Giovanni Cesaretti and to my dear mother Mabel E. Cesaretti, since without them I would certainly not be here. My last thought to the beautiful Bologna, to the great Italy and to the big Argentina.*

# Contents

<b>Introduction</b>	<b>ix</b>
<b>1 Electromagnetic characterization of materials overview</b>	<b>1</b>
1.1 Introduction . . . . .	1
1.2 Materials overview . . . . .	3
1.2.1 Introduction . . . . .	3
1.2.2 Intrinsic electromagnetic properties of materials . . . . .	4
1.2.3 Dielectric medium . . . . .	6
1.2.4 Complex permittivity definition and use . . . . .	7
1.2.5 Dielectric dispersion . . . . .	8
1.2.6 Dielectric mechanism . . . . .	9
1.2.7 Dielectric relaxation parameters and models . . . . .	11
1.2.8 Electromagnetic field interaction at the interface of two media . . . . .	15
1.2.9 Other macroscopic properties of materials . . . . .	16
1.2.10 General composite medium properties . . . . .	19
1.2.11 Extrinsic performance . . . . .	20
1.2.12 Applications of the complex permittivity knowledge . . . . .	21
1.3 Measurement techniques overview . . . . .	23
1.3.1 Introduction . . . . .	23
1.3.2 Characteristic features helping in technique selection . . . . .	29
1.3.3 Comparative diagram . . . . .	34
1.3.4 Open-ended coaxial probe technique . . . . .	36

---

1.3.5	Transmission line techniques . . . . .	38
1.3.6	Free-space techniques . . . . .	40
1.3.7	Resonant-cavity techniques . . . . .	42
1.3.8	Additional comments on the accuracy and resolution of the techniques . . . . .	45
<b>2</b>	<b>Open-ended coaxial probe Overview</b>	<b>47</b>
2.1	Introduction . . . . .	47
2.2	The ideal open-ended coaxial probe . . . . .	47
2.2.1	Introduction . . . . .	47
2.2.2	Basic geometry and definitions . . . . .	48
2.2.3	Discussion . . . . .	50
2.3	The performance of the probe . . . . .	51
2.3.1	Introduction . . . . .	51
2.3.2	The performance areas . . . . .	52
2.3.3	The parameters describing the performance . . . . .	55
2.3.4	Maximum frequency limit . . . . .	55
2.3.5	Minimum frequency limit . . . . .	56
2.3.6	Precision . . . . .	57
2.3.7	Admittance and permittivity accuracies . . . . .	59
2.3.8	Sensibility Depth . . . . .	60
2.3.9	Sensitivity or spatial resolution . . . . .	62
2.4	Simulation study for sensibility range and sensitivity . . . . .	62
2.5	Conclusions . . . . .	63
<b>3</b>	<b>Probe models and extraction schemes</b>	<b>65</b>
3.1	Introduction . . . . .	65
3.2	Probe models . . . . .	66
3.2.1	Introduction . . . . .	66
3.2.2	The probe models . . . . .	66
3.2.3	Classification of the probe models . . . . .	72
3.2.4	Features of hard models . . . . .	73

3.2.5	Discussion on features of hard models . . . . .	74
3.2.6	Features of soft models . . . . .	75
3.2.7	Discussion on features of soft models . . . . .	76
3.2.8	Conclusions . . . . .	77
3.3	Extraction schemes . . . . .	77
3.3.1	Introduction . . . . .	77
3.3.2	Descriptive features of an extraction scheme . . . . .	78
3.3.3	Main elements of parameter estimation procedure . . . . .	80
3.4	Point-Matching methods . . . . .	83
3.5	Simplex Point-Matching method . . . . .	84
3.5.1	Introduction . . . . .	84
3.5.2	Simplex Point-Matching extraction procedure . . . . .	86
3.6	Gradient Point-Matching method . . . . .	90
3.6.1	Introduction . . . . .	90
3.6.2	Actual-Future procedure's description . . . . .	90
3.6.3	Actual-Future procedure's flowchart . . . . .	91
3.6.4	List of states . . . . .	93
3.7	The PSO method . . . . .	96
3.8	Conclusions . . . . .	98
<b>4</b>	<b>Effective dielectric models for multilayer materials</b>	<b>99</b>
4.1	Introduction . . . . .	99
4.2	Effective medium theory for laminar composite media . . . . .	101
4.2.1	Introduction . . . . .	101
4.2.2	Quasi-static approach and Weiner bounds . . . . .	101
4.2.3	The Weiner bounds representation . . . . .	103
4.2.4	Oblique incidence Case . . . . .	107
4.3	Effective dielectric model for the open-ended coaxial probe . . . . .	110
4.3.1	Exponential behavior of the effective dielectric response	110
4.3.2	Effective dielectric model for the open-ended coaxial probe . . . . .	110
4.3.3	Oblique incidence model verification . . . . .	112

---

4.3.4	Circuital Representation of the Oblique Incidence Model	112
4.3.5	General multilayer model . . . . .	115
4.3.6	Consideration about finite-wavelength effects . . . . .	116
4.4	Validation and applications . . . . .	118
4.4.1	Introduction . . . . .	118
4.4.2	Performance of the effective dielectric models for model optimization usage . . . . .	120
4.4.3	Conclusions . . . . .	126
4.5	Conclusions . . . . .	128
<b>5</b>	<b>The imperfectness of the contact in open-ended coaxial probes</b>	<b>129</b>
5.1	Introduction . . . . .	129
5.2	The electric field at the aperture and the imperfect contact problem . . . . .	130
5.3	Discussion and assumptions on the surface profile nature . . .	134
5.4	Simulation role and permittivity extraction . . . . .	137
5.5	Lift-Off case: simulation results and conclusion . . . . .	141
5.6	Air brick case: simulation and conclusion . . . . .	143
5.7	Conclusions . . . . .	143
	<b>Bibliography</b>	<b>147</b>

# List of Figures

1.2.1	<i>Geometrical representation of the complex permittivity and its components. . . . .</i>	8
1.2.2	<i>Random Molecular structure of Water (Absence of an external electric field.) . . . . .</i>	10
1.2.3	<i>Molecular structure of Water aligned to an external electric field. . . . .</i>	10
1.2.4	<i>Dielectric mechanisms related to a solution of salt and water while an external electric field with variable frequency is applied. . . . .</i>	12
1.2.5	<i>Optical view of the electromagnetic wave interaction with a two-phases material. . . . .</i>	16
1.2.6	<i>Real and Imaginary part of water and some alcohols at room temperature and microwave frequencies. . . . .</i>	23
1.2.7	<i>Real part of Martini drink and its ingredients Gin and Vermouth at room temperature and microwave frequencies. . . .</i>	24
1.2.8	<i>Imaginary part of Beer, Lite Beer and water drinks at room temperature and microwave frequencies. . . . .</i>	25
1.2.9	<i>Real part of milk drink at room temperature and microwave frequencies after 1, 2, 3 and 4 periods of 8 hours each one. .</i>	26
1.3.1	<i>Comparative Diagram. Loss and Frequency for each technique.</i>	35
2.2.1	<i>Sketch of the ideal open-ended coaxial probe. Longitudinal cut section. . . . .</i>	49

2.3.1	Illustration of the low frequency limitation of an open-ended coaxial probe. In (a) a mapping sketch of Gamma and epsilon. In (b) a polar reflection coefficient plot at a low frequency (200 MHz). In (c) a polar reflection coefficient plot at a medium frequency (2.45 GHz). . . . .	58
3.5.1	<i>Flowchart of the algorithm for the Simplex Point-Matching Method Extraction.</i> . . . . .	87
3.5.2	<i>Table index nomenclature and definitions. In (a) the association relation between the permittivity elements in the Permlist table and the aperture admittance elements from the model (YM). In (b) the error elements and the recovery of the permittivity associated to the minimal error (<math>\epsilon_{i_0, k_0}</math>).</i> . . . . .	89
3.6.1	<i>Permittivity and Admittance Domains to show Gradient Point-Matching search. In (a) it is shown the initial state. In (b) the searching procedure. In (c) the final step.</i> . . . . .	91
3.6.2	<i>Flow chart of the Actual-Future Procedure for the Gradient Point-Matching Method.</i> . . . . .	94
4.2.1	Incident wave in laminar material. . . . .	102
4.2.2	Plane of complex permittivity showing the two points corresponding to the permittivity of the constituent of the composite. . . . .	103
4.2.3	<i>Diagrams of parallel-plate geometries with two materials arrangements for parallel (a) and series (b) responses according with field polarization with respect to the material's interface.</i> . . . . .	105

4.2.4	Sketch showing the graphical representation of a two-layers composite in the complex $\epsilon$ -plane. In (a) the values of the constituent's permittivity. In (b) the totally parallel case is depicted as a straight line. In (c) the totally normal case is depicted as a circular arc line. In (d) the delimited region $\Omega$ is shown. . . . .	106
4.2.5	Graphical interpretation of the oblique case from the extreme cases. In (a) the totally normal bound, its locus (black thick line) and its circle constructor (black thin dashed line). In (b) the totally parallel bound, its locus (black thick line) and its infinite-radius circle constructor (black thin dashed line). In (c) the oblique incidence cases, its locus (black thick lines for $\epsilon_{ry} = v_1$ and $v_2$ ) and its circle constructors (black long-short dashed-style lines). In (d) the contour map regions of isolines, the right one including all the possible values of $\epsilon_{ry}$ and the left one including the $\Omega$ region. . . . .	108
4.3.1	Exponential behavior of the effective dielectric response vs thickness for a two-layers composite of Teflon backed by air.	111
4.3.2	<i>Diagram of the equivalent circuit for the two layered case with general incidence as a capacitors network.</i> . . . . .	114
4.3.3	Summary of the effective dielectric model for general incidence in multilayer materials. . . . .	117
4.3.4	<i>Diagram of the geometrical locus showing the frequency effect for some points</i> . . . . .	119
4.4.1	Summary sketch of the validation of the series, parallel and general effective dielectric models. . . . .	121
4.4.2	Results of the case study for air backed by a lossy material, at left, and lossy material backed by air, at right. . . . .	123
4.4.3	Results of the case study for air backed by an FR-4 similar material (lossless). . . . .	123

---

4.4.4	Results of the case study for methanol backed by teflon for a small probe at 1 GHz. . . . .	125
4.4.5	Results of the case study for methanol backed by teflon for a large probe at 1 GHz. . . . .	125
4.4.6	Results of the case study for methanol backed by teflon for a small probe at 10 GHz. . . . .	126
4.4.7	Results of the case study for any lossy material combination.	127
5.2.1	<i>Electric field distribution in the OECC probe and air-gap problem illustration</i> . . . . .	132
5.2.2	<i>Equivalent Circuits</i> . . . . .	135
5.3.1	Employed Air-MUT profiles . . . . .	136
5.4.1	CST Issue . . . . .	138
5.5.1	Permittivity Diagrams for Lift-off case . . . . .	141
5.6.1	Permittivity Diagrams for Air Brick cases . . . . .	144

# Introduction

The impact of the technologies based on the knowledge of the electromagnetic properties of materials at microwave frequencies is growing both in academic and in industrial field. Nowadays, a great interest is focused in applications such as biomedicine, electromagnetic compatibility, food and agriculture, to mention some of them.

In fact, the knowledge of the frequency dependence of the complex electric permittivity and magnetic permeability of a material allows the prediction of the shielding effectiveness of a structure made of that material. Similarly, the signals interconnections can be designed with precision when the dependence of the frequency is known with the dielectric substrate; from the knowledge of the dielectric properties of biological tissues the spatial distribution of the incident electromagnetic field and the absorbed power can be determined in accurate manner. Also the differences, as for example, between healthy and carcinogenic tissues and between fresh and spoiled milk can be distinguished. The extraction of the characteristics of the complex electric permittivity of a material can be achieved in many ways according to the employed technique. Which technique to employ will depend on the material's properties, frequency and temperature of interest, sample machining, contacting requirements and accuracy.

The most popular technique according to its easiness of use and performance is the open-ended coaxial-probe frequency-domain reflectometry technique. The current commercially available versions of this technique assumes restrictions in the employed materials for on-line systems applications. This

restrictions are that the material must have perfect contact, homogeneous and infinite extension which reduces the overall accuracy and applicability of the technique.

In order to evaluate the current alternative performance and to formulate and to validate a model that extends the applicability of this technique to heterogeneous materials, particularly laminar materials, and that alleviates the contact perfectness restriction, a series of simulations and an analytical study have been realized.

The principal contribution of this thesis is then a model that extends the applicability of this technique to multilayer materials for on-line system application and a review and new classification of the available models according to its applicability to on-line systems and other outstanding characteristics. This thesis has been split in five chapters.

In Chapter 1 a general overview of the electromagnetic characterization of materials, specially for dielectrics, is presented. A description of the material referred to the electromagnetic properties, principally the complex permittivity, and the applications of its knowledge is shown in the first section.

A general overview of the different techniques for material characterization, focused mostly in microwave measurements is also shown in the second section of this chapter. There the features of each technique is given as a tool for technique selection.

In Chapter 2 a descriptive overview of the employed technique, the open-ended coaxial probe frequency-domain reflectometry, is presented, with details in the probe types and characteristics. Particular attention has been given to the performance, to the tools for the correct evaluation and selection. Finally a simulation study have been carried out regarding one of its performance parameters, the *sensibility depth* and the *sensitivity*.

In Chapter 3 the available probe models and extraction techniques are presented in brief detail and main features. Two main class of probe models and, as a consequence, of extraction schemes have been introduced, defined and discussed according to the applicability of the technique to on-line systems

with well distinguished features. In addition, two deterministic permittivity optimization techniques, utilizing two variants of the Point-Matching method are described together with the detailed algorithms. Finally, a Particle Swarm Optimization method is briefly described as a stochastic-search permittivity optimization method.

In Chapter 4 a new general effective dielectric model for any type of incidence and for multilayer material is presented. To describe its presentation, the Effective Medium Theory for laminar materials is introduced together with the formulation and verification process of the referred model.

In Chapter 5 a performed study about the imperfectness of the contact is presented. To describe it a theoretical discussion regarding the field structure at the interface is introduced together with a simulator-based analysis regarding different cases of lift-off and air elements in the interface, also aimed to discuss about the applicability of effective dielectric models to this kind of problem.



# Chapter 1

## Electromagnetic characterization of materials overview

### 1.1 Introduction

Nowadays and from last decades there is a continuous and increasing demand of industrial and academic areas in accurate data on constitutive electric and magnetic properties of materials at microwave frequencies, principally the complex electric permittivity and complex magnetic permeability.

The importance of the research on the electromagnetic properties of materials at microwave frequencies can be understood in the aspects that follow:

Firstly, though it is an old field in physics, the study of electromagnetic properties of materials at microwave frequencies is full of academic importance [1, 2, 3, 4], especially for magnetic materials [5, 6], superconductors [7] and ferro-electrics [8]. In addition, the knowledge gained from microwave measurements contributes to our information about both the macroscopic and the microscopic properties of materials, so microwave techniques have been important for materials property research.

Secondly, microwave communications are playing more and more impor-

tant roles in military, industrial, and civilian life, and microwave engineering requires precise and accurate knowledge of the electromagnetic properties of materials at microwave frequencies [9]. Since World War II, a lot of resources have been put into electromagnetic signature control, and microwave absorbers are widely used in reducing the radar cross sections (RCSs) of vehicles. The study of electromagnetic properties of materials and the ability of tailoring the electromagnetic properties of composite materials are very important for the design and development of radar absorbing materials and other functional electromagnetic materials and structures [10].

Thirdly, as the clock speeds of electronic devices are approaching microwave frequencies, it becomes indispensable to study the microwave electronic properties of materials used in electronic components, circuits, and packaging. The development of electronic components working at microwave frequencies needs the electrical transport properties at microwave frequencies, such as Hall mobility and carrier density; and the development of electronic circuits working at microwave frequencies requires accurate constitutive properties of materials, such as permittivity and permeability. Meanwhile, the electromagnetic interference (EMI) should be taken into serious consideration in the design of circuit and packaging, and special materials are needed to ensure electromagnetic compatibility (EMC) [11].

Fourthly, the study of electromagnetic properties of materials is important for various fields of science and technology. The principle of microwave remote sensing is based on the reflection and scattering of different objects to microwave signals, and the reflection and scattering properties of an object are mainly determined by the electromagnetic properties of the object. Besides, the conclusions of the research of electromagnetic materials are helpful for agriculture, food engineering, medical treatments, and bioengineering [12].

Finally, as the electromagnetic properties of materials are related to other macroscopic or microscopic properties of the materials, we can obtain information about the microscopic or macroscopic properties in which we are

interested, from the electromagnetic properties of the materials. In materials research and engineering, microwave techniques for the characterization of materials properties are widely used in monitoring the fabrication procedure and nondestructive testing of samples and products [13, 14].

This chapter aims to provide basic and general knowledges on the electromagnetic properties of materials to understand the results from microwave measurements and to help in understanding the techniques's operation. In that sense the intrinsic and extrinsic properties of materials are introduced together with the electromagnetic mechanisms that take place in the material when perturbed by external electromagnetic waves. In addition, a general introduction to the the microwave measurement techniques available in the current state of art is given. This introduction consist on a brief description of the features of the most used techniques.

## 1.2 Materials overview

### 1.2.1 Introduction

As it is well known a material is anything made of matter, constituted of one or more substances with certain physical properties. Wood, cement, hydrogen, air and water are all examples of materials. Materials are mostly used in the society structure as inputs to production or manufacturing and as diagnosis object.

Material's properties are quantities that help in their description and that allow its comparison with other materials to aid in materials selection.

Some material's properties are used in relevant equations to determine the attributes of a system a priori. For example, if a material of a known specific heat gains or loses a known amount of heat, the temperature change of that material can be determined.

There is a vast list of material's properties we are not presenting because they are out of the scope of this book .What is important to notice is that all those properties are given by the matter structure of the material at a

microscope scale where the molecular structure and the mass and volume are considered.

The matter structure is correlated to the manner in which the negative charge of an atom or a molecule is arranged in the three-dimensional space. This is determined by the electronic charge density distribution that is related to electron energy bands of the material. Thus, it determines directly the sizes and shapes of molecules, their electrical moments and, indeed, all of their chemical and physical properties.

Another consequence of it is that the different properties of the material can also be related to each other in many cases. This is an important aspect since it lets us calculate some properties from others, being a valuable alternative when the property of interest is difficult to measure directly.

We will fundamentally focus on the macroscopic electromagnetic properties, not entering in details in the microscopic notions neither in their relations to other material's properties.

### 1.2.2 Intrinsic electromagnetic properties of materials

The electromagnetic properties of a material accounts for its response to electromagnetic fields at a macroscopic scale and it can be generally described by the Maxwell's equations. Maxwell's equations can be expressed in many equivalent forms. The most general form is listed here:

$$\nabla \times \vec{E} = -\frac{\partial \vec{B}}{\partial t} \quad (1.2.1)$$

$$\nabla \times \vec{H} = -\frac{\partial \vec{D}}{\partial t} + \vec{J} \quad (1.2.2)$$

$$\nabla \cdot \vec{D} = \rho \quad (1.2.3)$$

$$\nabla \cdot \vec{B} = 0 \quad (1.2.4)$$

with the following constitutive relations:

$$\vec{D} = \epsilon \vec{E} \quad (1.2.5)$$

$$\vec{B} = \mu \vec{H} \quad (1.2.6)$$

$$\vec{J} = \sigma \vec{E} \quad (1.2.7)$$

where:

- $\vec{J}$  is the current density vector
- $\vec{E}$  is the electric field vector
- $\vec{D}$  is the electric flux density vector
- $\vec{H}$  is the magnetic field vector
- $\vec{B}$  is the magnetic flux density vector
- $\rho$  is the charge density
- $\epsilon$  is the complex permittivity of the media
- $\mu$  is the complex permeability of the media
- $\sigma$  is the conductivity of the media

Equations (1.2.1) to (1.2.7) indicate that the responses of a material to electromagnetic fields are determined essentially by three constitutive parameters, namely permittivity  $\epsilon$ , permeability  $\mu$ , and conductivity  $\sigma$ . These parameters also determine the spatial extent to which the electromagnetic field can penetrate into the material at a given frequency and how microwave energy propagates through a material.

This constitutive parameters are the basement for many other electromagnetic parameters that define properties of the material. They are *intrinsic* as they are governed by their respective underlying mechanisms, not by their geometries. Other intrinsic parameters can be derived from them according to the general properties of the typical kind of materials that can be considered and that generally includes dielectric materials, semiconductors, conductors, magnetic materials and artificial materials.

For dielectric materials, additional parameters such as the propagation parameters (propagation constant, wave impedance and refraction index) can be derived from the constitutive parameters as it is well known. We are not getting in detail on the formulation of these propagation parameters because they are well known.

The material's type considered here, in this present thesis, is a non-chiral non-magnetic dielectric material.

Chiral materials have a different constitutive parameters form and information on chirality can be found in [15, sec. 1.3.5.1].

For non-magnetic materials  $\mu$  is known and assumed to be 1. At high frequencies, the effect of  $\sigma$  can be ignored. This is because its effect varies inversely with frequency. This is true for most non-conductive materials. The exception is for metals. We don't consider non-magnetic also because most of the common materials are completely non-magnetic.

Consequently the attention will be focused more in the complex permittivity parameter and in dielectric materials.

We will start with an introduction to dielectric materials.

### 1.2.3 Dielectric medium

A dielectric is an electrical insulator that can be polarized by an applied electric field. When a dielectric is placed in an electric field, electric charges do not flow through the material, as in a conductor, but only slightly shift from their average equilibrium positions causing dielectric polarization. Because of dielectric polarization, positive charges are displaced toward the field and negative charges shift in the opposite direction. This creates an internal electric field which reduces the overall field within the dielectric itself. <sup>1</sup> If a dielectric is composed of weakly bonded molecules, those molecules not only

---

<sup>1</sup>Quote from Encyclopdia Britannica: "Dielectric, insulating material or a very poor conductor of electric current. When dielectrics are placed in an electric field, practically no current flows in them because, unlike metals, they have no loosely bound, or free, electrons that may drift through the material". [16]

become polarized, but also reorient so that their symmetry axis aligns to the field.

Although the term "insulator" implies low electrical conduction, "dielectric" is typically used to describe materials with a high polarizability. This latter is expressed by a number called the dielectric constant.

The study of dielectric properties is concerned with the storage and dissipation of electric and magnetic energy in materials.<sup>2</sup> It is important to explain various phenomena in electronics, optics, and solid-state physics.

### 1.2.4 Complex permittivity definition and use

The complex permittivity ( $\epsilon$ ) is a constitutive parameter that describes the interaction of a medium with an external electric field. In other words, permittivity is a measure of how an electric field affects, and is affected by, a medium. A material's permittivity is usually normalized to the permittivity of vacuum ( $\epsilon_0$ ) and known as relative permittivity ( $\epsilon_r$ ):

$$\epsilon_r = \frac{\epsilon}{\epsilon_0} = \epsilon_r' - i\epsilon_r'' \quad (1.2.8)$$

where  $\epsilon_0 \approx 8.85 \times 10^{-12} [F/m]$ .

The real part of the relative permittivity ( $\epsilon_r'$ ) is a measure of how much energy from an external electric field is stored in a material. The imaginary part of the relative permittivity ( $\epsilon_r''$ ) is called the loss factor and is a measure of how dissipative or lossy a material is to an external electric field.

Its fundamental dimensions are  $T^2Q^2M^{-1}L^{-3}$  where T, Q, M and L are time, charge, mass and length respectively. Normally this is expressed as farad per meter (capacitance per distance).

---

<sup>2</sup>Arthur R. von Hippel, in his seminar work, Dielectric Materials and Applications [3], stated: "Dielectrics... are not a narrow class of so-called insulators, but the broad expanse of nonmetals considered from the standpoint of their interaction with electric, magnetic, or electromagnetic fields. Thus we are concerned with gases as well as with liquids and solids, and with the storage of electric and magnetic energy as well as its dissipation."

When the complex permittivity is drawn as a simple vector diagram, the real and imaginary components are 90 out of phase (See figure 1.2.1). The vector sum forms an angle  $\delta$  with the real axis ( $\epsilon_r'$ ). The relative "lossiness" of a material is the ratio of the energy lost to the energy stored. This ratio is known as "loss tangent", "delta tangent" or dissipation factor:

$$\tan(\delta) = D = \frac{1}{Q} = \frac{\epsilon_r''}{\epsilon_r'} \quad (1.2.9)$$

In some cases is used the term "quality factor" or "Q-factor" with respect to an electronic microwave material. About the graphical representation of

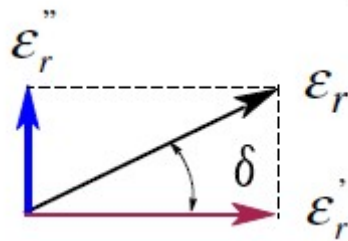


**Figure 1.2.1:** Geometrical representation of the complex permittivity and its components.

the complex permittivity. Usually it is used to plot the real and imaginary part vs frequency in two separate plots. But two other common ways to view permittivity are loss tangent plot, which is the imaginary part divided by the real part, vs. frequency, and Cole-Cole plot which is the imaginary part vs the real part (imaginary part on the y-axis, real part on the x-axis).

### 1.2.5 Dielectric dispersion

In general, a material cannot respond instantaneously to an applied field. The speed and manner of its response will depend on its matter's structure and is described by the dielectric relaxation. Usually its response can be studied considering the phase velocity of a wave propagating in the medium and its dependence with the frequency [17].

Dispersion most often refers to frequency-dependent effects in wave propagation. In the presence of dispersion, wave velocity is no longer uniquely defined, giving rise to the distinction of phase velocity and group velocity [18] as expressed in the following equation:

$$v_g = \frac{\partial \omega}{\partial \beta} = v + \beta \frac{\partial v}{\partial \beta} \quad (1.2.10)$$

where  $v_g$  is the group velocity,  $\omega$  is the angular frequency of the propagating wave,  $\beta$  is the propagation phase constant and  $v$  is the phase velocity.

Consequently a medium can be considered non-dispersive if a lineal relation exists between the angular frequency ( $\omega$ ) and the propagation phase constant ( $\beta$ ) resulting in frequency-independent group and phase velocity that are at the same time equals between them. This is the case of ideal dielectric media.

From equation (1.2.10) and propagation phase constant ( $\beta = \omega\sqrt{\epsilon\mu}$ ) we can see that the dispersion in a medium will occur if the constitutive parameters are frequency-dependent.

Consequently dielectric dispersion is the dependence of the permittivity of a dielectric material on the frequency of an applied electric field. Because there is always a lag, a momentary delay, between changes in material's response and changes in an electric field, what is known as dielectric relaxation, the permittivity of the dielectric is a complicated, complex-valued function of frequency of the electric field.

The description of the dispersion of dielectric medium is very important for the application of dielectric materials and the analysis of polarization systems.

### 1.2.6 Dielectric mechanism

As an illustration of the behavior of a material along the frequency domain we consider a salt/water solution starting as follows.

Let's consider the molecular structure of water. The water molecule consists of two hydrogen atoms and one oxygen atom. While the molecule is

electrically neutral its charge distribution is not constant over its volume. Because of its bonding mechanism, the hydrogen side of the molecule is more positive than the oxygen side. In the absence of any forces other than thermal energy, a group of water molecules will take on a random orientation as depicted in figure (1.2.2).

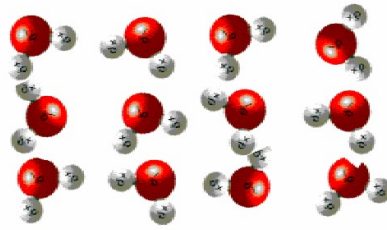


**Figure 1.2.2:** *Random Molecular structure of Water (Absence of an external electric field.)*

If a constant electric field is applied to this group of water molecules they will tend to orient with the applied field as depicted in figure (1.2.3). This orientation, or polarization, causes the water to have a particular capacitance per meter (Permittivity).

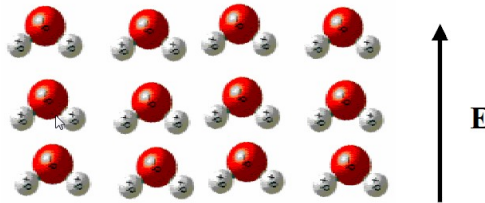


**Figure 1.2.3:** *Molecular structure of Water aligned to an external electric field.*

When salt is added to water positive and negative ions are created. The plot in figure (1.2.4) illustrates how the dielectric properties of this mixture, in this case represented by the complex permittivity, vary with the frequency of an applied electric field and let's use to introduce the different dielectric mechanisms that take place.

At low frequencies, the water molecules can follow and align the applied electric field resulting in maximum values of  $\epsilon_r'$  with low dipolar rotational loss. This polarization phenomena, known as dipole relaxation, is a form of energy storage. At these same frequencies, the positive and negative ions move in accordance to the electric field. This electric current corresponds to an ionic energy loss phenomena, that is part of the ionic relaxation mechanism and that is dominant at low frequencies.  $\epsilon_r''$  accounts for both ionic and dipolar losses.

As the frequency increases less time is given to the water molecules to keep up aligned with the changing electric field so the energy is differently distributed. The energy storage decreases while energy loss, dipolar rotational loss, increases. In addition, at these frequencies, the mass of the ions starts to prevent them from responding to the changing electric field. Consequently the ionic loss decreases so that the losses start to be dominated by the rotational losses.

At even higher frequencies the water molecules no longer respond to the electric field and both energy storage and loss still decreases. Permittivity usually is measured at frequencies below  $10^{11}$  Hz with microwave techniques. At microwave range below that frequency the permittivity variation is mainly caused by dielectric relaxation mechanisms (dipolar and ionic). Above this the water molecules are stretched and the variation of the permittivity is mainly given by the atomic polarization of the molecules. At even higher frequencies the water molecules are pulled apart and electronic polarization mechanisms take place.

In this thesis, the mechanisms that are going to be most influential on the dielectric response, because of the frequency range of interest (0.1GHz to 20GHz, microwaves) are the dielectric relaxation mechanisms.

### 1.2.7 Dielectric relaxation parameters and models

The dielectric relaxation mechanism, as in many other physical relaxation mechanisms, means the return of a perturbed system back to equilibrium.

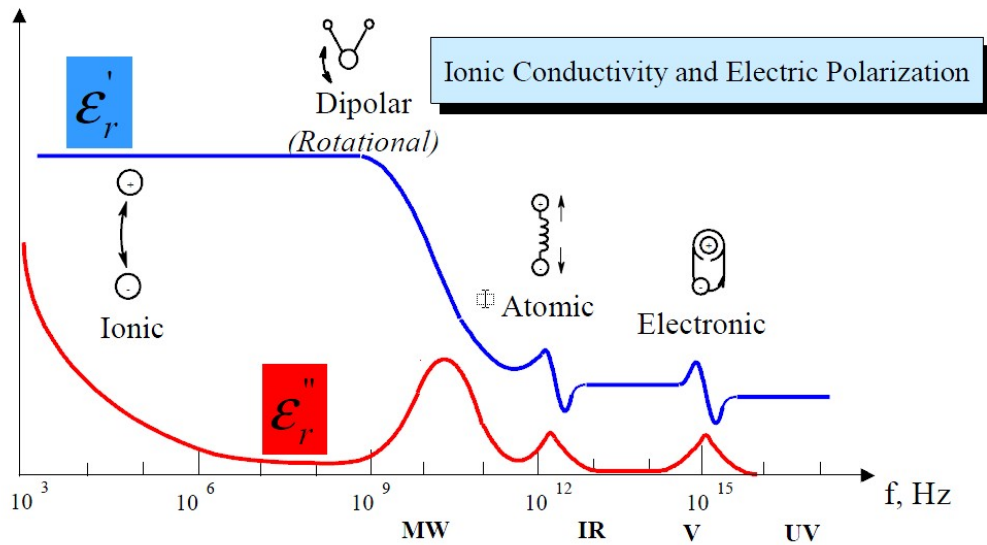


**Figure 1.2.4:** Dielectric mechanisms related to a solution of salt and water while an external electric field with variable frequency is applied.

The dielectric relaxation is often described in terms of permittivity as a function of frequency. In spite of their different origins, various types of polarizations at microwave and millimeter-wave ranges can be described in a similar qualitative way [15]. In this trend some theoretical and empirical models have been proposed accounting for an idealized representation of the dielectric relaxation phenomena.

All these models have in common these following three parameters that describe the fundamentally ideal behavior of a medium from the relaxation point of view:

- Static permittivity ( $\epsilon_0$ )
- High-frequency limit permittivity ( $\epsilon_\infty$ )
- Relaxation constant ( $\tau$ )

**Static permittivity ( $\epsilon_0$ )**

The relative permittivity of a material for a frequency of zero is known as its static relative permittivity or as its dielectric constant. Since at sufficiently low frequencies there is no phase difference between the polarization material and electric field,  $\epsilon_0$  is a real number. But the static permittivity  $\epsilon_0$  decreases with increasing temperature because of the increasing disorder.

**High-frequency limit permittivity ( $\epsilon_\infty$ )**

At sufficiently high frequencies, as the period of electric field  $E$  is much smaller than the relaxation time of the permanent dipoles, the orientations of the dipoles are not influenced by electric field and remain random, so the permittivity at infinite frequency  $\epsilon_\infty$  is a real number. As  $\epsilon_\infty$  is mainly due to electronic and atomic polarization, it is independent of the temperature too.

**Relaxation Constant ( $\tau$ )**

As in any relaxation process, the relaxation constant or time,  $\tau$ , characterizes the fundamental aspect of the relaxation. For dipolar dielectrics (such as water),  $\tau$  describes the time required for dipoles to become oriented in an electric field. (Or the time needed for thermal agitation to disorient the dipoles after the electric field is removed.).  $\tau$  is inversely proportional to temperature as all the movements become faster at higher temperatures and is closely related to the electrical conductivity. In a semiconductor it is a measure of how long it takes to become neutralized by conduction process. This relaxation time is small in metals and can be large in semiconductors and dielectrics.

**Debye model**

In most cases, the Debye Relaxation model can be applied. This model represents the dielectric relaxation response of an ideal, noninteracting population

of dipoles to an alternating external electric field. According to Debye theory, the complex permittivity of a dielectric can be expressed as:

$$\epsilon_r = \epsilon_{r\infty} + \frac{\epsilon_{r0} - \epsilon_{r\infty}}{1 + i\omega\tau} \quad (1.2.11)$$

where  $\epsilon_{\infty}$  is the permittivity at the high frequency limit,  $\epsilon_0$  is the static, low frequency permittivity, and  $\tau$  is the characteristic relaxation time of the medium.

### Cole-Cole model

The Cole-Cole equation is a relaxation model that is often used to describe dielectric relaxation in polymers.

It is given by the equation:

$$\epsilon_r = \epsilon_{r\infty} + \frac{\epsilon_{r0} - \epsilon_{r\infty}}{1 + (i\omega\tau)^{1-\alpha_{CC}}} \quad (1.2.12)$$

where  $\epsilon_r$  is the complex dielectric constant,  $\epsilon_0$  and  $\epsilon_{\infty}$  are the "static" and "infinite frequency" dielectric constants,  $\omega$  is the angular frequency and  $\tau$  is a time constant.

The exponent parameter  $\alpha_{CC}$ , which takes a value between 0 and 1, allows to describe different spectral shapes. When  $\alpha_{CC} = 0$ , the Cole-Cole model reduces to the Debye model. When  $\alpha_{CC} > 0$ , the relaxation is stretched, i.e. it extends over a wider range on a logarithmic  $\omega$  scale than Debye relaxation.

Cole-Cole relaxation constitutes a special case of Havriliak-Negami relaxation when the symmetry parameter ( $\beta_S$ ) is equal to 1. That is, when the relaxation peaks are symmetric. Another special case of Havriliak-Negami relaxation ( $\beta_S < 1$ ,  $\alpha_{CC} = 0$ ) is known as Cole-Davidson relaxation.

### Havriliak-Negami model

Havriliak-Negami relaxation is an empirical modification of the Debye relaxation model, accounting for the asymmetry and broadness of the dielectric

dispersion curve. The model was first used to describe the dielectric relaxation of some polymers [19] by adding two exponential parameters to the Debye equation:

$$\epsilon_r = \epsilon_{r\infty} + \frac{\epsilon_{r0} - \epsilon_{r\infty}}{(1 + (i\omega\tau)^{\alpha_{HN}})^{\beta_S}} \quad (1.2.13)$$

where  $\epsilon_r$  is the complex dielectric constant,  $\epsilon_0$  and  $\epsilon_\infty$  are the "static" and "infinite frequency" dielectric constants,  $\omega$  is the angular frequency and  $\tau$  is a time constant. The exponents  $\alpha_{HN}$  and  $\beta_S$  describe the asymmetry and broadness of the corresponding spectra.

For  $\beta_S = 1$  the Havriliak-Negami equation reduces to the Cole-Cole equation, for  $\alpha_{HN} = 1$  to the Cole-Davidson equation.

For additional information regarding the dielectric relaxation model consult [15].

### 1.2.8 Electromagnetic field interaction at the interface of two media

Since now we have considered the electromagnetic field interaction of a medium that is considered homogeneous, isotropic and generators lacking. We now consider the interaction with an heterogenous medium as the one depicted in figure (1.2.5) through an optic point of view. We do so to show the reflection and transmission mechanisms that can occur to the electromagnetic field while interacting with the transition between materials. Here also appears the usefulness of an intrinsic propagation parameter, the intrinsic impedance of each constituent phase of the medium, in the establishment of the modality of the reflection and transmission mechanisms.

The depicted medium has two transitions: Air-MUT and MUT-Air. The last transition is ignored for simplicity of the illustration in this case. So attention is focused to the first transition. The incident wave come from the left as depicted in that figure going through the air to incise in the material under test (MUT) phase through the transition. We will have incident, reflected and transmitted waves. Since the impedance of the wave in the material is differ-

ent (lower) from the free space impedance, there will be impedance mismatch and this will create the reflected wave. Part of the energy will penetrate the sample. Once in the slab, the wave velocity is slower and the wavelength is shorter according to the equations above. Since the material will always have some loss, there will be attenuation and insertion loss. For simplicity the mismatch on the second border is not considered.

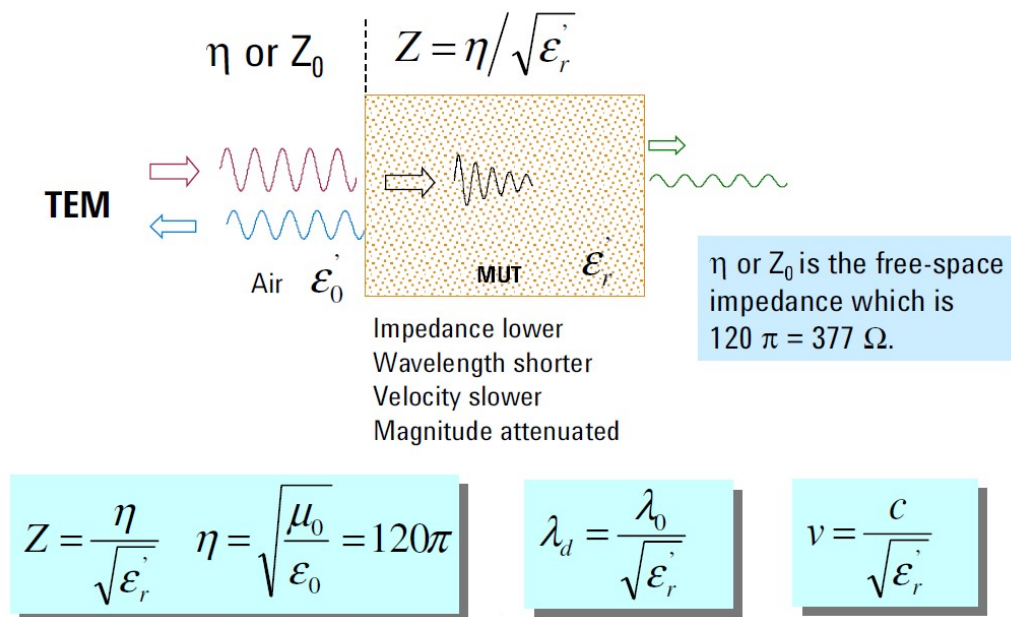


**Figure 1.2.5:** Optical view of the electromagnetic wave interaction with a two-phases material.

### 1.2.9 Other macroscopic properties of materials

Besides the macroscopic parameters discussed above, in materials research and engineering, some other macroscopic properties are often used to describe materials.

These are listed here:

- Linear and nonlinear materials

- Isotropic and anisotropic materials
- Monolithic and composite materials.

### **Linear and nonlinear materials**

Linear materials respond linearly with externally applied electric and magnetic fields. In weak field ranges, most of the materials show linear responses to applied fields. In the characterization of materials electromagnetic properties, usually weak fields are used, and we assume that the materials under study are linear and that the applied electric and magnetic fields do not affect the properties of the materials under test.

However, some materials easily show nonlinear properties as are the cases of ferrite materials and high-temperature superconducting (HTS) thin films.

In the present thesis, the treated technique works with weak fields so that the assumption of linear material system is valid.

### **Isotropic and anisotropic materials**

The macroscopic properties of an isotropic material are the same in all orientations, so they can be represented by scalars or complex numbers. However, the macroscopic properties of an anisotropic material have orientation dependency, and they are usually represented by tensors or matrixes. Some crystals are anisotropic because of their crystalline structures. More discussion on anisotropic materials can be found in Chapter 8 of [15], and further discussion on this topic can be found in [20].

The present thesis treats only isotropic material systems.

### **Monolithic and composite materials.**

According to the composition the material system can be classified as follows:

- Homogeneous
- Quasi-homogeneous

- Heterogeneous
  - Impure Medium
  - Stratified Medium

Homogeneous:

A homogeneous or monolithic material is a medium with a single constituent. Or what is the same, the constitutive parameters are the same in the whole volume of the considered material, they are spatially independent on the material. This concept has not to be confused with the concept of anisotropism or isotropism where material's parameters exhibit or not electric field orientation dependence but not spatial dependence.

Quasi-homogeneous:

A quasi-homogeneous material is a composite medium, that's a material with a host constituent and one or more constituents called inclusions or inhomogeneities, where the percentage of inhomogeneities are very less compared with the principal host compound and where the largest particle dimension is much smaller than a wavelength. This kind of materials can be approached as homogeneous materials.

Impure Heterogeneous:

An impure heterogeneous material is a composite medium where a homogeneous medium hosts inhomogeneities that are modeled with defined shapes (spheres, tubes, etc.). In some of those cases, authors refer to mixing formulas and laws that help predicting the effective permittivity of a mixture as a function of the permittivities, shapes, and volume fractions of the constituents [21, 22, 23, 24, 15].

Stratified Heterogeneous: A stratified, laminar or multilayer material is a medium that is divided in regions or layers with defined characteristics. This kind of material is going to be treated in this thesis.

### 1.2.10 General composite medium properties

The properties of a heterogeneous or composite medium are related to the properties and fractions of its constituents, so the electromagnetic properties of composites can be tailored by varying the properties and fractions of their constituents. The study of the electromagnetic properties of heterogeneous materials has attracted much attention, with the aim of developing composites with expected electromagnetic properties.

The prediction of the properties of a composite from those of the constituents of the composite is a long-standing problem for theoretical and experimental physics. The mixing laws relating the macroscopic electromagnetic properties of composite materials to those of their individual constituents have been a subject of enquiry since the end of the nineteenth century. The ability to treat a composite with single effective permittivity and effective permeability is essential to work in many fields, for example, remote sensing, industrial and medical applications of microwaves, materials science, and electrical engineering.

The mean-field method and effective-medium method are two traditional approaches in predicting the properties of composite materials [25]. In the mean-field method, we calculate the upper and lower limits of properties representing the parallel and perpendicular arrangements of the constituents. A practical method is to approximate the composite structure by elements of ellipsoidal shape, and various techniques are available to calculate the composite permittivity. For isotropic composites, closer limits can be calculated and, depending on morphological knowledge, more sophisticated limits are possible. In an effective medium method, we assume the presence of an imaginary effective medium, whose properties are calculated using general physical principles, such as average fields, potential continuity, average polarizability, and so on. Detailed discussion on effective medium theory can be found in [15, 26, 27, 24, 28].

To achieve more accurate prediction, numerical methods are often used in predicting the properties of composite materials. Numerical computation

of the effective dielectric constant of discrete random media is important for practical applications such as geophysical exploration, artificial dielectrics, and so on. In such dielectrics, a propagating electromagnetic wave undergoes dispersion and absorption. Some materials are naturally absorptive owing to viscosity, whereas inhomogeneous media exhibit absorption due to geometric dispersion or multiple scattering. The scattering characteristics of the individual particles (or the inclusions) in the composite could be described by a transition or T-matrix and the frequency-dependent dielectric properties of the composite are calculated using multiple scattering theory and appropriate correlation functions between the particles [29, 30, 31, 32].

In this present thesis we are going to deal with the accurate prediction through numerical methods of the effective complex permittivity of multi-layer composite materials for the particular case of open-ended coaxial-probe frequency-domain reflectometry technique.

More references on monolithic and composite materials can be found in [15].

### 1.2.11 Extrinsic performance

As the performances of electromagnetic materials and structures depend on their geometries, the performance-related properties are usually extrinsic [15, 1.4.2]. The design of functional materials and structures is to realize the desired extrinsic performances based on the intrinsic properties of the raw materials to be used. In a same manner the design of a measurement technique that characterizes the electromagnetic properties of a material, has to take into consideration the extrinsic performance of the measurement system based on the intrinsic properties of the measured material.

There are varieties of extrinsic performances and as an illustration we cite the characteristic impedance of a transmission line as one of them.

### 1.2.12 Applications of the complex permittivity knowledge

Because the material's permittivity changes with molecular changes, its measurement has found application in many industries. It can be used to determine the suitability of materials used to package microwaveable foods. Chemical reactions can be monitored. Bio-mass can be measured in fermentation. Measurements can detect the presence of cancerous tumors. Drug/protein interaction can be observed. Moisture content can be monitored in real time.

Here is list of the most applicable areas:

- Food Science
- Chemistry
- Biology
- Medicine
- Drug Discovery
- Agriculture
- Non-destructive testing
- Electrical/Electronic Devices
- Stealth Vehicles

Here is a partial list of material properties that have been related to the dielectric properties:

- Moisture content
- Bulk density
- Bacterial content
- Chemical reaction

- Mechanical stress
- structure
- consistency
- Concentration
- Fruit ripeness
- Most other physical, chemical and biological properties

The amount of water in a solid or liquid can be determined by measuring the material's permittivity. The advantage of using microwave techniques over the traditional oven dried methods is that permittivity can be measured in near real time. Bio-mass can be measured in fermentation. Cancer cells have a different permittivity than healthy cells. As chemicals react the permittivity of the mixture changes.

As illustrations of the difference in permittivity between different materials, the following graphics present measured cases courtesy of Agilent Technology Inc. All the measurements were made with the open-ended coaxial probe technique that will be introduced further in this chapter and in the following since it is the main topic of this thesis.

In figure (1.2.6) the complex permittivity of water and three different alcohols (methanol, ethanol and isopropanol) are plotted vs frequency in two separate plots, one for the real part and the other for the imaginary part. We can appreciate storage and lossiness of these materials. You can see that each alcohol and the water have their peak loss at different frequencies.

In figure (1.2.7) the real part of permittivity of a "Martini" mixture drink is plotted vs frequency together with its two constituent drinks "Gin" and "Vermouth". Measuring the permittivity of this and other mixtures would allow you to determine the concentration of the mixture.

In figure (1.2.8) there is a look at the differences between beer, lite beer and water. The green trace is water, the purple trace is lite beer, and the

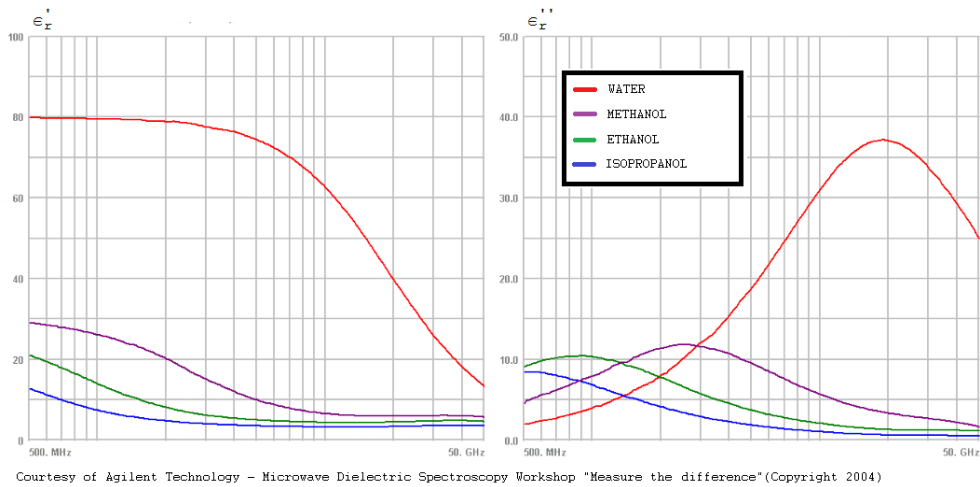


**Figure 1.2.6:** *Real and Imaginary part of water and some alcohols at room temperature and microwave frequencies.*

blue trace is regular beer. At first glance, one may think that lite beer is just beer with water added. But looking closer, you can see that the maximum value of the two beers are lower frequency of the water. Adding water to beer will not give the same result as lite beer.

In figure (1.2.9) there is the plots of milk, a glass of room temperature milk, measured over and eight hours period. The milk changed from being drinkable to spoiled. This suggests that bio-content can be correlated to dielectric properties.

## 1.3 Measurement techniques overview

### 1.3.1 Introduction

Materials properties may be determined by standardized test methods. Many of such test methods have been documented by their respective user communities and published through ASTM International.

Dielectric spectroscopy measures the dielectric properties of a medium as

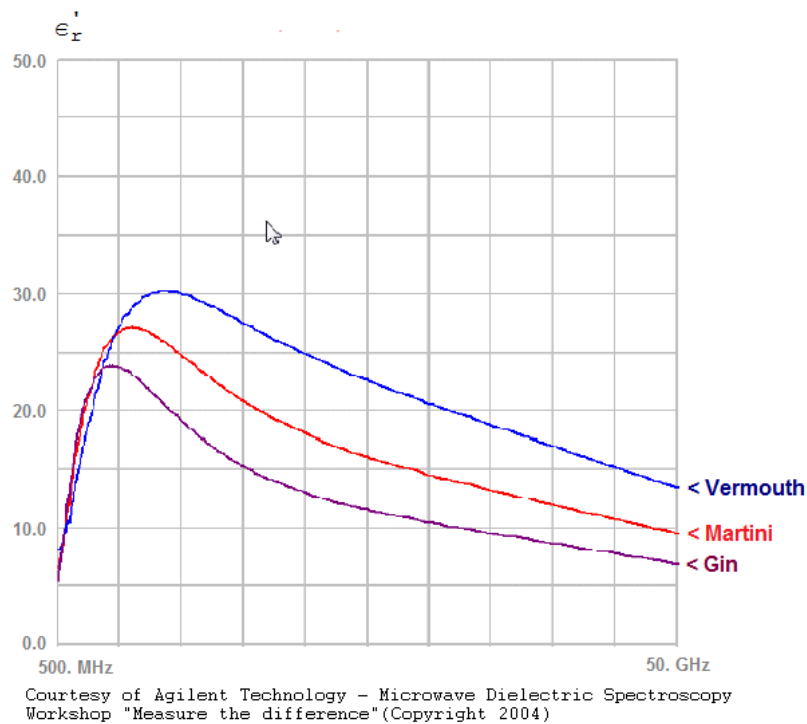


**Figure 1.2.7:** Real part of Martini drink and its ingredients Gin and Vermouth at room temperature and microwave frequencies.

a function of frequency. To accomplish it the measurement method requires the evaluation of the performance of one or more extrinsic parameters that are based on one or more intrinsic properties of the material.

These extrinsic parameters usually depend on the geometries of the structures of the material and of the measurement probe or holder. They can be directly measured or the measurement of these can be accomplished in a significantly simpler way than the intrinsic parameters.

Usually the most employed techniques measure the Z-parameters (impedances), Y-parameters (admittances) or S-parameters (scatterings) as extrinsic parameters over a frequency range and the estimation of the intrinsic parameters from those requires the geometry of the probe or holder system to be in some way previously known or considered. From these extrinsic parame-

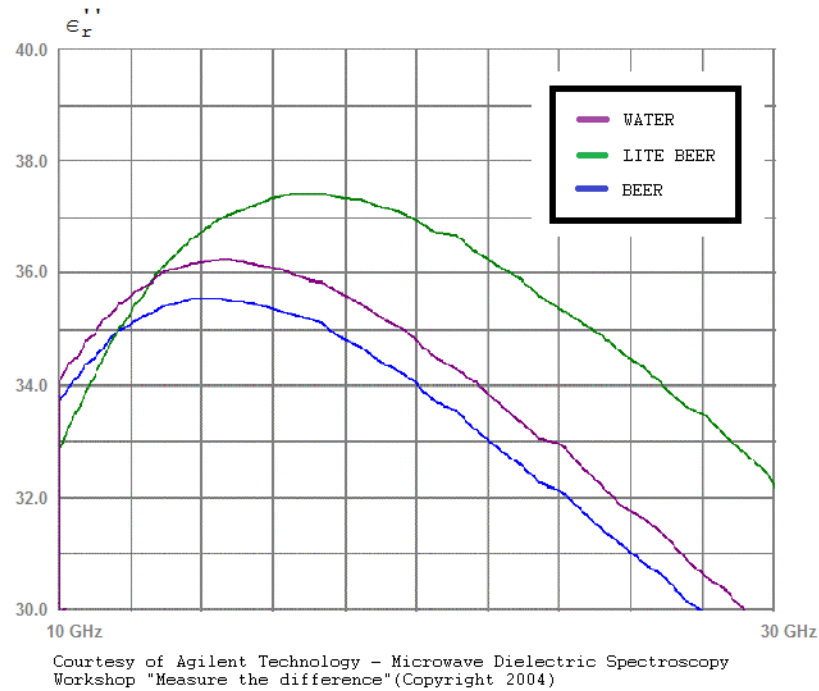


**Figure 1.2.8:** *Imaginary part of Beer, Lite Beer and water drinks at room temperature and microwave frequencies.*

ters what is measured over the frequency range are both the magnitude and phase, the real or imaginary part, or its resonance characteristics according to the technique in question.

The estimation of the complex permittivity can be achieved over a wide range of frequencies by using different variants of dielectric spectroscopy, covering nearly 21 orders of magnitude from  $10^{-6}$  to  $10^{15}$  Hz. The dielectric constant of a material can be found by a variety of static electrical measurements. Also, by using cryostats and ovens, the dielectric properties of a medium can be characterized over an array of temperatures.

In order to study systems for such diverse exciting fields, a number of measurement setups are used, each adequate for a special frequency range. A general list of them, classified by the main methods (resonant or non-resonant) and by their frequency application is presented here:

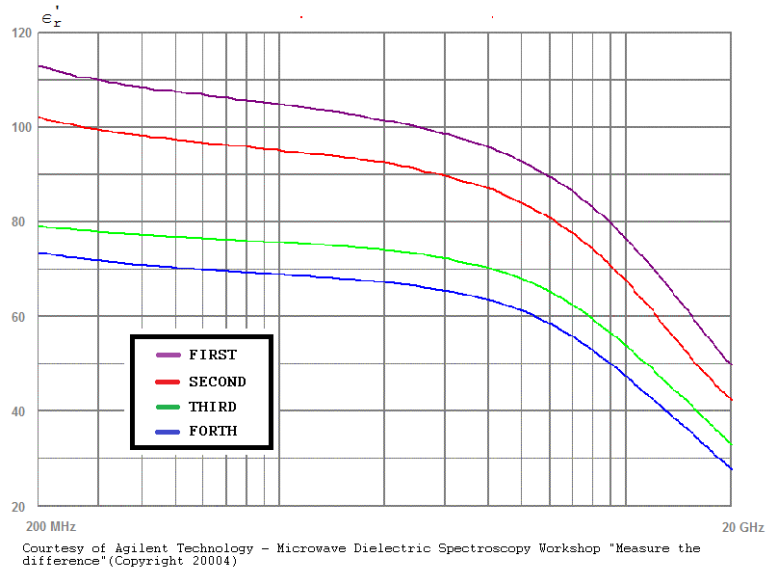


**Figure 1.2.9:** Real part of milk drink at room temperature and microwave frequencies after 1, 2, 3 and 4 periods of 8 hours each one.

- Low-frequency methods [33]
  - time domain methods ( $10^{-6} - 10^3$  Hz)
  - frequency domain methods ( $10^{-5} - 10^6$  Hz)
- High-Frequency non-resonant methods [15]
  - Reflection methods ( $10^6 - 10^{10}$  Hz)
  - Transmission/Reflection method ( $10^8 - 10^{15}$  Hz) [15]
- High-Frequency resonant methods [15]
  - Reflection methods ( $10^9 - 10^{11}$  Hz)
  - Transmission methods ( $10^9 - 10^{11}$  Hz)

The frequency ranges assigned to each method are only indicative and they are shown to be conservative.

Most of these techniques are outlined by Chen *et al.* in [15].

Low-frequency time- and frequency-domain techniques are reviewed by Iskander *et al.* in [33] and in most of the case are boarded by voltammetric, galvanometric, comparison and zero-equilibrium bridge methods. I.e., Rajendran *et al.* in [34] introduce a AC De Sauty Bridge Measurement system and Agilent Technologies Inc. has optimized a parallel plate capacitor measurement system to work also upto the UHF-L bands with the help of a LCR meter or impedance analyzer.

High-frequency methods are divided in non-resonant and resonant methods. Non-resonant methods are broad-band but less accurate, while resonant methods are narrow- or single-band and more accurate and sensitive. Most of the non-resonant methods are frequency-domain methods but when they are seriously affected by unwanted signals, time-domain methods give better performances and the combination with the Fourier-transform method let also to reach the terahertz frequency range and even more. Terahertz time-domain spectroscopy is reviewed by Schmuttenmaer in [35]. Both non-resonant and resonant methods can be one-port or two-port methods according to if reflection or tranmission/reflection parameters are measured and can use transmission line or free-space (HF/microwave/mm-wave) methods according to the properties of the material and of the measurement system and to the frequency range of interest.

This previous list represents the current state of art of all the generalized measurement technique that the user community (industrial, academic and amateur) has developed.

During the first year of Ph.D. course of the author, the attention was focused in methods in the low microwave frequency range according to the instrumental availability. Now, for discussion and illustration, we present a little wider range, from 1 MHz to 100GHz. A list with the most known microwave techniques available and applicable to those methods previously presented is listed below.

List of most diffused microwave techniques for material characterization:

1. non-resonant reflection methods
  - open-ended aperture probe techniques
  - monopole antenna probe techniques
  - planar-circuit probe techniques
  - shielded probe techniques
  - free-space reflection techniques
2. non-resonant transmission-reflection methods
  - transmission line technique (coaxial air-lines, hollow waveguides, dielectric waveguides, planar lines)
  - Free-space technique
3. resonant transmission methods
  - dielectric resonance technique
  - resonant-cavity perturbation technique

The techniques based on non-resonant reflection methods obtain the test sample permittivity from the measurements of the reflection coefficient (the scattering parameter  $S_{11}$ ) at a defined reference plane (usually at the interface of the test dielectric). The reflection coefficient may be measured by a slotted line or a network analyzer, or by forming a resonator terminated by the sample as described in [36], in the frequency domain (FD), or by a time domain (TD) spectrometer. Most of the techniques shown in the previous list are reviewed by Stuchly *et al.* in [37] and by Chen *et al.* in [15].

In this thesis we will completely focus on the open-ended coaxial probe FD reflectometry technique that is type of open-ended aperture probe technique.

The techniques based on non-resonant transmission-reflection methods obtain the test sample permittivity from the measurement of both the reflection and transmission coefficients (the scattering parameters  $S_{11}$  and  $S_{21}$ ) at defined reference planes. These coefficients may be measured by a network

analyzer in the frequency domain (FD). Most of these techniques, shown in the previous list, are reviewed by Chen *et al.* in [15].

The techniques based on resonant reflection or transmission methods obtain the test sample permittivity from the measurement of the reflection coefficient ( $S_{11}$ ) or transmission coefficient ( $S_{21}$ ) respectively. These coefficients may be measured by a network analyzer in the frequency domain (FD). Usually the most commonly used are the one based on transmission methods. Most of these techniques, shown in the previous list, are reviewed by Chen *et al.* in [15].

In the following sections of this chapter we are going to introduce the most common techniques giving their most characteristic features and commenting their usage and functionality. We will start from the techniques based on reflection methods. There we are only introducing the open-ended coaxial probe because it is the most representative and performant of its group. Then we are going to present the transmission techniques and the resonant techniques.

### 1.3.2 Characteristic features helping in technique selection

The following list represents the most common features that can help in the technique selection. These features refer to the characteristic features of the material and to the characteristic features of the measurement system.

Characteristic features:

- Frequency range of interest
- Expected value
- Required accuracy
- Material properties
- Sample size restrictions

- Destructivity
- Material's contact
- Passive and Active
- One or two port
- Complexity

A brief discussion of these different aspects or features that can describe the methods and techniques is presented here:

### **Frequency range of interest**

This is one of the fundamental factors that helps in the technique selection. Leaving to a side the low-frequency methods, the most difficult choice is between the resonant and non-resonant methods. The distinctive characteristics of each one of these methods take us to a compromise between the broadness of the frequency range and the accuracy. Non-resonant methods, once calibration is established, are capable to give a broad view of the material in frequency at a reasonable accuracy (a few percents) but have difficulties to measure low-loss materials. On the other hand, resonant methods gives the best accuracy and are capable to measure low-loss materials because of their higher sensitivity but at a single frequency. Resonant methods can be combined with dielectric relaxation models, assuming that they fit well the material's dielectric relaxation nature, to account, after some frequency points, a broad view in frequency.

Between the non-resonant methods, because of the transmission line characteristics, different band performance can be achieved. Usually coaxial line are wider in band than the waveguides. In free-space methods the broadness of the band will be given by the characteristics of the employed antennas.

**Expected value**

Any estimative expectation in the value of the complex permittivity and of the loss of the material can be useful for a correct choice of the technique. Expectation on the complex permittivity can be particularly useful for techniques that possess a numerically tough extraction of the parameter as is the case of open-ended coaxial probes technique, when no reference standards are employed, in order to give an initial condition on the extraction algorithms. Expectation on the lossiness of the material can be useful when choosing between resonant and non resonant methods.

**Required accuracy**

The measurement accuracy requirement will be given by the required application. Applications that require low accuracy are mostly applications involving systems' diagnosis, i.e. that require the comparison between materials as for example in decision schemes in industrial processes. The joker card will be the requirements in resolution or sensitivity that will depend on the problem's nature to solve. Applications that require high accuracy are most involved in systems' design. Accurate data in the complex permittivity and in its dispersion characteristic are a continuous demand, i.e, in PCB circuits for working at higher frequencies as the technology advances. For sheet materials and low-loss, as maybe we previously mention, the best techniques are the one based on resonant methods.

**Material properties**

According to the material's nature some technique are more performant than others. If the material is macroscopically homogeneous, most of the techniques work well. If the material is macroscopically heterogeneous, the applied technique needs to have its sensible area (area where the material influences the system response) including a certain percent of the inhomogeneities to work. Also in this case specialized homogenization models have

to be employed according to the nature of the treated problem. If the material is isotropic most of the techniques works well, but if it is anisotropic some particular techniques need to be used, as for example, special wave modes can be excited in some particular waveguide techniques to study its anisotropism. According to the material's phase, for liquids most of the techniques are applicable but the best performant are the techniques that are immersed in the liquid as is the case of the open-ended coaxial probe. For solids the transmission line, reflection-transmission techniques are between the best if machining them is allowed.

### **Sample size restriction**

Usually the techniques will restrict the sample size according to various reasons. Minimal and maximal dimensions will be restricted by: 1) accomplishing the ideal assumptions that the models used in the technique assumes; 2) the frequency range of interest; 3) the value of the material's permittivity; 4) the energetic restriction regarding the minimal volume of the material for a detectable response; The techniques that allows the smallest samples are the resonant techniques since they are the most sensitive. The techniques with the most freedom in the sample size are the free-space techniques and the open-ended coaxial probe technique. Usually at lower frequencies, sample sizes are required to be larger what in some cases become impractical.

### **Destructivity**

Depending on the case, each electrical characterization measurement to be made for a material or an object, would require or not a previous preparation and transportation of the material. The methods where a special preparation of the material is needed are called destructive methods. In this sense the preparation turns the material useless of other applications.

In some applications, it is required to know the exact electrical characterization of the material in the state it works. This means that the less processing the material suffers the best. This requires for that type of methods a non-

destructive method.

The technique open-ended coaxial probe is non-destructive because its configuration, in some cases like solids or semi-solids, lets the application of the material to a side of the probe with minimal base preparation. However its accuracy is considerably reduced because of the imperfectness of the contact and specialized models need to be considered.

For liquids the problem ceases or is lower since they are easily manipulated to fit in the measurement holder and, in some cases, they also can be shipped without or with reduced changes in the characteristics to measure and can be applied back again.

### **Material's contact**

Some samples, because of various reasons cannot be in contact with the measurement holder or probe. The sample can be at a very high or low temperature or need to be kept under certain environmental conditions or the redesign of the measurement system can be expensively increased in cost. In such cases the free-space is the most preferable technique since the redesign cost is in most of the cases minimal compared to other techniques to work at such conditions.

### **Passive and active**

In a passive technique, the microwave source and the dielectric being measured are independent of each other. In contrast, in an active method the opposite occurs. Generally mostly of the method were analyzed at the bibliographical research were passive, but the microwave oscillation loop, that uses a kind of resonant method was an active one [38].

### **Ports**

We can think of the device containing the MUT like a network with a defined quantity of ports, that have to be the only opened interfaces between it and

the tester devise. The discussed methodologies were of 1 and 2 ports only. Generally the reflection methods, being resonant or not, were all one port, while the others where two ports. In the two-ports case, the advantage is the possibility of measuring both transmission and reflection signals from the MUT's device what in some cases gives two independent conditions to extract at the same time two constitutive parameters of the material. Usually they are used to extract both the complex permittivity and the complex permeability. On the contrary, in a one-port method only the reflected signal can be used and just one constitutive parameter at a time can be estimated.

### Complexity

This aspect would depend not only on the difficulty of executing the direct measurement (measurement setup and calibration), but also the later calculation needed to arrive to the required information, indirectly.

Because of the complexity of the relation between the electric parameters like the complex permittivity and the measured parameters (Reflexion coefficient), an analytical and direct resolution would be difficult or impossible in many cases. In this sense many of those methods would have the difficulty of needing to recur to an inverse problem solution by mean of numerical methods.

### 1.3.3 Comparative diagram

As a first comparative glance between the three major methods we introduce this scheme as depicted in figure (1.3.1). The axis are two important determining factors in deciding which technique to choose. On the x-axis we have frequency of interest, from the low MHz to 500GHz. And on the y-axis is how lossy the material under test will be. At the bottom we have low loss materials and at the top, high loss materials.

“Coaxial probe” represents the non-resonant reflection methods, mostly in the open-ended coaxial probe technique and is shown its extended application for high loss materials. The “Transmission line” represents the

non-resonant transmission-reflection with the transmission line technique and the “Free space” the non-resonant transmission-reflection with the free-space technique. Both of them are highly applicable to medium loss materials and inclusively are the most capable to be extended to the millimeter wave regions. The “Resonant cavity” represents the resonant methods. The extension in the “resonant cavity” block with dashed lines represents the advances in quasi-optic methods applied to resonators as the microwave Fabry-Perot resonator that extend the applicability of the resonators to millimeter wave regions.

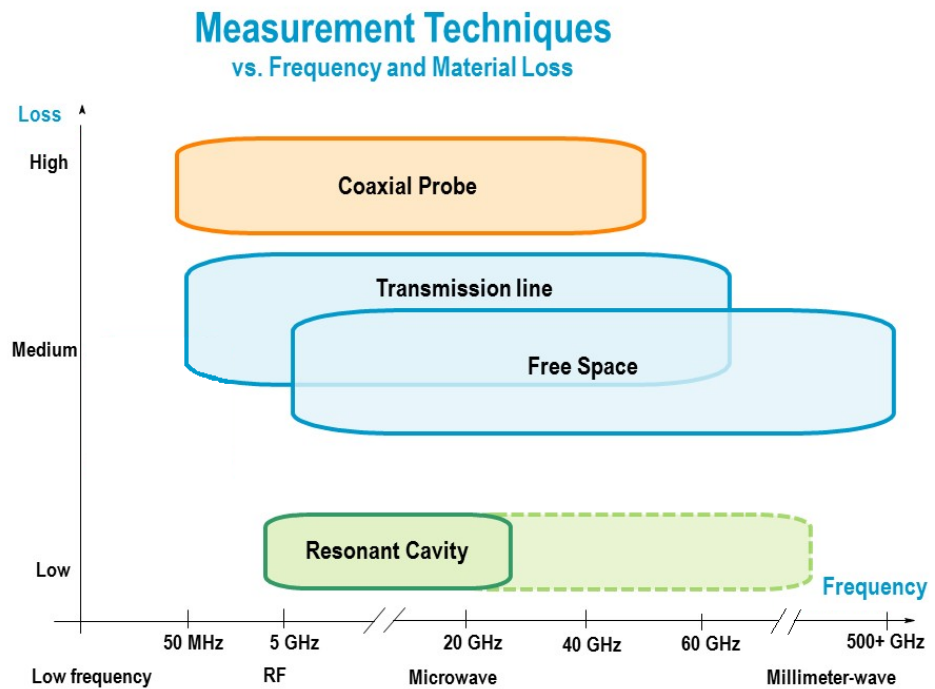


**Figure 1.3.1:** Comparative Diagram. Loss and Frequency for each technique.

A description of the previously mentioned techniques is presented here:

### 1.3.4 Open-ended coaxial probe technique

#### Characteristic aspects

The most important aspects of this technique are:

- Broadband frequency range: Offers broadband response according to the coaxial probe geometry and material in a range that goes from VHF to low EHF bands (0.2 GHz to 50 GHz).
- Good for highly lossy materials: Works well for highly lossy materials, principally liquids and semi-solids. Powders and solids can be measured if they present a good contact. In theory it can be applicable to an extensive range of materials. Magnetic materials can also be measured by accomplishing two independent reflection measurements.
- Regular Accuracy: From 1 to 10% approx.
- Sample Size restriction: Necessary to cover the active area of the probe, so depends on the probe geometry. Depending on the extraction model, samples can be heterogeneous or of a defined thickness.
- Minimal destructivity: Minimal for liquids and biological tissues. Solids may need to be prepared to improve its contact with the probe, specially in the active area.
- Needed material's contact: Needed, specially in the central area of the probe.
- passive
- 1-port
- Regular Complexity: Convenient and easy to use. Measurement setup may require other known liquids standards or ad-hoc Open-Short-Load standards to be measured for calibration purpose according to the used

models for the extraction. The reflective response can be easily measured and the probe is easily designed. Materials need minimal preparation and calibration can be done faster than in transmission techniques. Extraction models are widely available from simple and less accurate to complex and more accurate. The most expensive part that makes its complexity is the extraction algorithm and the error corrections.

### Comments about this type of technique

The coaxial probe technique is a technique based on the non-resonant reflection method. The main and common features of this system consist of an open-ended coaxial probe in contact at a side with the material sample to be tested (MUT) and connected to the other side through an adequate transition for a correct adaptation to the tester line, a single port to a network analyzer. The dielectric properties can be calculated from the reflection response of the probe at the reference plane in the aperture of the probe in contact with the material through the use of appropriate extracting algorithms.

The coaxial probe technique usable frequency range goes from about 200MHz to near 50GHz. The upper frequency limit is hardly extended because of the unrealizable small dimensions of the probe. The lower frequency limit is conditioned by the fact that a phase distinction starts to be difficult, specially for low loss materials, to resolve and the lack on resolution start to be impractical.

This technique is best for characterizing permittivity of highly lossy materials. Examples are human phantoms for Specific Absorption Rate (SAR) tests, tissue samples for medical research, and any sample with a high water content, such as food products and agricultural or mineral materials.

The accuracy and validity range of open-ended coaxial probe techniques depends on the probe diameter and on the model relation that derives the permittivity from the measured reflection coefficient [39, 37]. Air gaps between a solid and the probe tip, and bubbles in a liquid will cause significant errors and should be carefully controlled.

This technique is extended in the following chapters where a detailed presentation of each of its features is given and the introduction to the main work of this thesis is done.

### 1.3.5 Transmission line techniques

#### Characteristic aspects

The most important aspects of this technique are:

- Broadband or banded frequency range: Offers broadband or banded response according to the transmission line holder and material in a range that goes from VHF to low EHF bands (0.05 GHz to 75 GHz).
- Good for averagely lossy materials: Works well for moderately lossy materials, principally hard solid materials. Can measure magnetic materials. Liquids, powders, and gases must be contained.
- Good Accuracy: From 1 to 5% approx. Conditioned for air-gap between the sample and walls of the holder. Better performance than the coaxial probe techniques.
- Sample Size restriction: Needs to fit in the holder cavity, so dependent on the probe geometry. Needs large samples for low frequencies. Needs flat faces, perpendicular to long axis. Needs Sample Thickness  $> 20/360\lambda$ .
- Considerable destructivity: Solids require extensive machining to fit the holder's cavity.
- Needed material's contact: Needed, good contact with all the walls of the cavity, principally the most actives one.
- passive
- 2-port

- Regular Complexity: Measurement setup requires samples that fit the holder and the calibration can be relatively simple if ad hoc TRL (Thru-Reflect-Line) standards or similar are available. The extraction algorithms are of medium difficulty, depending on the features of the extraction model.

### Comments about this type of technique

The transmission line sample holders can be made from coaxial airlines, waveguide straight sections or strip-line or microstrip-line sections. They possess two ports so that the reflection and transmission coefficient can be measured with the appropriate device, usually a vector network analyzer.

Coaxial fixtures (beadless airlines) are broadband but require a sample shaped into a flat-faced torus. Waveguide fixtures are band-limited but operate at higher frequencies and accept a simpler rectangular shape. Samples must completely fill the cross section of the transmission line without gaps at the fixture walls. Faces at either end must be flat, smooth and perpendicular to the long axis.

The material's thickness (length) is needed to be known for the extraction. The sample must be long enough to contain enough of the wavelength to be measurable. Ideally it is recommended a minimum of 20 degrees, but this is conservative and with today sensitive network analyzers, reasonable measurements can be obtained with even shorter samples. If air gaps are significant, correcting algorithms can considerably reduce the largest source of error.

This technique can measure both the complex permittivity and permeability of the material. It works best for hard solids that can be machined, but it is also possible, although more difficult, to contain liquids and powders inside these using dielectric dams. High loss materials can be measured too if the sample is kept relatively thin.

Although it is more accurate than the coaxial probe techniques, it is still somewhat limited in resolution for low loss materials.

Grim *et al.* in [40] presents a strip-line and microstrip-line applicators for this technique. Additional variants and techniques can be found by Chen *et al.* in [15]

### 1.3.6 Free-space techniques

#### Characteristic aspects

The most important aspects of this technique are:

- Broadband frequency range: from SHF to EHF bands and even more (5 GHz to 500 GHz). Range set by antennas, material and network analyzer. Minimal Frequency is set by maximum practical sample length.
- Good for planar materials: Good for planar block and for high temperature materials.
- Good Accuracy: Typical 1 to 2%
- Sample Size requirements: Sample sizes (transversal size) larger than the wavelength of the electromagnetic wave (at least twice larger) for scattering minimization. Flat parallel sample faces. Very large samples needed at low frequencies. Sample thickness (longitudinal size) larger than 20 degrees ( $> 20/360\lambda$ ), but smaller than 1 wavelength ( $\lambda$ ) because multiple root mathematical errors can occur. These are conservative estimations.
- Poor destructivity: Needed to ensure a flat surface and the required size.
- No needed material's contact
- passive
- 2-port

- Regular Complexity: Measurement setup requires the placement of the samples in the far-field non-reactive region (antenna theory) and the 3dB beam spot of the antennas contained in the sample. Calibration can be relatively simple if ad hoc TRL (Thru-Reflect-Line) standards or similar are available. The extraction algorithms are of medium difficulty, depending on the features of the extraction model.

### Comments about this type of techniques

The free-space technique is just a variation of the transmission line technique and uses the same algorithms to calculate permittivity and permeability. Materials are placed between antennas for a non-contacting measurement under free space conditions.

This non-contacting condition makes that the sample finds itself isolated from the other hardware in the system what remarks the potential application of this technique in remote sensing and materials at high temperatures. Special ovens can be purchased with microwave “windows”. The sample is placed inside and the test equipment can remain safe outside.

The free space technique works best for large, flat, thin, parallel-faced solid materials (sheet materials), but granular and powdered materials can also be measured in a fixture. It is very useful for many applications such as non-destructive testing, measuring materials that must be heated to very high temperatures, or measuring a large area of material that is non-uniform such as honeycomb or a composite.

High loss materials can be measured too if the sample is kept relatively thin. Common materials measured with the free space technique are various types of radar absorbing materials such as low observable coatings for military aircraft, as well as other coatings such as painted car bumper materials for collision avoidance. In addition, this technique is often used for measuring permittivity of radome materials, materials used to cover antennas. Even though these materials are usually fairly low loss, the form factor of the large sheet of radome material fits the technique well and the accuracy of the real

part of permittivity is usually adequate for the application.

The transmission line technique has a frequency range of around 50MHz to about 75GHz. Above 75GHz, it gets difficult to fit a sample into the microwave transmission line that is used as a sample holder. If you know anything about waveguide sizes, you know how small waveguide in this frequency range is, 75GHz rectangular waveguide is approximately 1x2 mm. So at higher frequencies, free space technique becomes more practical because everything, including the required sample size, becomes larger and easier to work with. With the free space technique, we can go all the way up to 500GHz and even beyond. By contrast, on the low frequency end, free space becomes more difficult because things become very large. The free space technique works at low frequencies, but at 3 - 6GHz, a sample would have to be a few feet wide and at that point it can become easier to fit the sample into a transmission line. Unless of course the sample is a large sheet of material, in which free space may still be a practical solution.

A typical free-space system consists of a vector network analyzer, two antennas facing each other and a sample holder between them placed at the “far-field” non-reactive region of both antennas. Transmission and Reflection Coefficients are calculated from those measurements and then the electrical characteristics of the material are determined using an appropriate model and a fitting technique [41].

### 1.3.7 Resonant-cavity techniques

#### Characteristic aspects

The most important aspects of this technique are:

- Single frequency: from SHF to low EHF bands (1 GHz to 100 GHz). Just a single frequency. Some techniques reach to give few frequencies through special structures and mechanisms. The difficulty to overcome at high frequencies is that start to become difficult to separate out the usable resonant frequency modes.

- Good for low loss materials and thin films. High loss materials need very small sample size.
- Very Good Accuracy: From 0.1 to 2%
- Sample Size requirements: Necessary to fit in the holder cavity, so depend on the probe geometry. Since the method is more sensitive than other methods, smaller samples can be required.
- Considerable destructivity: Solids require extensive machining to fit the holder's cavity. In liquids the holder can become tube that can be routed through the cavity for real time fluid measurements.
- Needed material's contact: Needed, good contact with all the walls of the cavity, principally the most actives one.
- passive
- 2-port
- Regular complexity: Measurement setup requires the placement of the samples inside the cavity. Vector calibration is not required. The extraction algorithms are of medium difficult, depending on the features of the extraction model.

### Comments about this type of technique

The resonant cavity technique is a technique based on a resonant method. The main features of this system consist of a resonant structure, with inside the material sample, connected between two ports of a network analyzer with coax cables. The dielectric properties can be calculated from the transmission response of the cavity, measured empty and then with the sample.

The port aperture has to be small enough to ensure the cavity to be a close volume. This can be done with a magnetic loop coupler protruding slightly into each port wall. The cavity volume has also to be known for calculating the complex permittivity.

There are several extracting algorithms. The ASTM 2520 is a fairly simple and commonly used method. This algorithm is dependent on the center frequency and Q measure with and without the sample inserted. The volume of the empty cavity and sample are also required. Other more accurate and complex methods have been developed at NIST.

There are many different types of resonant structures. There is the 10GHz Split Cylinder resonator, which was recently adopted as an IPC standard test method. The Split Post Dielectric Resonator developed by Dr. Jerzy Krupka at QWED in Poland, and an older ASTM waveguide resonator. For the Split Cylinder and the Split Post resonators the sample must be in the form of a thin flat sheet. For the ASTM resonator, the sample is a long rod or rectangle.

The resonant-cavity technique is particularly suited for thin film and sheet materials. For both the Split Cylinder and Split Post resonators, the ideal sample thickness is 1 mm and below. The sample size requirement for the Split Cylinder stays the same, no matter what frequency, but with the Split post resonator, the sample size scales with frequency. For lower frequencies, the sample must be larger, and for higher frequencies the sample must be smaller.

The Split Post resonator fixtures are tuned to measure one frequency mode each. So, to get data at multiple frequency points, multiple fixtures must be used. With the split cylinder resonator, it is possible to use multiple resonant frequencies in the same fixture. Which of these points are, is determined by the electrical properties of the material under test and the samples thickness.

Kent in [42] presents a cylindrical waveguide resonant-cavity perturbation tester with a slot for substrate sample insertion and two coupling loops for input and output signals. Additional techniques are presented by Chen *et al.* in [15].

An active technique is presented by Tian and Tinga in [38]. They introduce a microwave oscillation loop circuit for dielectric constant measurement. Since this technique is active, the microwave source and the dielectric being

measured are dependent of each other.

### 1.3.8 Additional comments on the accuracy and resolution of the techniques

About the performance of the techniques in accuracy and resolution, we found that the ones to have better accuracy and resolution are the resonant techniques specially for measuring the imaginary part of permittivity and loss tangent. Usually the resolution for the Split Post Dielectric Resonator and the Split Cylinder Resonator techniques is equal or better than  $10^{-4}$ . On the contrary, techniques based on non-resonant methods have larger resolutions going from  $10^{-3}$  for the transmission techniques (line and free-space) to  $10^{-1}$  for the coaxial probe techniques. The accuracy of the techniques based on the non-resonant methods is largely determined by the quality of the vector calibration. By contrast, techniques based on resonant methods don't need vector calibration and the accuracy is determined by the Q factor of the empty resonant cavity fixture what is very high for the Split Cylinder Resonator and the Split Post Dielectric Resonators.



# Chapter 2

## Open-ended coaxial probe

### Overview

#### 2.1 Introduction

This chapter is dedicated to the open-ended coaxial probe technique in its functional aspect with the measurement system. In the first section the basic geometry of the ideal probe and the main functional aspects of each geometrical and physical parameter are introduced. The performance of the probe is then illustrated. The performance areas of interest and the performance parameters are introduced with a detailed description. Finally a simulation study is shown with respect to one of the performance parameter, the Sensibility range.

#### 2.2 The ideal open-ended coaxial probe

##### 2.2.1 Introduction

Perhaps the first theoretical works on open-ended coaxial probe were done not exactly intended as a permittivity measurement tool but as a circular

diffraction antenna at the end of the 40's and beginning of the 50's of the XX century, with the works of Pistolkors [43], and Levine and Papas [44]. The most diffused for the application as a permittivity measurement tool was certainly the one of Levine and Papas that was also published in a Waveguide handbook ([45]). But that occurred later at the beginning of the 80's. The first works were conducted by Gadja, Stuchly, Mosig *et.al.* and Burdette in [46, 47, 48, 37, 49, 50] and from those the research on this technique started to increase so as to gain in these last three decades a position of pre-eminence among the nondestructive methods for the measurement of permittivity due to its several advantages (e.g. the ease and speed of operation and the flat frequency response).

The hardware of the probe is simple and has fundamentally not changed along these last decades in all the reviewed publications. What has unquestionably changed and improved is the usage and modeling of it.

The first works on the technique utilized an ideal geometrical configuration, as for example, the one introduced by Levine & Papas [44]. The ideal geometrical model, the ideal sketch of the probe is introduced in the following subsections together with comments and discussion regarding its parameters and features.

### 2.2.2 Basic geometry and definitions

A sketch of the ideal open-ended coaxial probe is shown in figure 2.2.1. The sketch shows an illustration as a coaxial line that at a side (left) is infinitely extended and at the opposite side (right) connects with the material under test (MUT from now on) through an open-ended coaxial aperture transition. As can be seen in the sketch, the principal features that describes the probe, in particular its coaxial section, are:

- $R$ : the “axial ratio” or “radius ratio”;
- $b$ : the outer radius of the coaxial section;

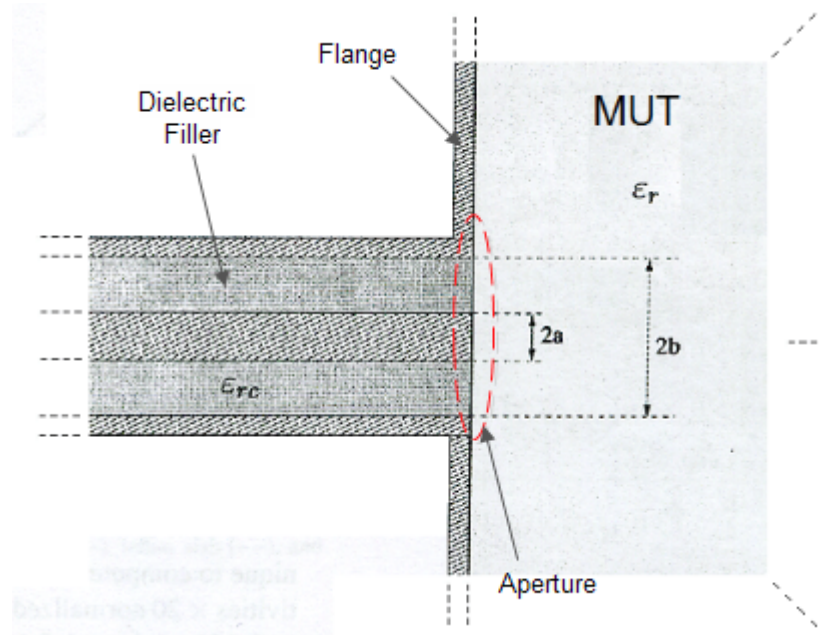


**Figure 2.2.1:** Sketch of the ideal open-ended coaxial probe. Longitudinal cut section.

- $Z_0$ : the characteristic impedance.

In addition to those three features, another two features are commonly cited:

- $a$ : the inner radius of the coaxial section;
- $\epsilon_{rc}$ : the permittivity of the probe's dielectric filler.

The axial ratio feature of the probe is defined as the ratio of the outer and inner radii of the coaxial section:

$$R = \frac{b}{a} \quad (2.2.1)$$

and its value goes inside the domain defined by  $1 < R < \infty$ .

The “characteristic impedance” of the probe is defined as the extrinsic performance parameter based on the intrinsic parameters of the coaxial filler and axial ratio of the coaxial section:

$$Z_0 = \frac{1}{2\pi} \sqrt{\frac{\mu}{\epsilon}} \log(R). \quad (2.2.2)$$

Here  $\log$  is the natural logarithm. Usually the filler is a low loss or lossless dielectric material so that its most influential intrinsic parameter is the dielectric constant ( $\epsilon_{rc}$ ).

In addition to those features, the ideal probe is assumed to have an infinitely extended flange and an infinitely-extended homogeneous material at the right half-space delimited by the aperture of the probe. This is a condition usually given by the aperture admittance models to explain the probe's response. Those models define the admittance at the aperture plane of the probe (see figure 2.2.1). One example of aperture admittance model is the one given by Levine & Papas in equation (6.1) in [44]. That and other aperture admittance models are going to be introduced in detail in chapter 3.

### 2.2.3 Discussion

With the use of the features “axial ratio”, “radius  $b$ ” and “characteristic impedance” the probe is completely characterized. The “axial ratio” gives a measure of the openness of the aperture of the probe to its left half-space where the material under test is placed and straightforwardly influences the probe's performance and defines the probe's applicability. The “radius  $b$ ” gives a measure of the largeness of the section of the probe and helps in its size classification as “small”, “medium” or “large” probes. The “characteristic impedance” gives a measure of the probe's performance and its value helps to characterize the behavior of the probe in its completeness, i.e., with the material under test.

The dielectric constant ( $\epsilon_{rc}$ ) of the filler of the probe is principally chosen to keep a desired “characteristic impedance”, but small values of it are also wanted to improve the probe's performance from the boarding field effect as it's going to be seen in chapter 5 when studying the imperfectness of the contact problem.

About the “radius  $a$ ”, its knowledge is also important to characterize the main area of intensive field predominance and to decide the threshold from

which elements (inclusions or inhomogeneities) at the material half-space side, in touch with the aperture plane, can be neglected.

Finally, about the flange and material assumptions, they are mostly conservative conditions based on the employed aperture admittance models. The infinitely extended flange condition can be broken to include no-flange or small flange cases for practical applications. This is not drastically changing the probes performance but affects the overall accuracy and conditionate the interpretation of the probe response according to the employed model used, mostly if it is one of type of hard models. Soft models can include its effect in their parameters according to its nature. Hard and soft models are going to be introduced in chapter 3.

The infinitely-extended homogeneous material assumption can also be broken and how it affects will depend in the aperture admittance models. Usually how the structure and composition of the MUT affects the overall response of the probe will depend on the characteristics of the probe, principally the sensitivity depth that will be introduced in the following section. In case there is a change on the response given by the structure and composition of the MUT, an effective response is seen. This response can be traduced by the use of specialized aperture admittance models taking into consideration the material structure and composition as will be seen in chapter 3.

## **2.3 The performance of the probe**

### **2.3.1 Introduction**

In the previous section was given a general overview of the geometry of an ideal open-ended coaxial probe where the respective definitions for each geometrical feature was introduced and comments regarding the functionality of each one of them were presented.

In this section the attention is focused on the performance of the probe. Its performance is examined with respect to: 1) the operable frequencies; 2) the

maximum sensibility to detect changes in the structure or composition of the MUT; 3) the maximum range, i.e. the closest a changer element, like for example a new component layer of the MUT, has to be to produce a change in the response of the probe.

For evaluating it a serie of performance parameter needs to be defined so as to allow an open and neat comparison between different probes and also of this employed technique with other techniques.

### **2.3.2 The performance areas**

The performance parameters of the probe have the function of describing the overall functionality of the probe in a performance area. The performance areas are some of the characteristic features introduced in subsection 1.3.2 and even more.

The considered areas are:

- Frequency range
- Precision
- Accuracy
- Sensibility range
- Sensitivity

#### **Frequency range area**

In this area the performance of the probe is evaluated according to the upper and lower limits of the frequency operation of the probe. Inside the region delimited by the two limits, the probe operates in the normal conditions the probe was designed and warranted to work as.

### **Precision area**

In this area the performance of the probe is evaluated according to its precision. The same is given as a result of the uncertainty analysis carried out to the probe system. The probe will be considered more precise as smaller radius of the uncertainty circle is.

### **Accuracy area**

In this area the performance of the probe is evaluated according to its accuracy. Since the accuracy is fundamentally a relative quantity, we need to refer it to a target or reference. In this sense there can be two modalities of evaluations: 1) accuracy with respect to the aperture admittance; 2) accuracy with respect to the permittivity of MUT. The first one is less convenient in the point of view of an absolute exactness, since is referred to an aperture admittance model that is considered much more accurate than other models to be considered as reference. The inconvenience yields in that no probe's model will be as accurate as the real MUT as a reference. Because of that the second one, that makes the evaluation with respect to the MUT, is more convenient because gives a more absolute indicator. But it is less convenient from the application point of view since is more challenging to achieve that the former one.

### **Sensibility range area**

In this area the performance of the probe is evaluated according to its *sensibility range*, i.e., the range in which the probe shows its ability to be used. This range is defined as the spatial area behind the probe's aperture, in the right half-space containing the MUT, where the system can resolve changes in the structure or composition of the MUT.

The *Sensibility Range* is intimately related to the electric field spatial distri-

butions in the half-space outward of the aperture plane. The more intensive and normally oriented is the field in that range, the more sensitive the probe will be to detect smaller elements principally if they are very low in permittivity compared with the permittivity of the host medium. See page 34 in [51]. The electric field is more intensive in the space surrounding the annular aperture, principally at the central conductor level. Outside this aperture the field intensity decrease, diminishing also the influence. A boundary to it, as suggested by Stuchly *et al.* in [37], is where the magnitude of the electric field is at least two orders of magnitude smaller with respect to what seen at the inner conductor tip at the probe's aperture.

The distribution of the electric field intensity and of its normal and parallel components can be found easily by considering a longitudinal cut section, paying attention to the half-space in the MUT next out to the coaxial aperture. A more detailed information can be obtained with assistance of a CAD. We have been helped out in this by a commercial electromagnetic simulator (CST Microwave Studio, [52]).

Usually the parameter describing most this range is the *sensibility depth*. In addition, a simulation study has been carried out to attain a description of this range. The same will be described in the following section 2.4.

### Sensitivity area

In this area the performance of the probe is evaluated according to its sensitivity, i.e., the ability of the probe system to detect perturbations or agents, inside the sensibility range, that make to changes in the probe's response. By perturbations or agents we mean changes in the composition or structure of the MUT.

### 2.3.3 The parameters describing the performance

In order to evaluate the performance of the probe in the previously cited areas, performance parameters are defined as elements carrying out in one or more performance areas.

A list of the most spread parameters is:

- Maximum frequency limit
- Minimum frequency limit
- Precision
- Admittance accuracy
- Permittivity accuracy
- Sensibility Depth
- Sensitivity or spatial resolution

### 2.3.4 Maximum frequency limit

The maximum operative frequency will be conditioned by the dimensions of the coaxial line and considerations of simplifying nature regarding the modes in play and the radiation disregard. There are aperture admittance models that can take into consideration also high-order modes to increase the overall accuracy of the model. The coaxial line operates in TEM mode and does not support the propagation of higher order modes so the excited modes at the aperture discontinuity are evanescent in the coaxial line and its contribution to the energy balance needs to be considered for increasing the overall accuracy of the model. A single TEM mode operation is achieved when the frequency operation is conditioned by the TEM-mode cut-off frequency in a coaxial line.

If apart from that it is desired to ignore the radiation effects, the conductance

of the aperture should be neglected and that occurs for frequencies smaller than this following frequency:

$$f_m = \frac{20}{(b-a)\sqrt{\epsilon_r}} [\text{MHz}] \quad (2.3.1)$$

The above expression was extracted from the Levine & Papas expression (6.7) in [44] at the low frequency limit, i.e., when the propagation phase constant ( $k$ ) is much more smaller than the reciprocal of  $a$  (see also [37, 47, 53]), and, as suggested by Otto *et al.* in [54], when the wavelength of the sample is much bigger than the aperture of the coaxial probe, i.e.,  $\lambda_m > 15(b-a)$ .

### 2.3.5 Minimum frequency limit

At low frequencies material measurements can become less accurate due to the physical quantity used by the measurement method in question as an intermediate quantity, directly measured, in an indirect measurement context. If the material measurement is based on the method that uses the determination of the complex reflection coefficient Gamma ( $\Gamma$ ) as the intermediate quantity, the measurement accuracy is compromised at low frequencies.<sup>1</sup>

In the following we give an illustration of the Gamma-based measurement method problem. We illustrate focusing on network analyzers since they operate on the Gamma determination principle.

The accuracy of the network analyzer is expressed as a certain percentage of Gamma, both magnitude and phase. As shown in the sketch (a) of figure 2.3.1, the measured reflection coefficient Gamma corresponds to the complex permittivity of the measurement material. In other words, there is a bidirectional mapping of the complex permittivity, epsilon sub r ( $\epsilon_r$ ), and the reflection coefficient, Gamma ( $\Gamma$ ). This illuminates how a polar display of Gamma is transformed into values of the real part of the complex permittivity ( $\epsilon_r'$ ) and loss tangent ( $\tan(\delta)$ ), i.e., the complex permittivity ( $\epsilon_r$ ). The

<sup>1</sup>This knowledge was extracted from the Agilent forum:  
<https://forums.tm.agilent.com/community/>

figure below presents the mapping of the complex permittivity ( $\epsilon_r$ ) of the material into a polar reflection coefficient plot for two frequencies, 200 MHz and 2.45 GHz. The 200 MHz plot (sketch (b) of figure 2.3.1) depicts a random Gamma vector and on the tip of the vector, there is a circle, representing the uncertainty (not to scale). Compare the display at 200 MHz and 2.45 GHz (sketch (c) in figure 2.3.1). At 200 MHz, a wide range of complex permittivity, from 1 to 100 for the real part ( $\epsilon_r'$ ) of the complex permittivity and from 0 to 2 for the loss tangent ( $\tan(\delta)$ ) is compressed into a small area of the polar plot. This implies that a small percentage uncertainty for measuring reflection coefficient now becomes a large percentage error for real part of permittivity and loss tangent. The complex permittivity error at 200 MHz is much larger than the error at higher frequencies. This explains the start (low) frequency limitations on the probe.

Contrary to what happen with network analyzer, impedance analyzers operate on different principles. They measure impedance directly via an RF-IV methodology. The RF-IV based impedance analyzers do not measure reflection coefficient Gamma. Thus they are able to produce better results at low frequencies than the network analyzer. Impedance analyzers do not exhibit the same advantage at higher frequencies.

### 2.3.6 Precision

The precision parameter gives information on the uncertainty of the measurement and is calculated with an uncertainty analysis performed to the probe. Well-characterized uncertainties are mandatory for trustable measurement [51]. For accomplishing it, identification and evaluation of the factors affecting the uncertainty of the measured permittivity are crucial.

Usually the uncertainty factors can be some of the ones listed here:

1. Magnitude of the measured complex reflection coefficient
2. Phase of the measured complex reflection coefficient

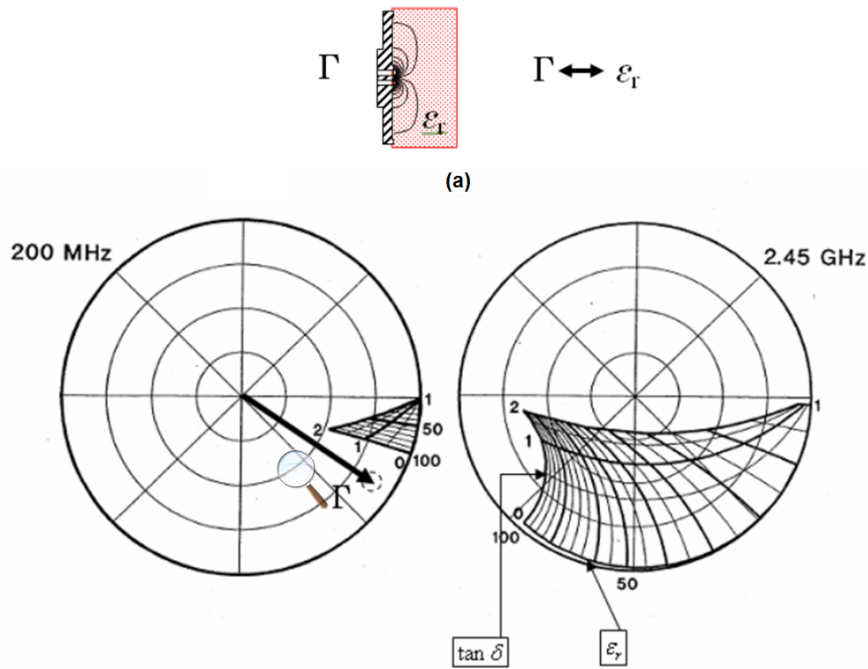


**Figure 2.3.1:** Illustration of the low frequency limitation of an open-ended coaxial probe. In (a) a mapping sketch of Gamma and epsilon. In (b) a polar reflection coefficient plot at a low frequency (200 MHz). In (c) a polar reflection coefficient plot at a medium frequency (2.45 GHz).

3. Permittivity of dielectric filler
4. Operating frequency
5. Outer conductor diameter ( $2b$ )
6. Inner conductor diameter ( $2a$ )
7. Parameters of soft models

Additional factors can be included if new conditions are included to the probe system. The above given factors are enough for characterizing the uncertainty of an homogeneous material. For composite materials, where the composition and structure are introduced in the MUT's completeness, new factors

appear, as for example, the uncertainty factors related to the dimension and permittivity value of each constituent according to the problem's type. In problems where the temperature is also included, this is also added as a new uncertainty factor.

The previously enlisted factors are used according to the problem type and models assumptions. The mandatory factors are the measured complex reflection coefficient uncertainty, both magnitude (point 1) and phase (point 2), together with the dielectric filler permittivity uncertainty (point 3) and the operating frequency (point 4).

Points from 5 to 7 are chosen according to the model's assumptions. If the model is one of the hard type (see chapter 3), knowledge on the dimensions of the probe are needed and consequently an uncertainty analysis of those needs to be performed and considered. Soft models require the uncertainty produced by the parameters to be considered too.

For calculating the uncertainty of a given problem a worse-case differential uncertainty analysis is considered assuming no cross-correlation. In this case, only the complex reflection coefficient is considered, since other uncertainty are negligible due to the fact that their combinations result in less uncertain responses. The expression for the real part of the complex permittivity to carry out the analysis is:

$$\Delta\epsilon'_{rm} = \sqrt{\left(\frac{\partial\epsilon'_{rm}}{\partial|\Gamma_m|}\Delta|\Gamma_m|\right)^2 + \left(\frac{\partial\epsilon'_{rm}}{\partial\theta_m}\Delta\theta_m\right)^2} \quad (2.3.2)$$

A similar equation can be written for the imaginary part of the complex permittivity  $\epsilon''_{rm}$ . Implicit differentiation can be used to find the necessary derivatives. The aperture admittance models need to be considered at this point for the derivatives calculation. Some derivatives examples are given by Baker-Jarvis *et al.* in [55].

### 2.3.7 Admittance and permittivity accuracies

Since the complex permittivity is an intrinsic parameter of the medium, the knowledge regarding the exactness of its value is conditioned by the accuracy

of the models used for its study, i.e., the ability of these to give a trustable value. The models gives a bidirectional mapping between this intrinsic parameter and an extrinsic parameter as for example the reflection coefficient at the probe's aperture that can be easily achieved to measure with the available methods.

As we considered and discussed previously, we can think about the *admittance accuracy* as usable only for the cases in which the extrinsic parameter for both models, the object and the reference, is the same. Otherwise the *permittivity accuracy* is recommendable to use.

Consequently what is recommendable to do is to characterize the accuracy of the most accurate aperture admittance model (object model) with a *permittivity accuracy* approach, comparing the permittivity extracted with the object model to the one extracted with the reference model. The reference model use a different methodology and is considered more accurate. Resonant methods as the resonant-cavity techniques can be used as reference models as known to be the most accurate of all.

Once the most accurate aperture admittance model is identified and its accuracy evaluated, it can serve as a reference for other aperture admittance models and the *admittance accuracy* approach can be used.

The accuracy of the model in question is then studied by evaluating this model with the reference, in their response (extrinsic parameter evaluation) when subjected to the same input (intrinsic parameter).

### 2.3.8 Sensibility Depth

The sensibility depth is a parameter that gives information about the sensibility range of the probe. Its value indicates the distance, from the probe's aperture, toward the half-space where the material is placed, where the probe turns itself insensible to structural or compositional changes in the material, i.e., no changes in material after that range are detected by the probe.

Following this information some researchers along these last decades have

found that the *sensibility depth* can be interpreted as:

1. the sample thickness at which the effective permittivity ( $\epsilon_{\text{eff}}$ ) in a two layered medium agrees with this following expression:<sup>2</sup>

$$(\epsilon_{\text{eff}} - \epsilon_2) = 0.98 (\epsilon_1 - \epsilon_2) \quad (2.3.3)$$

2. the sample thickness large enough with respect to the outer radius of the probe so as to consider the sample as "infinitely thick".<sup>4</sup>
3. the sample thickness large enough as for the magnitude to be at least two orders of magnitude smaller behind the sample that at the interface (aperture plane) with the coaxial line [37].

Following the first interpretation, one can suppose that the permittivity of the back-layer does not influence the measured permittivity when the thickness of the first layer is larger than the sensitivity depth. The measured permittivity will be lower (or higher) than the true permittivity of the layer when the thickness of the layer is lower than the sensitivity depth, if an infinite two-layer sample is assumed in the calculations. This is in agreement with what happens in reality and will be discussed more in detail in the chapter 4 when introducing the effective medium theory to this technique.

Following the second and third interpretations it is found that the active area of the probe (*sensibility range*) is approximately twice the dielectric diameter of the probe (*4 times b*).

---

<sup>2</sup>Definition given by Folgeroe *et al.* in [56] and taken from a parallel capacitive homogenization model.<sup>3</sup>  $\epsilon_1$  and  $\epsilon_2$  are the permittivities of each constituent of the material. "0.98" is an empirical value found by these authors.

<sup>4</sup>Interpretation given by Anderson *et al.* and Fan *et al.* in [57, 58]. Their interpretations was found to be independent of the permittivity of the sample and of the frequency when the radiation from the probes is negligible.

### 2.3.9 Sensitivity or spatial resolution

The *Sensitivity* or spatial resolution is a parameter for evaluating the performance of the probe along the *Sensitivity* area that accounts for how sensitive the probe is inside its *Sensibility Range* to resolve small elements that compound the material.

According to that definition one can redefine the *Sensitivity* parameter as the minimum dimensions of an element inside the *Sensibility range* to be detectable by the probe.

A simulation study conducted to evaluate the *Sensitivity* of the probe throws like an estimation that air brick elements whose thicknesses are smaller than 1 micrometer, or whose section is less than a quarter of the square of the inner radius ( $a^2$ ), can be neglected.

## 2.4 Simulation study for sensibility range and sensitivity

A simulation study was carried out with the assistance of a commercial electromagnetic simulator (CST Microwave Studio, [52]) to evaluate the probe performance in relation to the *Sensibility Range* area and its *Sensitivity*. The evaluation consisted in several simulations of the probe connected to a MUT (Methanol modeled by Cole-Cole relaxation model) at a range of frequency that goes from 500 MHz to 15 GHz. In each simulation, the MUT acted as a host material for an air element with a brick-shape that was placed at a different position for every simulation. The position of the air element was chosen as relative to the center of the inner conductor at the probe's aperture plane. The dimensions and position of the brick were varied according to the performance test to do. For evaluating the *Sensibility Range* a brick with fixed dimensions, smaller than the inner conductor, but big enough for being detectable and with a variable position was considered. For evaluating

the *Sensitivity* a brick with variable dimensions but fixed in position was considered. The air brick element was approximated moved from the center of the aperture toward the flange side. Simulations where the brick moves normally to the aperture's plane were not considered because of spherical symmetry with respect to the inner conductor.

The simulations conducted to evaluate the *Sensitivity Range* took as a reference the scattering parameter  $S_{11}$  at the probe's aperture for the absence of the brick and the spherical boundary was identified as the position at which the  $S_{11}$  parameter changes considerably its magnitude.

The simulations conducted to evaluate the *Sensitivity* took as a reference the scattering parameter  $S_{11}$  at the probe's aperture for the absence of the brick and the smallest detectable element was identified as the minimal element size at which the  $S_{11}$  parameter changes considerably its magnitude.

In all the cases by a "considerable change" it was meant a 10% change.

The result of the set of simulations helped to define the *Sensitivity Range* as a space with a half sphere shape. The radius of the sphere was found to be about 3 times the outer radius of the inner conductor ( $\approx 3a$ ) in order to keep the "Stuchly magnitude condition" [37]. This result, as maybe less conservative because of the 10% change consideration, is in agreement also with the second and third interpretation for the *Sensitivity Depth* discussed in the previous subsection.

A simulation study conducted to evaluate the *Sensitivity* of the probe throws as an estimation that an air brick elements whose thicknesses are smaller, less than 1 micrometer, or whose section is less than a quarter of the square of the inner radius ( $a^2$ ), can be neglected.

## 2.5 Conclusions

In this chapter the ideal probe was introduced together with a detailed description of each one of its parts and the functionality of each part, according

to the author's experience earned during the duration of the course.

The most important contribution of this chapter is in the performance study that was carried out to the probe's system. There the most important performance parameters were identified trying to order them in a formal way according to the bibliographical research and to the conducted analytical and numerical studies.

The importance of those resides in a better characterization of the probe's capability and of the measured material. This last is crucial because of the importance of more detailed information on the measurement uncertainty.

# Chapter 3

## Probe models and extraction schemes

### 3.1 Introduction

In this chapter the fruits of the bibliographical study together with maturation reached along the course are given concerning the probe's model and the extraction schemes utilized in the "open-ended coaxial-probe frequency-domain reflectometry" technique.

The probe models started, as it was mentioned in earlier chapters, with the introduction of the Levine & Papas model in the early 50's. Successive models started at the early 80's together with the extraction schemes since at that time the probe started to be considered as a material measurement tool, not only as an antenna and its technology was object of several transformation along these three decades.

This chapter will give the readers the basic notions of probe models and extraction schemes and will introduce them to the various alternatives to do the best use of the probe according to the problem requirement in object.

The classification of the probes in hard and soft is introduced in response to the model functionality in the measurement system context. The same is done for the extraction schemes in robust and modular.

Finally, as permittivity optimization schemes, two Point-Matching methods are introduced: the simplex and gradient methods. They were elaborated as part of the permittivity extraction technique in the early period of the Ph.D. course. In this same period a Particle Swarm Optimization (PSO) scheme was employed as an alternative technique in collaboration with others researchers.

## 3.2 Probe models

### 3.2.1 Introduction

In this section the probe models are introduced. First a descriptive classification of each one of its features is given so as to help in the models selection. Then a classification is done, principally into two main classes, the hard and soft models.

### 3.2.2 The probe models

#### Introduction

The conducted bibliographical research threw a significant quantity of available models, each one of them with defined features that highlight them with respect to others.

The models that are emphasized here are aperture admittance models, that represent a bidirectional mapping between the aperture admittance, i.e. the admittance at the aperture plane, and the complex permittivity of the material under test (MUT). The aperture admittance is easily related to the complex reflection coefficient through the transmission line theory.

According to the models assumptions regarding the material, the referred permittivity can represent the real permittivity of the MUT or an effective permittivity of the MUT. Effective permittivity will require the use of effective dielectric models to map it with the parameters that that model owns,

that may refer to the structure and composition of the material.

In this subsection we are introducing the most diffused models with a brief detail in their functionality.

### The ideal open transmission line

Before introducing the probe models, as a starting point, the concept of ideally open transmission line is introduced here. This is also done to give the readers the association of the probe behavior with that of an ideally open coaxial line to help in the understanding of the probe limitation and behavior.

The open-ended coaxial probe approximates an ideally open transmission line, even more if the MUT is a lossless low-permittivity material. This is also a reason why this technique is not appropriate when this kind of material is measured.

The boarding effect can be seen as a representation of the separation to this ideal condition and does to its resolution. In fact, the boarding effect is what makes to the usefulness of the technique as it allows the resolution of different cases of MUT.

An ideally open coaxial line section has this expression:

$$Y_{in} = iY_0 \tan [2\pi f \sqrt{\mu\epsilon} l] \quad (3.2.1)$$

where  $\mu$  and  $\epsilon$  are the intrinsic parameters of the coaxial filler,  $l$  is the length of the coaxial line section,  $f$  the operating frequency and  $Y_0$  is the characteristic impedance of the line.

At the aperture plane, ideally the admittance should be zero. If the admittance, there, is not null, then the boarding field are the responsible giving the impression of an even more extended line that can be modeled with the above expression (eq. 3.2.1) [59]. This interpretation is then taken for the virtual line model introduced later in this section.

**List of most diffused probe models**

A list of the most diffused probe mode is the following list:

- Single-layer linear capacitive model [60, 61, 15]
- Single-layer radiation model [47, 62, 15]
- Single-layer non-linear capacitive model [63]
- Single-layer virtual line model [15]
- Single-layer rational function model [15]
- Single-layer quasi-static model [64]
- Single-layer full-wave model [44]
- Two-layers capacitive model [65]
- Two-layers quasi-static model [58, 56]
- Two-layers full-wave model [66]
- Three-layers full-wave model [55]
- N-layers full-wave model [67, 68]

Note: soft and hard models are two class of models that are going to be introduced later in section 3.2.3.

**Single-layer linear capacitive model [60, 61, 15]**

This soft model is an equivalent-circuit empirical model with two capacitors in a parallel connection for a single-layer MUT. An introductory description is given by Chen *et al.* in [15, Capacitance model - sec. 3.2.1.1]. Since in this model the admittance is purely reactive, the conductance seen at the aperture has to be insignificant, so it is valid for low microwave frequencies (See 2.3.4).

**Single-layer radiation model [47, 62, 15]**

This soft model is an equivalent-circuit empirical model with two capacitors and a conductance in a parallel connection for a single-layer MUT. An introductory description is given by Chen *et al.* in [15, Radiation model - sec. 3.2.1.1]. In this model the admittance is complex, both active and reactive parts are present and its validity is extended more in frequency than the previous one. This is based on the early work of Gajda, in reference [47, 62], and has been mostly applied to biological materials.

**Single-layer non-linear capacitive model [63]**

This soft model is an equivalent-circuit empirical model with three capacitors in a parallel connection for a single-layer MUT. An introductory description is given by Gajda & Stuchly in [63]. Since in this model the admittance is purely reactive, the conductance seen at the aperture has to be insignificant, so it is valid for low microwave frequencies only (See section 2.3.4). This model is more accurate than the linear capacitive model because of the introduction of the third capacitance, so as to match better the non-linearities of the boarding field.

**Single-layer virtual line model [15]**

This soft model is an empirical model representing an equivalent line accounting for what is seen from the aperture out when a single-layer MUT is used. An introductory description is given by Chen *et al.* in [15]. Since in this model the admittance is purely reactive, the conductance seen at the aperture has to be insignificant, so it is valid for low microwave frequencies only (See 2.3.4). This model can compete with the non-linear capacitive model because it is also a non-linear model for the permittivity of the MUT and uses a parameter less (just the probe and virtual line lengths,  $D$  and  $L$ , respectively).

**Single-layer rational function model [15]**

This soft model is an empirical model representing a rational function with a large number of parameter, N in the numerator and M in the denominator. An introductory description is given by Chen *et al.* in [15, Rational function model - sec. 3.2.1.1]. In this model the admittance is complex, so both active and reactive parts are considered and the model can accomplish a good fit with hard full-wave models.

**Single-layer quasi-static model [64]**

This hard model is quasi-static model for a single-layer MUT. An analytical close-form mathematical expression is given by Misra in [64, sec.II]. Since in this model the admittance is purely reactive, the conductance seen at the aperture has to be insignificant, so it is valid for low microwave frequencies only (See 2.3.4).

**Single-layer full-wave model [44]**

This hard model is a full-wave model for a single-layer MUT. A non-close-form mathematical expression is given by Levine & Papas in [44]. In this model the admittance is complex, both active and reactive parts are considered and can accounts also for higher-order modes (The higher-order modes expressions can be identified in the article [44], previously to the introduction of the fundamental mode in eq. (6.1)).

**Two-layers quasi-static model [58, 56]**

This hard model is a quasi-static model for a two-layers MUT that accounts for a two capacitance equivalent-circuit expression. An introductory description is given by Fan *et al.* in [58] and also in [56, sec.2.2]. In this model the capacitances are calculated with an electrostatic approach and a two-layers material is considered so the first capacitance account for the capacitances effect described in the *linear capacitance* and *tadiation* models. Works well for

low-loss materials with real dielectric constants of " $< 25$ " but it was found that can underestimate the permittivity of semi-infinite samples by about 20% as demonstrated in [56, sec. 4.2].

### **Two-layers capacitive model [65]**

This soft model is an empirical equivalent-circuit model with three capacitors in a parallel connection for a two-layers MUT. An introductory description is given by Chen *et al.* in [65]. This model was derived by a Schwarz Conformal transformation in complex function theory whose demonstration is found in [65, Appendix].

### **Two-layers full-wave model [66]**

This hard model is one of the full-wave types. An analytical close-form mathematical expression is given by Li *et al.* in [66]. It assumes a two-layers lossy MUT with a flanged probe and can also account for higher-order modes.

### **Three-layers full-wave model [55]**

This hard model is one of the full-wave types. A non-close-form mathematical expression is given by Baker-Jarvis *et al.* in [55, sec.II-C]. It assumes a three-layers MUT and can account for the higher-order modes. This model is practical for many applications according to its three layers assumption. It can estimate the permittivity of a liquid layer with high accuracy for frequencies below 10 GHz provided that the layers thickness is known and takes into account of the reflections in the liquid layer. However, the computation time is long.

### **N-layers full-wave model [67, 68]**

This hard model is one of the full-wave types. There were found two non-close-form mathematical expression. One given by Bakhtiari *et al.* in [68, 15] and the other by De Langhe *et al.* in [67]. Both of them assume a multi-layer MUT

and can account for the higher-order modes. The Bakhtiari's expression was found easier to work with for more than two layers. This model is practical for many applications according to its multi-layer assumption.

### 3.2.3 Classification of the probe models

The probe models represent a bidirectional mapping between the aperture admittance, i.e. the admittance at the aperture plane, and the complex permittivity of the material under test (MUT). The mapping is formally represented by a mathematical expression. This expression can have or not a *closed analytical* form,<sup>1</sup> and can be composed by variables and parameters that are considered independent from other elements in the model (other variables, parameters, etc.). The variables usually are the complex permittivity and the frequency for the type of aperture models treated in this work under the dielectric material assumption. The parameters can be of two types: *setting* (or *soft*) or *analysis* (or *hard*).<sup>2</sup> The *setting* parameters are those needed for optimizing the model. In the single-layer capacitive model, they are the empirical parameters, the  $C_0$  and  $C_f$  in [15, Capacitance model - sec. 3.2.1.1]. The *analysis* parameters are those needed for analyzing or evaluating the model with a given set of input variables. In the single-layer full-wave model, they are the geometrical and physical parameter  $a$ ,  $b$  and  $\epsilon_{rc}$  (Permittivity of the dielectric filler).

Models needing to be optimized, to fit best the experimental data before being employed for the extraction, are usually models that are empirical,

---

<sup>1</sup>When referred to a mathematical expression, by *analytical* it is understood an expression constructed using well-known operations that lend themselves readily to calculation. By *close* it is understood an analytical expression that is given in terms of a bounded number of certain *well-known* functions. Typically, these well-known functions are defined to be elementary functions: constants, one variable  $x$ , elementary operations of arithmetic ( $+$ ,  $-$ ,  $\times$ ,  $\div$ ),  $n$ th roots, exponent and logarithm (which thus also include trigonometric functions and inverse trigonometric functions). Learned from [69].

<sup>2</sup>This parameter classification is introduced by the author and is useful to distinguish between soft and hard models.

optimizable (or fittable). A new denomination for them, according to their function in the measurement system, is *soft*. The importance of this type of models will emerge later when introducing the extraction schemes.

Not all the models need to be optimized. Only soft models do. The rest are denominated hard models. Hard models possess the hard parameters (analysis parameters) whose only function is to allow the model evaluation, i.e. the model's value calculation under an input set conformed from the complex permittivity and frequency.

In conclusion, a new classification of the aperture admittance models according to the need or not to be optimized is introduced here, leading to distinguish between soft and hard models.

In the following subsections the features of each type of model is given.

### 3.2.4 Features of hard models

The principal features of hard models are:

- Hard evaluation:
  - No direct inverse form,
  - Computationally expensive,
  - More time consuming,
  - Impractical for on-line systems;
- Offer more capability to the measurement system:
  - Wider frequency range,
  - More accuracy,
  - No need of known material reference;
- Useful for studying the probe:
  - Behavior under variation of probe (geometry, filler), MUT and frequency

- Performance of the probe features (Sensibility Depth, Sensitivity, Precision, etc.);
- Applications:
  - Permittivity extraction;
  - Soft model calibration;
  - probe design.

### 3.2.5 Discussion on features of hard models

#### Hard evaluation

For evaluation we understand the calculation of the model's value for a given input set. Since most of this model are given as non-closed-form expression or as analytical expression that are expensive to evaluate, we consider this type of model hard to evaluate. The most important consequences of this is that: 1) it would be difficult to achieve an inverse form to help in the extraction since a bounded algebraic expression is also hard to accomplish; 2) It would be impractical for on-line systems because of the time consuming and the computational resources.

#### Offer more capability to the measurement system

Most of these models are full-wave models so they can account for higher-order modes and their expressions represent complex admittances, that includes also the conductance. As a consequence of it, the widest frequency range and the best accuracy can be accomplished for the probe if also calibration and measurement system stability are satisfactory.

In addition, this kind of model don't need known material references.

#### Useful for studying the probe

These models can be used for studying the probe behavior while the geometry, the filler, the MUT and the frequency are varied. Also the probe perfor-

mance can be evaluated through its features (Sensibility Depth, Sensitivity, Precision, etc.).

### Applications

The most important applications are these following three:

Permittivity extraction: Through the use of the appropriate permittivity optimization scheme, the permittivity can be extracted. This is introduced in detail in the extraction scheme section.

Soft model calibration: For the optimization of soft models, the hard model, that will become the reference model in the optimization task, will need to have its parameters and variables predefined. The predefinition will consist of an input set of values for the complex permittivity and frequency variables according to the optimization requirements and of an input set of values for the parameters according to the reference model requirements (dimensions of the geometry and material of the probe).

probe design: In probe design some measurement specification can be given (material's assumptions, frequency of interest, etc.) and from them an estimation of the capacitances can be reached and those related to the probe geometry. This type of model is well suited for design of open-ended coaxial probes according to the Sensibility Range performance and to the apparent (effective) permittivity.

#### 3.2.6 Features of soft models

The principal features of soft models are:

- Easy evaluation:
  - Can have direct inverse form,
  - Computationally cheap,
  - Less time consuming,
  - Practical for on-line systems;

- Offer benefits to the measurement system;
- Applications: Permittivity extraction.

### 3.2.7 Discussion on features of soft models

#### Easy evaluation

For evaluation we understand the calculation of the model's value for a given input set. All these models are given as close analytical expressions that are of easy evaluation. The most important consequences of this is that: 1) it is easy, in some cases, to achieve an inverse form to help in the extraction; 2) it is practical for on-line systems because of the time consuming and the computational resources are much less than in hard models.

#### Offered benefits to the measurement system

The contribution in benefit for the measurement system when using soft models is mostly the embeddability<sup>3</sup>. This type of models, as it will be seen in the section dedicated to extraction schemes, can be ensembled with other models and this can reduce the number of parameters to fit. Also this includes the calibration.<sup>4</sup> In this way the overall system can be described by a close algebraic expression, that is easily invertible or where the extraction of the permittivity is accomplished easier than for hard models. Another advantage of the embeddability is that the model is improvable, i.e. it can learn, for example, from the reference model or material and this is used for improving the performance of the model and of the measurement system.

The disadvantages are that it needs references for the model optimization and these references can be known materials or more accurate models, specially hard models.

---

<sup>3</sup>the ability to be embedded

<sup>4</sup>An example of this is found in [56, sec. 2.1]. There, the linear capacitance model and the two-port error model are combined to give a new model for the permittivity (estimated) with only two model parameters of the soft type.

### **Applications: permittivity extraction**

Through the use of the appropriate permittivity optimization scheme, the permittivity can be extracted. This is introduced in detail in the extraction scheme section.

#### **3.2.8 Conclusions**

In this section the results of the bibliographical research referred to the probe model were presented. They consist in that there is a vast quantity of models from single to multi-layers, from lumped-elements to full-wave, from close to not close form in mathematical expression. All this research allowed to introduce a new classification in soft or hard models according to whether the model require to be optimized or not. This classification has been found to be useful since it allows a new interpretation of the extraction schemes as it will be seen in the following section.

## **3.3 Extraction schemes**

### **3.3.1 Introduction**

The mechanism or procedure for obtaining the complex permittivity from the measured data is described by the extraction scheme. In this section we aim to describe the most important parts of the extraction scheme, the features they have, the classification and their impact on the measurement system. To that purpose we start with a description of the features that an extraction scheme should have, the main elements and the type of extraction schemes. To finish, two permittivity optimization methods are presented in detail. The first one, the Point-Matching method, that was developed by the author during the first year of the Ph.D. course with its two variants: simplex and gradient. The second and last one, the PSO method, that was also developed in collaboration with other researchers.

### 3.3.2 Descriptive features of an extraction scheme

#### Introduction

In order to compare different extraction schemes some features to compare are needed. In this subsection we aim to present the most important features that describe the extraction scheme performance and that help to the appropriate selection according to the application in question.

The most important features to take into consideration are:

- modularity
- internal embedding
- robustness
- speed
- accuracy
- computational cost

All these above features are in their majority given by the probe model.

#### Modularity

By modularity it is understood the feature of the extraction scheme that accounts for its ability to be divisible in modules or parts, each one of them with the following characteristics: 1)independent on each other; 2)specific function definable; 3)interchangeable with other modules of same type.

The degree with which these above presented characteristic is filled does to the modularity degree of the scheme.

This modularity concept requires that a module's type definition is presented to make effective the division of the scheme in areas (type) to be occupied by module of that type.

Following this concept we can define the following module's type:

- aperture admittance type
- effective dielectric type
- calibration type
- dispersion type
- temperature type

All these module's type are modular since all fulfill the above mentioned characteristics of independence, function definable and interchangeableness.

### **Internal embedding**

By internal embedding is understood the feature of the extraction scheme that accounts for the ability of the modules or parts to embed themselves with other type of modules resulting in a reduction of the overall model's parameters.

The more embeddable is the scheme, the more types of module can integrate in a unitary expression with a reduction in its overall model's parameters. It is desirable the integration in a unitary expression for reason that does to the simplification of the extraction. I.e. an scheme with a good embeddable degree will have all its type's of module integrated in a single expression.

Usually most of the module's type are embeddable modules, with the exception of some of the probe module. Some hard models, the ones that are in a not close nor analytic form expression, are no easily embeddable with other modules, since their integration, will not reduce the number of parameters nor simplify the expression and, contrarily, can increase.

### **Robustness**

By robustness is understood the feature of the extraction scheme that accounts for the ability of to withstand accurate results with the minimum of reference and for a spread range of conditions.

This is a special characteristic of hard models that are of robust nature.

**Speed**

By speed is understood the feature of the extraction scheme that accounts for the ability to accomplish the extraction with rapidness keeping a reference accuracy.

This is a special characteristic of soft models that are fast for nature.

**Accuracy**

By accuracy is understood the feature of the extraction scheme that accounts for the ability to accomplish the extraction with accuracy at a given time or general condition.

This is a special characteristic of hard models that are of robust nature. But soft models can improve the overall accuracy of the system with appropriate reference and conditions. By that we mean that in soft models, their parameters, when calibrated with a hard model, they can learn a percentage of the hard model potential, like a heritage.

**Computational cost**

By computational cost is understood the feature of the extraction scheme that accounts for the ability to accomplish the extraction with low computational cost.

This is a special characteristic of soft models that are of reduced complexity and whose embedding nature contribute to the overall reduction of the scheme.

**3.3.3 Main elements of parameter estimation procedure**

The parameter estimation procedure is the procedure that allows to estimate the intrinsic parameter, in this case the complex permittivity, from the measured extrinsic parameter, in this case the complex reflection coefficient at the appropriate reference plane.

According to how this procedure is structured, there are principally two type of extraction scheme perfectly distinguished between them. They are the *robust* and *embeddable* schemes. Their names were suggested according to their principal functions.

The robust scheme is a tough, robust, time-consuming and accurate scheme. The embeddable scheme is soft, flexible and fast scheme. Their principal characteristic they get from the probe model to be hard for the robust scheme or to be soft for the embeddable scheme.

Each one of these scheme has its extraction procedure divided into two main parts. For the robust extraction scheme, the first part is the calibration and the second one is the hard permittivity optimization. For the embeddable extraction scheme, the first part is the model optimization and the second one is the soft permittivity optimization.

### Calibration

The calibration, the first part of the robust scheme, is the calibration procedure to move the measurement reference plane from the entrance of the network analyzer to the aperture of the probe (interface between probe and MUT). To achieve it a standard one-port calibration is performed with three calibration standards that usually model the three extreme behaviors of ideally open, ideally short and perfectly matching load. This calibration can be accomplished following two paths according to the availability of standards and resources.

The first path is divided into two stages. The first stage carries the reference plane not to the aperture but to the opposite extreme of the probe. This will be easy to achieve with the standard multi-purpose calibration kit. After that, the second stage carries the reference plane to the aperture through a phase correction carried out using a transmission line section model with its length characterized. The probe section length can be known from fabrication or can be measured by the use of a known reference MUT.

The second path uses ad-hoc calibration standards used at the probe aper-

ture plane that is accessible as it is to the MUT. Here not reference nor knowledge of the probe section length is required for performing the calibration. What is hard to accomplish are good ad-hoc standards that performs acceptable calibration since the ad-hoc standards have to match perfectly the probe section and all the open, short and load standard present particular difficulties of design.

### Permittivity optimization

The permittivity optimization procedure is mostly used for estimating the permittivity from a probe model, being it hard or soft. Usually for hard models that are hard to evaluate, special optimization schemes are used. Here we mention two that were operated during the Ph.D. course: 1) the Point-Matching (PM) method and 2) the Particle Swarm Optimization (PSO) method. They are detailed in the following sections.

Soft models can also be optimized by the above mentioned methods but since usually they easily reach polynomials or they reach easily invertible functions, the permittivity can be estimated with the use of root finding algorithms and inversion procedures too.

In hard permittivity optimization, the previously performed calibration serves to input the measured aperture admittance to the hard model. After that the permittivity optimization procedure is carried out to the hard model with the input and the conditions that do to the probe configuration for estimating the permittivity.

In soft permittivity optimization, there is no previously performed calibration, since the calibration model (error network) is embedded to the soft model (together with other models responding to different module's type if present). This results in a new embedded model object to the model optimization. This type of optimization is carried out to improve the model functionality to the light of the measurement requirements. Once the model is optimized, it is ready for the soft permittivity optimization. The measured input is the reflection coefficient at the entrance of the network analyzer (or

other measurement device). This optimization can be carried out with the use of the hard permittivity optimization schemes, as PM or PSO, but due to the optimized model characteristic, it can be preferable to use other methods as root finding algorithms and inversion procedures.

### Model optimization

The model optimization procedure is mostly used for estimating the model's parameters from other reference as measurements data or a more accurate model.

The optimization requires an optimization strategy as the 2-norm (euclidean norm) or the 1-norm that represents an error function to minimize as a quality control tool to decide when an acceptable fit has been reached.<sup>5</sup> The optimization also requires an optimization method to decide how the model is evaluated according to the problem requirements and to the indicators inherent to the optimization method. The optimization procedure requires a number of experiments greater or equal than the number of unknown parameters to optimize. The experiments are the set of inputs and outputs well correlated that become the essential piece for the optimization and that establish an algebraic equation system to solve.

## 3.4 Point-Matching methods

The Point-Matching methods have their name due to their strategy to decide when the best fitting element have been found. That element represents the permittivity point in the complex permittivity domain that matches best the measured data point in question. This is a sort of optimization where the strategy is a 1-norm strategy of a single experiment, the measured point, and where the evolution of the search is done according to these two methods: simplex and gradient. The strategy takes into consideration the error tolerance that decides when the appropriate element has been found.

---

<sup>5</sup>For definition of traditional strategies see [70, pag. 6].

The simplex method establishes the evolution of the search in a very slow way. Two stages are identified. The first one is a bidirectional mapping of all the elements of the considered permittivity domain to all the elements of the aperture admittance domain that is carried out to keep trace of the link between elements in both sets. The second one is the identifying the elements most appropriate element according to the strategy's specifications.

The gradient method establishes the evolution of the search in a more fast way. Here no intensive bidirectional mapping is done but an initial element in the permittivity domain is chosen according to problem's specification and experience, and then a search based on the evolution of an admittance element linked to its counterpart in the permittivity domain is carried out until the strategy specification is fulfilled. The search methods here is a gradient method in the sense that 8 different directions are evaluated in the permittivity domain and its response on the admittance domain is observed and considered to decide how to evolve, i.e., which will be the next element considered closer to the measured admittance element.

In the following subsections both the simplex and the gradient point-matching methods are introduced with details in their algorithms and calculation procedure.

## 3.5 Simplex Point-Matching method

### 3.5.1 Introduction

The two stages mentioned in the introduction for the simplex method are a solution procedure to what is known as an inversion problem. The first stage, the mapping, is done by solving a forward or direct problem for each element of the permittivity domain.<sup>6</sup> The second stage is the error analysis, or separation analysis with the objective of finding the element with minimum error or separation to the measured admittance. This error analysis evaluates an

---

<sup>6</sup>For definition of direct and inverse problem see [70, pag. 2].

error function. From this analysis we take into consideration the value of  $\epsilon$  that has shown the best matching.

We will suppose that the measured aperture admittance ( $Y_{mi}$ ) was appropriately obtained from a measurement with a network analyzer with the needed calibration and Gamma-Y transformation (Gamma for reflection coefficient and Y for admittance) to elaborate it.

This is then the measurement data with which to create the error function. The other part of the function to complete its creation is the object function, i.e., the probe model.

The probe model considered here is the Levine & Papas model, a single-layer full-wave model but the definite version of it. We extract it from eq. (3) in [61]:

$$G = \frac{(Y_0\sqrt{\epsilon})}{\sqrt{\epsilon_C} \log(\frac{b}{a})} \int_0^{\frac{\pi}{2}} \frac{1}{\sin(\theta)} (J_0(k_0\sqrt{\epsilon}b \sin(\theta)) - J_0(k_0\sqrt{\epsilon}a \sin(\theta)))^2 d\theta \quad (3.5.1)$$

$$B = \frac{(Y_0\sqrt{\epsilon})}{\pi\sqrt{\epsilon_C} \log(\frac{b}{a})} (\int_0^\pi 2\text{Si}(k_0\sqrt{\epsilon(a^2 + b^2 - 2ab \cos(\theta))}) d\theta - \int_0^\pi \text{Si}(2k_0\sqrt{\epsilon}a \sin(\frac{\theta}{2})) d\theta - \int_0^\pi \text{Si}(2k_0\sqrt{\epsilon}b \sin(\frac{\theta}{2})) d\theta) \quad (3.5.2)$$

To evaluate  $G$  and  $B$  for every input set (permittivity and frequency) with the characteristics of the probe predefined (outer and inner radius) we use a numerical integration method or a series expansion representation.

To solve the inverse problem, we would use an error function. This error function will be defined, following the 1-norm strategy, as the sum of the absolute values of the distance in the real and imaginary parts between the measured admittance and the probe model admittance:

$$\text{Err}_G(\epsilon, f) = |\Re(Y_{mi}(f)) - G(\epsilon, f)| \quad (3.5.3)$$

$$\text{Err}_B(\epsilon, f) = |\Im(Y_{mi}(f)) - B(\epsilon, f)| \quad (3.5.4)$$

Such that:

$$\epsilon \in \mathbb{R} \wedge M \geq \epsilon \geq m \geq 1 \quad (3.5.5)$$

$$f \in \mathbb{R} \wedge N \geq f \geq n \quad (3.5.6)$$

The point of  $\epsilon$ , at constant  $f$ , where these error functions are minimal or null, is the point, value of  $\epsilon$ , that according to the adopted model would associate itself to the calculated admittance from the measured data and then to the same measure.

Since we are interested on the nulling or minimal value of both functions of errors  $Err_G$  and  $Err_B$ , an error function representing the sum of them is employed instead:

$$Err = Err_G + Err_B \quad (3.5.7)$$

From here it is possible with the same procedure to calculate a set of solutions ( $\epsilon_{sol}$ ), that match the measured value  $Y_{mi}$ . That would be the function  $\epsilon_{approx}(Y_{mi}(f))$ .

This is a discrete function where for each measured value from the admittance  $Y_{mi}$  at a given frequency  $f$  we made to correspond a permittivity,  $\epsilon$  with the better approximation.

Then with the set  $P$  of tern ( $\epsilon_{approx}^i, Y_{mi}^i, f_i$ ) it is possible to obtain a "best fitting function" that let to obtain an approximative generalization.

### 3.5.2 Simplex Point-Matching extraction procedure

A procedure describing the permittivity extraction with the Simplex Point-Matching extraction procedure is presented here. The procedure is illustrated with the help of a flow chart. This chart describes the algorithm with all the necessary parts to accomplish the extraction.

The flow chart is depicted in figure (3.5.1). There, the procedure starts with the START state. This state is the initial one and carries immediately to the DECLARATION state where all the registers (variables, arrays, etc.) are declared in memory. Once that task is accomplished, the control is passed to the next INITIALIZATION state that initialize the previously declared registers. Here the measured admittance data are loaded as a 1D array reg-

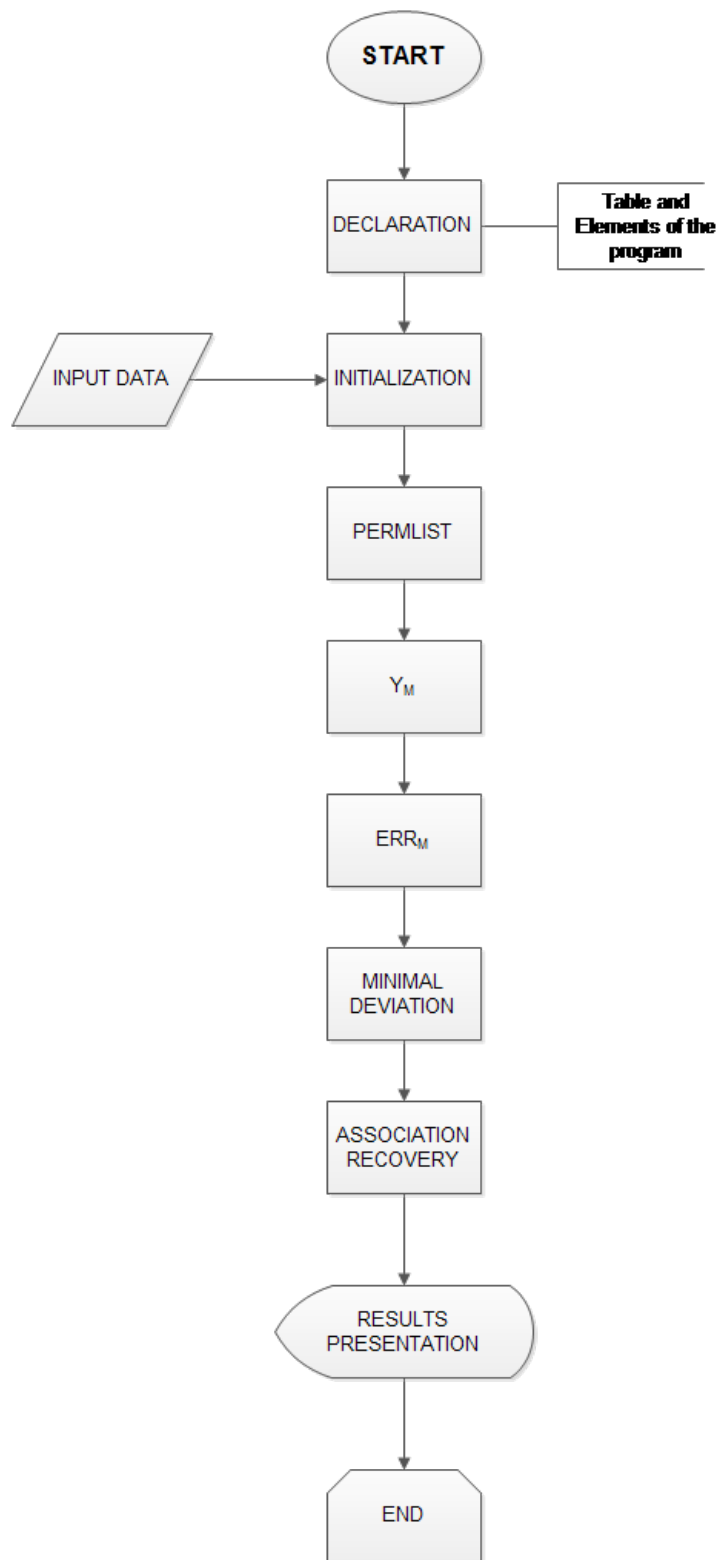


**Figure 3.5.1:** Flowchart of the algorithm for the Simplex Point-Matching Method Extraction.

ister with this index notation  $YE_j$  where the index  $j$  directs the attention to distinguish between the elements of the vector  $YE_j$  according to the frequency (each element of this register represents a different frequency). In addition to the initialization of that register, other variables are initialized as the information regarding the estimation of the permittivity, i.e., all the information that helps in reducing the computation area in the permittivity domain to define the working windows and the resolution. Once all this is accomplished the control is passed to the PERMLIST state. Here a 2D array, whose elements are the discrete points of the permittivity domain, is created making use of the information regarding the working windows and the resolution loaded in the previous state. This array is defined as a 2D one by this index notation  $\epsilon_{i,k}$  where the indexes  $i$  and  $k$  refer to the real and imaginary parts of the permittivity respectively. Once this array is created, the control is passed to the ASSOCIATION ( $Y_M$ ) state. In this state, making use of the previously created permittivity array ( $\epsilon_{i,k}$ ), a 3D array of association is created. The association meaning come of the association a particular admittance to a particular admittance through the mapping described by the probe model. This array is calculated using the probe model and its index notation is  $YM_{i,k,j}$  where the indexes  $i$ ,  $k$  and  $j$  correspond to the indexes of the real part of the permittivity, to the imaginary part of the permittivity and to the frequency, respectively. The relation of association is depicted in figure (a) of 3.5.2. Once the association array is created, the control is passed to the DEVIATION ( $Err_M$ ) state. In this state a 3D array of deviation is created with this index notation  $ErrM_{i,k,j}$  whose indexes are equal in meaning to the association array. This array is created as the deviation or separation between each element of the association array at a particular  $j$  (constant frequency) to each the correlated element in the admittance array as is depicted in figure (b) in 3.5.2. Once the deviation array is created, the control is passed to the MINIMAL DEVIATION state where a 1D array is created representing the minimal deviation for a constant frequency and its index notation is  $MinErrM_j$ . This array is calculated searching for the

minimum at a 2D level of the 3D array for a particular  $j$ . Once this array is created, the control is passed to the ASSOCIATION RECOVERY state. There, the deviation array is ranged to locate the elements ( $ErrM_{i_0,k_0,j}$ ) producing the minimal deviation at a particular  $j$ . The  $i_0$  and the  $k_0$  denote the values of the indexes  $i$  and  $k$  for the optimum element, i.e. the element with the minimum deviation. From the  $(i_0, k_0)$  coordinate it is possible to identify the associated permittivity ( $\epsilon_{i_0,k_0}$ ) to the minimal error.

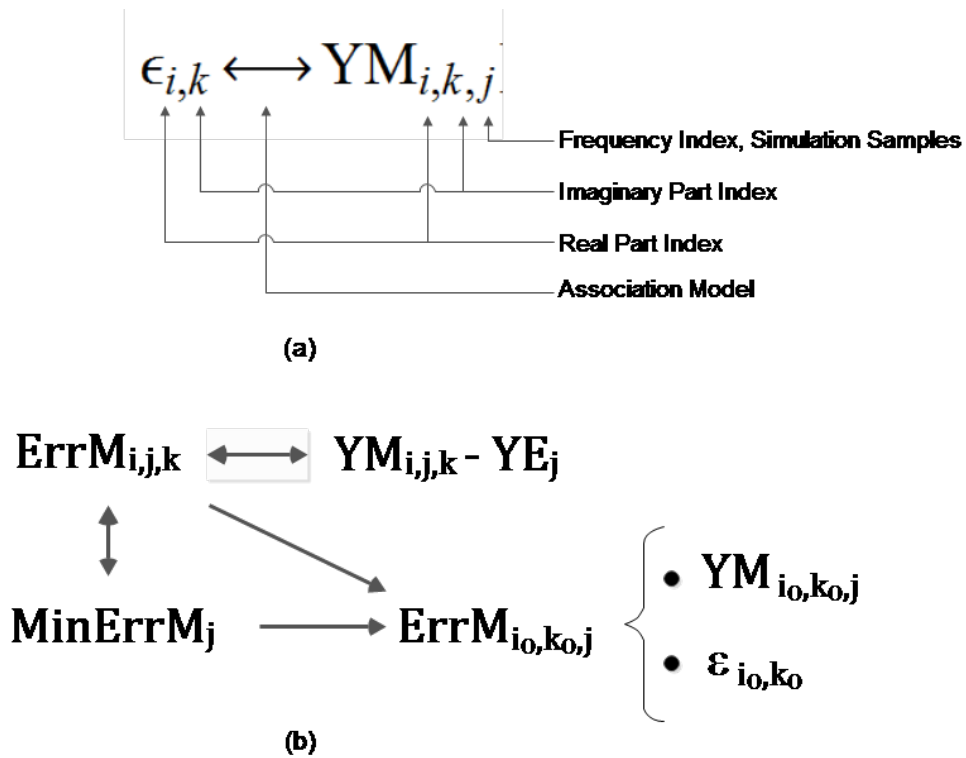


**Figure 3.5.2:** Table index nomenclature and definitions. In (a) the association relation between the permittivity elements in the Permlist table and the aperture admittance elements from the model ( $YM$ ). In (b) the error elements and the recovery of the permittivity associated to the minimal error ( $\epsilon_{i_0,k_0}$ ).

## 3.6 Gradient Point-Matching method

### 3.6.1 Introduction

In the simplex method, in order to do the estimation it was needed to create a permittivity table whose elements would be the domain of input data for the research defined by the analysis windows (minimal and maximum permittivity considered) and by the resolution (distance between elements). Then from this permittivity table the admittance table was created through the use of the apertura admittance model. The last step is to find from that admittance table, the element that approaches best the measured value. Since the association between the admittance elements and permittivity elements is kept, then it is possible to recovery the permittivity. So then the estimations end. In the gradient method, we don't calculate a permittivity table as we did in the previous method. We define the same analysis windows and we take decisions as how a movement in the permittivity plane affects in the admittance plane so to get closer to the measured value. In this way the estimation takes place.

### 3.6.2 Actual-Future procedure's description

This procedure is depicted in figure 3.6.1. In figure (a) of the initial state is shown, where  $\epsilon_0$  is the initial point in the permittivity domain to start the search. The separation vector  $\Delta Y_0$  is considered as a proximity indicator (proximity to the Measured Admittance  $Y_M$  in the admittance domain).

In figure (a) of The separation vector  $\Delta Y_0$  is considered as a proximity indicator (proximity to the Measured Admittance  $Y_M$ ).

Since a displacement in the Permittivity plane corresponds to an unknown displacement in the Admittance plane, we utilize a tester (searcher) vector to analyze in all the direction (usually 8 are considered), with normalized step (the magnitude of the movement is a fixed value), which is the response in

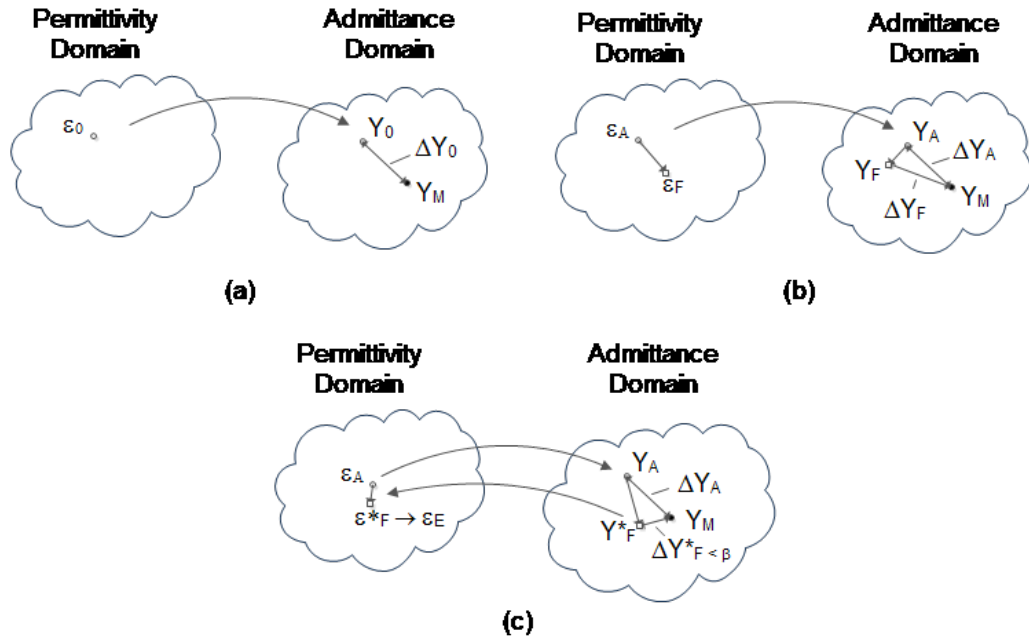


**Figure 3.6.1:** Permittivity and Admittance Domains to show Gradient Point-Matching search. In (a) it is shown the initial state. In (b) the searching procedure. In (c) the final step.

the Admittance plane using as indication of goodness the proximity indicator  $\Delta Y_0$ .

The starting point for every search step is called the Actual point denoted as  $\epsilon_A$  and  $Y_A$  in each plane respectively. The ending point for every search step is called the Future point and is denoted as  $\epsilon_F$  and  $Y_F$  in each plane respectively.

### 3.6.3 Actual-Future procedure's flowchart

In figure 3.6.2 is depicted the flow chart of the Actual-Future procedure for the gradient point-matching search method.

As it can be seen, there are 6 main states with internal and external actions. An internal action is an action that is done inside the state without a change of state and is depicted in the figure by an arrow that starts in that state

and finishes in the same state drawing a curve with a large curvature. An external action is an action that takes to a change of state and is depicted in the figure by an arrow that starts in that state and finishes in a different state.

The INITIAL state has defined two internal actions and five external actions and is the initial part of the program where declaration and initialization are carried out.

The internal actions are  $Y_0$  and  $M_0$ . The first one represents the determination of the initial starting point in the admittance plane and to accomplish that action needs to use an aperture admittance model (or probe model). The second one is the determination of the initial merit and to accomplish that action needs to determine the distance to the measured point (measured admittance data point) and evaluate it with respect to the reference minimal tolerance.

The external actions of the INITIAL state are the starting (the external call to give the control to this state), the download of the analyzing windows (AW), the download of the initial starting point in the permittivity plane ( $\epsilon_0$ ), the download of the object point in the Y-plane ( $Y_M$ ) and the upload of the merit and position data for the actual state evaluation.

For download and upload is understood the external action that takes (download) and gives (upload) data from and to the memory register according to each case.

When the INITIAL state upload the  $M_0$  data also gives the control to the ACTUAL state. This state is characterized by two internal actions and 8 external actions and is the operation center of the program where directives are given for decision on where to move and when the optimized position have been reached.

The internal actions are the evaluation of the initial or j-future merits to decide if the nearest allowed point have been reached (BMP? - best matching permittivity?) and the determination of the tester vector magnitude to generate the future states through the determination of 8 (eight) new  $\epsilon_j$  (TV).

The external actions are the download of the initial or j-future merits ( $M_j$  for  $j = 0, 1, \dots, j, 8$ ), and the upload of the merit verdict ( $OP = 1$  or  $0$ , as a decision “YES or NO” in the sense of having or not reached the most optimized point), of the 8 (eight) points valued as  $\epsilon_j$  to generate the J-FUTURE states, and pass to them the control, in case of a negative verdict ( $OP = 0$ ) and of the optimized position in case of positive verdict ( $OP = 1$ ) together to the control pass to the FINAL state.

The J-FUTURE states, for J ranging from 1 to 8, are the states created for evaluating where to place the future ACTUAL state and position and have the task of evaluating the position with respect to the measured admittance ( $Y_M$ ). These states also have associated three elements that are used for the merit verdict to identify which is the most performant J-FUTURE state to change the ACTUAL state at its position.

The internal actions of the J-FUTURE states are the determination of the position in the plane Y ( $Y_i$ ) for which task need to use the probe model and the determination of the merit ( $M_i$ ) for which task need to determinate the distance to the measured point ( $Y_M$ ) and to evaluate it with respect to the reference minimal tolerance.

The external actions of the J-FUTURE states are the download of the  $\epsilon_j$  points with which to determine the position and merit and the upload of the j-merit and j-position data ( $M_j$ ) for the evaluation that performs the ACTUAL state.

The FINAL state is the last state of the program with one internal and one external actions. The external action (OP) download the merit veredict when ( $OP = 1$ ) to take the control and to read the optimized position. Then it presents the result with the internal action P.

### 3.6.4 List of states

INITAL state:

- Internal Actions

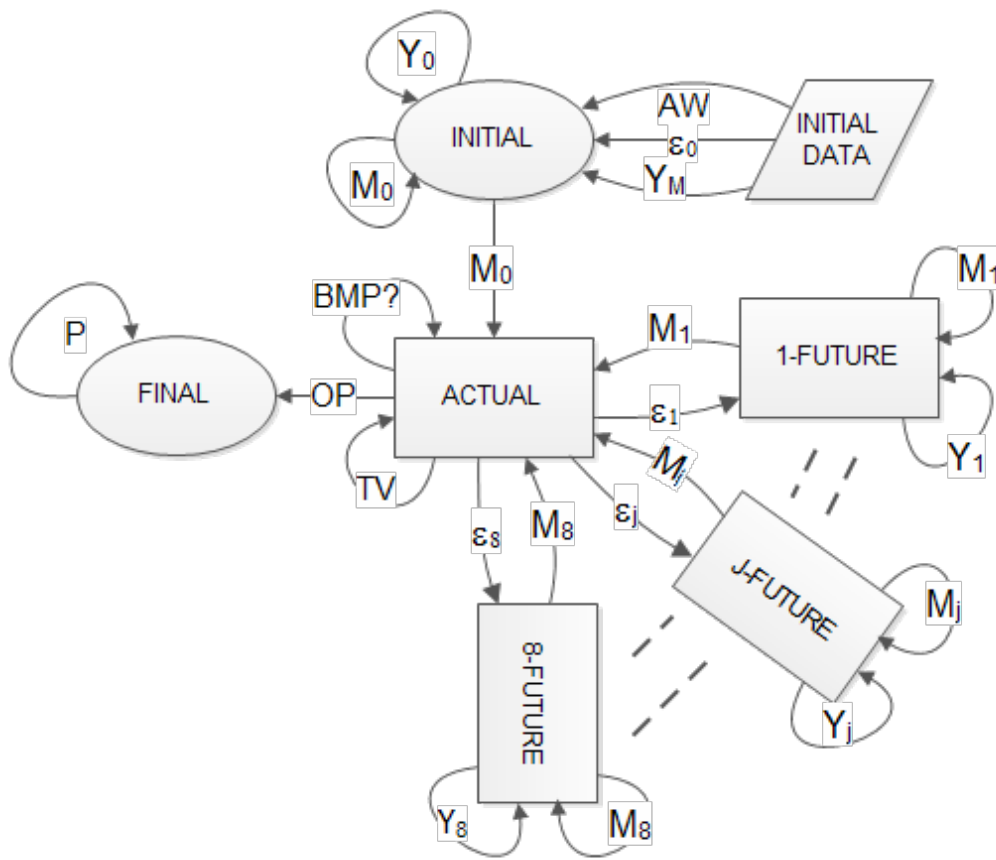


**Figure 3.6.2:** Flow chart of the Actual-Future Procedure for the Gradient Point-Matching Method.

- Determination initial starting point in admittance plane ( $Y_0$ ): Need to use admittance model.
- Determination initial Merit ( $M_0$ ): Need to determine distance to measure point and evaluate it with respect to the reference minimal tolerance.
- External Actions
  - Start
  - Download Analyzing windows (AW): Minimum and Maximum of

the real and imaginary part of the permittivity in which to make the search.

- Download initial starting point in permittivity plane ( $\epsilon_0$ ). Which is the content in Permittivity domain (Quadrant identification)? Initial assumptions regarding the problem's nature.
- Download object point in the Y-plane ( $Y_M$ ).
- Upload merit and position data ( $M_0$ ) for actual state evaluation.

ACTUAL state:

- Internal Actions
  - Evaluate initial or j-future merits to decide if the nearest allowed point have been reached (BMP? - best matching permittivity?)
  - Determine Tester vector magnitude to generate the future states through the determination of 8 new  $\epsilon_j$  (TV).
- External Actions
  - Download initial or j-future merits
  - Upload merit verdict as decision (YES or NO in the sense of having or not reached the optimized point)
  - Upload the 8 points valued as  $\epsilon_j$  to generate the j-future states in case of a negative verdict.
  - Upload the optimized position in case positive verdict.

j-FUTURE state:

- Elements
  - Position in plane  $\epsilon$  ( $\epsilon_i$ )
  - Position in plane Y ( $Y_i$ ).
  - Merit ( $M_i$ )

- Internal Actions
  - Determination of position in plane Y ( $Y_i$ ). Need to use admittance model.
  - Determination of Merit ( $M_i$ ). Need to determine distance to measure point and evaluate it with respect to the reference minimal tolerance.
- External Actions
  - Download  $\epsilon_j$  point
  - Upload j-merit and j-position data for actual state evaluation.

FINAL state:

- Internal Actions
  - Prepare and Present Result (P)
- External Actions
  - Download Optimized Position from Actual state in case of positive verdict (OP)
  - Finish

### 3.7 The PSO method

The particle swarm optimization (PSO) method is a metaheuristic<sup>7</sup> computational method that optimizes a problem by iteratively trying to improve a candidate

---

<sup>7</sup>“Ordinarily I would call the subfield stochastic optimization. But that is too general a term; it includes important algorithms like Markov Chain Monte Carlo (MCMC) or Gibbs Sampling, which are not in this category. Metaheuristics has lately been the term of use, but I think its profoundly misleading and weird. When I hear “metadiscussion” I think: a discussion about discussions. Likewise when I hear metaheuristic I think: a heuristic about (or for) heuristics. Thats not at all what these algorithms are about! Perhaps the lesser-used term black box optimization would be better, though it too comes with some

solution with regard to a given measure of quality. PSO optimizes a problem by having a population of candidate solutions (particles), and moving these particles around in the search-space according to simple mathematical formulae over the particle's position and velocity. Each particle's movement is influenced by its local best known position (its own flying experience - cognitive term) and is also guided toward the best known positions in the search-space (other swarm experience - social term), which are updated as better positions are found by other particles. This is expected to move the swarm toward the best solutions.

A PSO algorithm was implemented into two works [72, 73] during the Ph.D. course in collaboration with other researchers for the extraction of the parameters of three dispersion models (Havriliak-Negami, Cole-Cole and Debye) of the complex relative permittivity of dispersive materials.

The implemented algorithm was aimed to fit the aperture admittance unknown parameters (the dispersive parameters  $\epsilon_0$ ,  $\epsilon_\infty$ ,  $\tau$ ,  $\alpha$  and  $\beta_S$ ) to the experimental data (the measured aperture admittance). It was tested against the measured data of the methanol admittance published in [61]. This material was chosen as its aperture admittance experimental results are available in many papers. However, the results obtained showed that the proposed extraction procedure have a wide validity and can be applied to different materials.

Due to the influence of the fitting criterion on the calculation speed and accuracy of the fit, the investigation was initially aimed to compare two fitting criteria: (a) area fitting criterion, minimise the area between the experimental and the calculated curves; (b) distance fitting criterion, minimise the maximum distance (for each point) between the experimental curves and the calculated ones. As a result of this investigation was found that the more representative of the physical situation was the distance criterion.

---

additional baggage. Weak methods is also too broad a term: it doesnt imply stochasticity. Sometimes the term stochastic search is used: but I usually define search problems as all-or-nothing: either you find the solution or you dont. Were not doing search; were doing optimization."Quoted from Sean Luke in [71].

It was also found that all the dispersive models can both satisfactorily model the complex relative permittivity of methanol.

The proposed procedure was validated by comparing the aperture admittance characteristic as a function of frequency, calculated numerically with the single-layer full-wave Levine & Papas model, in its definite fundamental-mode form, using any one of the three dispersive models with the one calculated with a commercial electromagnetic simulator (CST Microwave Studio, [52]) using the values of the complex relative permittivity extracted from the measured data with the Cole-Cole model, and with the gradient method.

### 3.8 Conclusions

As a result of the bibliographical research and of the study of several papers along the Ph.D. course, a classification of the probe model was done with the identification of two main types of models (hard and soft) with defined characteristics. It was found that these models are useful in different situations according to the problem's specification and the model's nature. For example, the hard model is good for probe design and model's optimization and the soft model for on-line application. These classification helped to distinguish and characterize two main type of extraction schemes (robust and embeddable) that inherit the probe model features. The embedded scheme is more applicable for on-line system and is adaptable to a wide number of applications. Even more, this scheme can replace completely the robust scheme. The robust scheme is more suitable for laboratory test or when accuracy is a priority and when ad-hoc standards and well characterized probes are available.

# Chapter 4

## Effective dielectric models for multilayer materials

### 4.1 Introduction

A vast majority of the investigations carried out to date, which concern the use of open-ended coaxial-line probes, considers the ideal case of "homogeneous" dielectric samples, i.e., samples which consist of a single dielectric material layer that is infinitely thick.

The probe models to which these investigations refer, under the "homogeneous" dielectric assumption, can be used to obtain an effective dielectric response of the material under test, when this material is "heterogeneous" or composite.

Models that give a bidirectional mapping between the effective dielectric response of the probe and the structure and composition of the material under test can be considered of interest on characterization of composite materials. The current state of art in characterization of composite materials with the open-ended coaxial probe shows two directions that along these decades have been taken. One direction is the modeling of the aperture admittance that

includes in the formulation a multilayer material<sup>1</sup>. The other direction is the introduction of effective dielectric models.

In the trend of this second direction, maybe the earliest works were also addressed to layered materials and are dated to the middle of the 90's with the introduction of an empirical effective permittivity model, form to which is associated a two *parallel capacitors* model in [74, 75, 65, 56]. A model associated to a two *series capacitors* model has also been introduced in [76]. More recently also effective dielectric model of the kind of host with inclusions have been investigated in [21].

The parallel capacitor model has been found useful for liquid layers [56] at acceptable accuracies. The *series capacitors* model was not found mature enough compared to that former model and needed further developments.

In the trend of developing that later model and studying both models' nature, the *Effective Medium Theory* (now also EMT) has been studied for laminar composite system in the open-ended coaxial probe context. Consequently a generalized effective permittivity model, extended to multilayer materials, is presented.

This generalized model was formulated for trying to respond to the question: "Is it possible to formulate a model for multilayer materials that is more simple<sup>2</sup> than the alternatives in literature and general for any number of layers? Coming back to the effective dielectric model definition, from its concept we specifically define the effective permittivity ( $\epsilon_{eff}$ ) as the complex permittivity of a homogeneous material which reproduces the complex capacitance when it is inserted in place of a sample of a multilayer material. The multilayer material overall size must also be smaller than the wavelengths and attenuation lengths in the composite and composite's components. This is then described as a transformation of the multilayer problem to single-layer problem. Then this effective permittivity results in a quantitative description

---

<sup>1</sup>For multilayer materials the probe models analyzed in chapter 3, named "two-", "three-", and "N-layers" model are of this type.

<sup>2</sup>By *more simple* we refer to both in computational (extracting algorithm) and experimental terms. Also that include an empirical or equivalent circuit formulation.

given in terms of its composition and structure.

## 4.2 Effective medium theory for laminar composite media

### 4.2.1 Introduction

The effective medium theory has as objective to determine the dielectric function of macroscopically homogeneous and microscopically heterogeneous or composite materials.<sup>3</sup> The material can be considered macroscopically homogeneous if the dimensions of the phases are smaller than the wavelength of the measuring electromagnetic wave. In that sense is valid the approach that we are considering here.

A material with its “homogeneous” attribute defined in that way, allows itself to be treated following a quasi-static approach according to the effective medium theory.

We base our study on previous studies of effective dielectric response of composite and thin film materials that act as laminar systems (one-dimensional inhomogeneities) [77, 78, 79, 80, 28].

We start by taking into consideration a material composed of two layers and an EM wave whose polarization  $E$  is entering the interface between both materials as depicted in figure 4.2.1.

### 4.2.2 Quasi-static approach and Weiner bounds

In the quasi-static state (also called long-wave length state) the considered dimensions (thicknesses of the layers) have to be much smaller than the operative wavelengths and attenuation lengths in play . Under these assumptions two extreme bounds are valid from the Effective Medium Theory and they

---

<sup>3</sup>The terms macroscopically and microscopically are referred to the relation of the structure to the operation wavelengths.

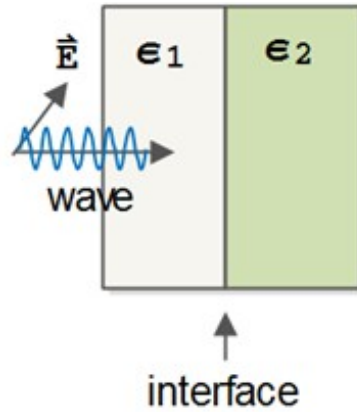


**Figure 4.2.1:** Incident wave in laminar material.

are known as the Wiener Absolute Bounds. These bounds are applied to  $\epsilon$  and are described by the equations (13) and (14) in [78] as extreme incidence cases for a laminar sample.

The word *bound* implies restriction of the effective permittivity to a region of the complex plane. Regions may be defined by simple geometric constructions. Elements of the geometry are also assumed to be much smaller than the wavelengths and the attenuation lengths<sup>4</sup> involved in the composite and component materials. The oscillating electric field within the multilayer material is treated as curl-free, i.e., inductive effects are neglected. (These effects may be important if there are filamentary conducting paths in the composite, with high values of self-inductance.)

The word *absolute* implies that no matter what the structure is, there can never be less screening or more screening than these bounds. In other words, the bounds are absolute because the region of the complex  $\epsilon$ -plane enclosed by them must contain all physically realizable quasi-static values of  $\epsilon$  for two-phase composites regardless of composition or structure. For a description of how the bounds are derived see [77].

<sup>4</sup>practically dimensions smaller than  $0.1\lambda$  and  $0.1\delta$  can be considered, where  $\lambda$  and  $\delta$  refer to the wavelength and attenuation length respectively

For studying the effective dielectric response we observe them in the complex plane. We identify, as shown in figure 4.2.2, both of the permittivity of the constituents of the laminar materials  $\epsilon_1$  and  $\epsilon_2$ .

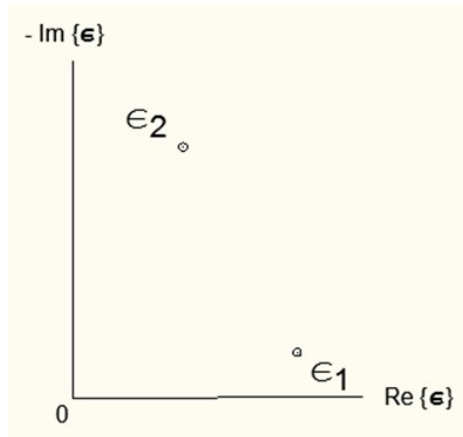


**Figure 4.2.2:** Plane of complex permittivity showing the two points corresponding to the permittivity of the constituent of the composite.

### 4.2.3 The Wiener bounds representation

In accordance with the Effective Medium Theory, the effective permittivity, in that way obtained, should be restricted inside the two Wiener absolute bounds [77, p.301]. One of them represents the extreme case of totally normal incidence of the electromagnetic wave in the interfaces between components and is a normalized weighted average function of the reciprocal of the permittivity. The other represents the extreme case of totally parallel incidence and is a normalized weighted average function of the permittivity.

#### Mathematical representation

These two bounds can be respectively related to the *series* and *parallel capacitors* models for a two-layers case with defined volume fractions (Hashin and Shtrikman bounds when thicknesses of the constituents can be estimated). Consequently we can redefine the *parallel capacitors* and *series capacitors*

models as follows.

For the *parallel capacitors* Model:

$$\epsilon_{\text{eff}} = \xi_1 \epsilon_1 + \xi_2 \epsilon_2 \quad (4.2.1)$$

For the *series capacitors* Model:

$$\epsilon_{\text{eff}}^{-1} = \xi_1 \epsilon_1^{-1} + \xi_2 \epsilon_2^{-1} \quad (4.2.2)$$

In these previous equations  $\xi_1$  and  $\xi_2$  are the volume fractions of the composite, i.e. for the whole volume considered for the electromagnetic object in analysis, how it is fractioned into the constituents.  $\epsilon_1$  and  $\epsilon_2$  are the permittivity's value of the constituents nro.1 and nro.2 in the two-layers material.

The constraint:

$$\xi_1 + \xi_2 = 1 \quad (4.2.3)$$

comes from the normalized weight nature of the function and implies that all the components' fractions sum the entire volume.

The *series capacitors* and *parallel capacitors* models are defined in a parallel plate (electrodes) configuration context as shown by the schemes in 4.2.3 with a transversal section area  $A$  and with thickness  $t_1$  and  $t_2$  for the respective numerated layers.

### Graphical representation

We now focus on the graphical representation of these two expressions in the complex plane of the effective permittivity to show the geometrical description of each one of them to help us to study the geometrical and mathematical properties that will help toward the generalization into a new model.

We use the fact that all bounds delimiting the effective permittivity are circular arcs in the complex plane and we use this to give a representation of  $\epsilon$  for two-phase composites in which the compositional and screening parameters are clearly identified.

The Wiener bounds are easily built as can be seen in figure 4.2.4. In (a)

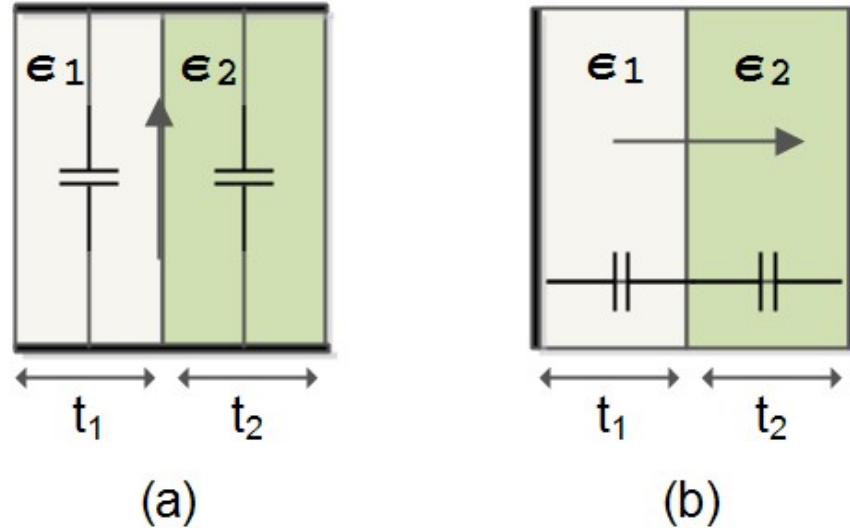


**Figure 4.2.3:** Diagrams of parallel-plate geometries with two materials arrangements for parallel (a) and series (b) responses according with field polarization with respect to the material's interface.

of that figure, the permittivity values of the two constituents are drawn as points in the complex  $\epsilon$ -plane. According to if the interaction of the electric field with the material is completely parallel, a straight line locus is drawn from both permittivity points ( $\epsilon_1$  and  $\epsilon_2$ ) as depicted in (b) of that figure. Its mathematical representation is the eqn. 4.2.1. If the interaction of the electric field with the material is completely normal, a circular arc line locus is drawn from both permittivity points ( $\epsilon_1$  and  $\epsilon_2$ ) as depicted in (c) of that figure. Its mathematical representation is the eqn. 4.2.2. In (d), the superposition of the locus of each extreme case is shown. They enclose a region denominated “ $\Omega$ ” where the effective dielectric response will be confined to exist. So it is clear that where the response will be inside of that region, will depend on the volume fractions of each material and depend on which is the totally incidence field at all boundaries.

We found that the locus described are spherical and hyperspherical non-

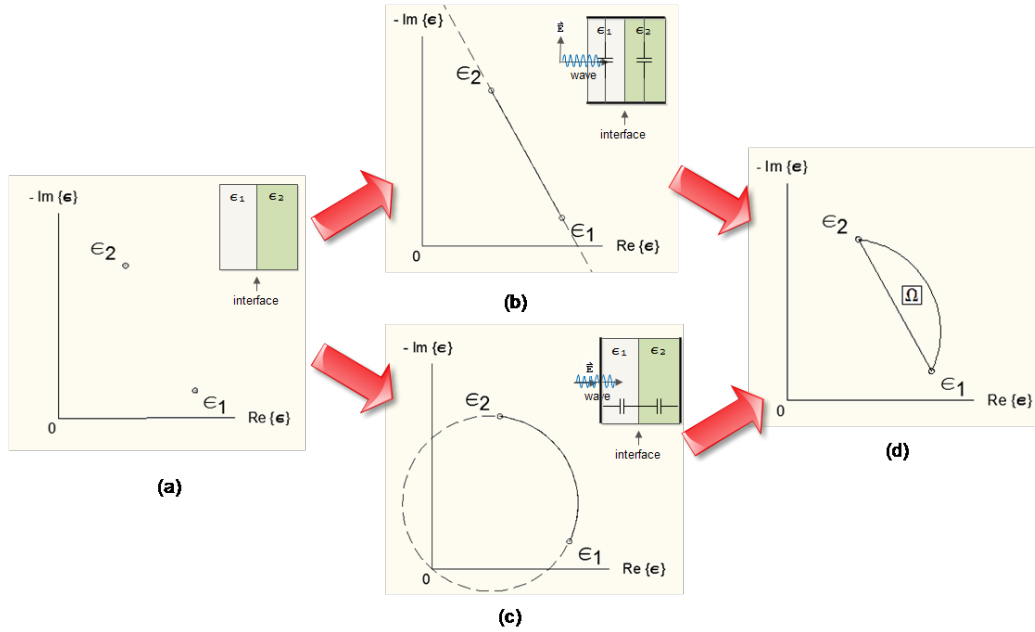


**Figure 4.2.4:** Sketch showing the graphical representation of a two-layers composite in the complex  $\epsilon$ -plane. In (a) the values of the constituent's permittivity. In (b) the totally parallel case is depicted as a straight line. In (c) the totally normal case is depicted as a circular arc line. In (d) the delimited region  $\Omega$  is shown.

euclidean geometries projected to the plane. For more of three constituents the geometries are hyperspherical.

For example, the circular arc line locus is a type of non-euclidean straight line that is called geodesic or 1-sphere sector enlightened by an angle. That line is described as an arc of a circle. That circle passes through the two points  $\epsilon_1$  and  $\epsilon_2$  and by the origin of the plane ( $\epsilon = 0$ ). Every point in the locus is referenced according to the volume fractions. Since the volume fractions are constrained to unity, one of them is enough for representing all the points in the locus if we are in presence of a two-layers composite as we are. So we define  $\xi_1$  for  $0 < \xi_1 < 1$ .

The straight line locus can be considered as a case similar to the circular arc line, but with a circle of infinite radius.

Through the geometries of the bounds in the complex plane we understood that there has to be a model that generalizes both extremes models described by the bounds, extends to multilayer cases, and that can be found by geometrical methods analyzing the geometries in the complex plane. We noted then that since both bounds can be described as circular arcs, then they should be a connection to the Spherical Non-Euclidean Geometries. In that tendency we followed two independent paths. One to generalize the model for considering oblique incidence cases (cases in which not all the boundaries are parallel or perpendicular to the field) and to extend it to N-layered materials. Consequently we applied this new general effective dielectric model to the open-ended coaxial probe technique to propose a new model.

#### 4.2.4 Oblique incidence Case

##### Graphical consideration

To generalize the model for considering oblique incidence cases we consider the figure 4.2.5 and the following regarding the line that connects the permittivity of the constituents materials for a two layered case:

1. in the totally normal case the line is a geodesic line belonging to a circle (constructor) passing through  $\epsilon_a$ ,  $\epsilon_b$  and the origin.<sup>5</sup> This is shown in (a) in figure 4.2.5;
2. in the totally tangential or parallel case the line is a straight line or a geodesic line belonging to a circle (constructor) passing through  $\epsilon_a$ ,  $\epsilon_b$  and the  $\infty$ . This is shown in (b) in figure 4.2.5.

This takes us to assume that these third points, the ones taking zero (0) and infinity ( $\infty$ ) for the normal and parallel case, can connect both models and generalize it in a new one.

In this trend we assume that these points belong to a new parameter whose

---

<sup>5</sup>Here,  $\epsilon_1 = \epsilon_a$  and  $\epsilon_2 = \epsilon_b$ . In this chapter these two equalities are keep always unless otherwise specified.

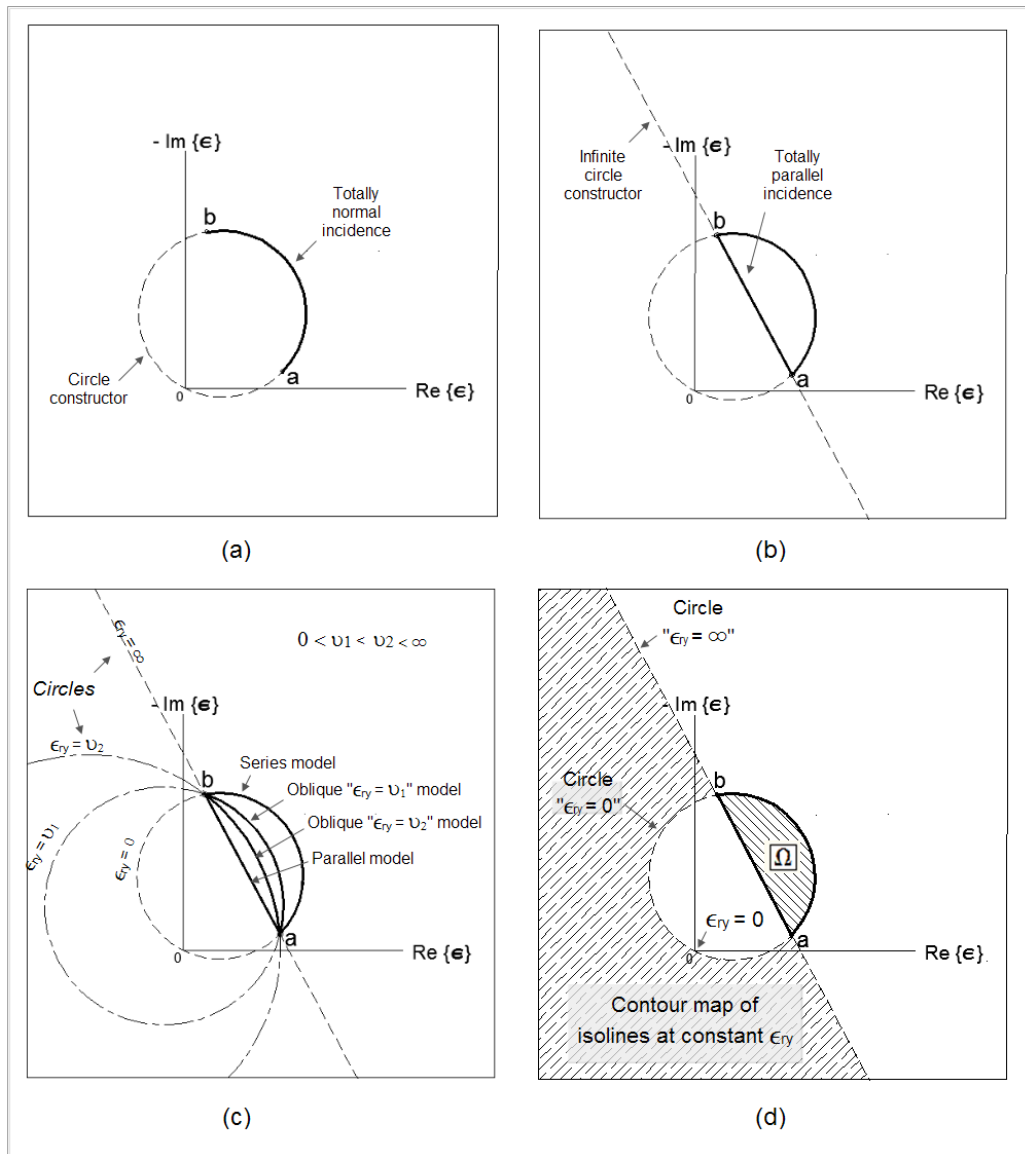


**Figure 4.2.5:** Graphical interpretation of the oblique case from the extreme cases. In (a) the totally normal bound, its locus (black thick line) and its circle constructor (black thin dashed line). In (b) the totally parallel bound, its locus (black thick line) and its infinite-radius circle constructor (black thin dashed line). In (c) the oblique incidence cases, its locus (black thick lines for  $\epsilon_{ry} = \nu_1$  and  $\nu_2$ ) and its circle constructors (black long-short dashed-style lines). In (d) the contour map regions of isolines, the right one including all the possible values of  $\epsilon_{ry}$  and the left one including the  $\Omega$  region.

symbol is  $\epsilon_{ry}$ , that we will call from now on the *incidence's* parameter and that is bounded by the extreme cases, i.e.  $0 < \epsilon_{ry} < \infty$ .

Thus we observe that there has to be a circular arc line described by the circle passing through  $(\epsilon_{ry}, \epsilon_a$  and  $\epsilon_b)$  inside the region,  $\Omega$ , delimited by the extreme cases. Let's suppose there is a circular arc line, of that type, defined by a constant incidence's parameter ( $\epsilon_{ry} = v_1$ ) and shown in (c) of figure 4.2.5 as an *oblique model*. This new circular arc line can describe any point of the region  $\Omega$  given the appropriate value for  $\epsilon_{ry}$ . Another circular arc line can be defined for  $\epsilon_{ry} = v_2$  where  $0 < v_1 < v_2 < \infty$  as also depicted in (c) of figure 4.2.5 as an *oblique model*. These respective inner circular arc lines define a contour map of isolines for constants values of the incidence's parameter in the  $\Omega$  region.

The region delimited to the right by the infinite line  $\epsilon_{ry} = \infty$  and outward by the circle  $\epsilon_{ry} = 0$  as depicted in (d) of figure 4.2.5 is another contour map of isolines for constants values of the incidence's parameter. All the possible values of the incidence's parameter will be inside this last region,

A generalization of the extremes models for taking into account the indoor cases is then presented in (c) of figure 4.2.5 as the *oblique model*. In the next subsection we will introduce the mathematical representation.

### Mathematical representation

The above graphical representation regarding the oblique incidence curve and the incidence's parameter open the door to find a mathematical representation that models that geometrical curve.

We found through several tentatives that this following representation is the best:

$$\epsilon_{\text{eff}} = \left( \xi_a (\epsilon_a - \epsilon_{ry})^{-1} + \xi_b (\epsilon_b - \epsilon_{ry})^{-1} \right)^{-1} + \epsilon_{ry} \quad (4.2.4)$$

The next step is then to apply this formulation as a model for the open-ended coaxial probe.

## 4.3 Effective dielectric model for the open-ended coaxial probe

### 4.3.1 Exponential behavior of the effective dielectric response

For the passage from the extreme models (totally parallel and normal incidence models) given by the Effective Medium Theory for laminar composite to models that can be used by the open-ended coaxial probe technique as effective dielectric models, a new definition of the volume fractions ( $\xi_a$  and  $\xi_b$ ) needs to be found in function of the thicknesses of the layers.

An analytical work performed by us shows that the volume fractions (the  $\xi$ s) depend exponentially on the thickness of each respective material layer. This was found by studying the effective dielectric response with other full-wave and quasi-static models. In figure 4.3.1 an example showing the exponential behavior is depicted. The example corresponds to Teflon backed by Air evaluated by a two-layers Bakhtiaris model and extracted with a single-layer Bakhtiari's model.

### 4.3.2 Effective dielectric model for the open-ended coaxial probe

This exponential behavior let us define the effective dielectric response by this model where all type of incidence is considered:

$$\epsilon_e(y, \epsilon_a, \epsilon_b) = (e^{-C_y y} ((\epsilon_b - \epsilon_{ry})^{-1} - (\epsilon_a - \epsilon_{ry})^{-1}) + (\epsilon_a - \epsilon_{ry})^{-1})^{-1} + \epsilon_{ry} \quad (4.3.1)$$

where:  $\epsilon_e$  is the effective dielectric response or effective permittivity,  $\epsilon_a$  and  $\epsilon_b$  are the complex permittivities of the composite constituents,  $y$  is the thickness of the layer closer to the aperture of the probe.<sup>6</sup>, and  $\epsilon_{ry}$  and  $C_y$  are the

<sup>6</sup>In these multilayer materials, the last layer is considered infinitely extended.

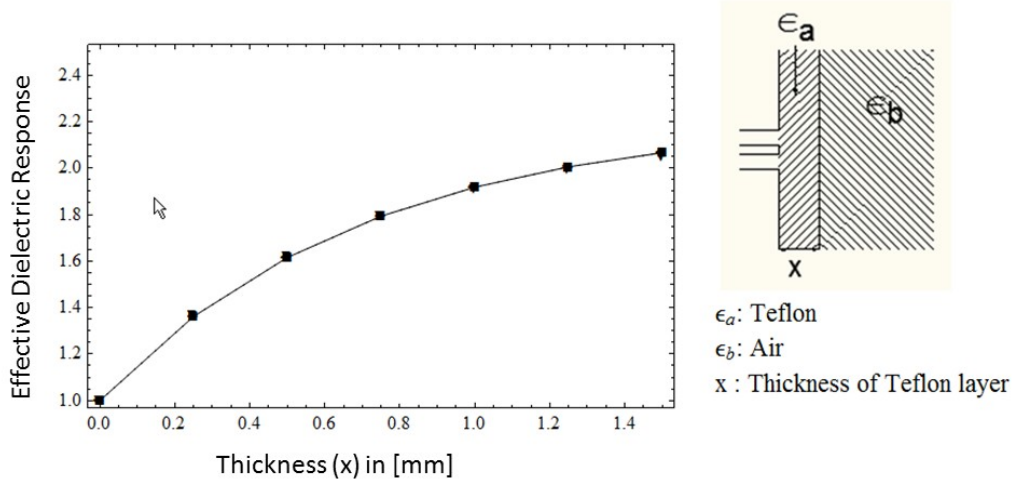


**Figure 4.3.1:** Exponential behavior of the effective dielectric response vs thickness for a two-layers composite of Teflon backed by air.

fitting (setting or soft) parameters of the model.

When  $\epsilon_{ry} \rightarrow 0$ , we are in the *totally normal* case or *series capacitive* Case:

$$\epsilon_e(y, \epsilon_a, \epsilon_b) = (e^{-C_y y} (\epsilon_b^{-1} - \epsilon_a^{-1}) + \epsilon_a^{-1})^{-1} \quad (4.3.2)$$

When  $\epsilon_{ry} \rightarrow \infty$ , we are in the *totally parallel* case or *parallel capacitive* case:

$$\epsilon_e(y, \epsilon_a, \epsilon_b) = e^{-C_y y} (\epsilon_b - \epsilon_a) + \epsilon_a \quad (4.3.3)$$

The models presented here are all empirical whose parameters can be found by known-material measurement fitting or by other models fitting (Model Optimization - see sec.3.3.3).

From these models, the one that appears clearly in literature is the *parallel capacitive* model ([74, 75, 65, 56]). The *series capacitive* model was also proposed in reference [76] but in a different manner.<sup>7</sup>

With the introduction of this new, Oblique Incidence model, we give to all of them a formal representation so that things can return clearer.

<sup>7</sup>The Arai's model was expressed in a not-so-clear way because of the few information detailed in the referred article with respect to the model's parameter, specially the definition and specification of  $t_2$ .

### 4.3.3 Oblique incidence model verification

The model's parameters can be fitted by minimizing the

$$\text{Err}(C_y, \epsilon_{ry}) = \sum_{i=1}^N |\epsilon_e(y_i, \epsilon_a, \epsilon_b) - \epsilon_i| < \kappa \quad (4.3.4)$$

given  $\epsilon_a$ ,  $\epsilon_b$  and  $N$  experiments  $(y_i, \epsilon_i)$ .

For testing purpose we generate some experiments by the use of the Bakhtiari's admittance expression for one and two layers cases. The two-layers case was defined to have one layer of a material with a permittivity  $\epsilon_a$  and thickness  $y$  and the other layer with a material with a permittivity  $\epsilon_b$  and infinitely thick. The one-layer case was defined to have an infinitely thick material with permittivity  $\epsilon$ . For the case where both cases are equal, i.e. its admittances are equals, we have that  $\epsilon$  would be the effective permittivity of the two-layers case. So for any  $y$  in the two-layer case, will correspond an  $\epsilon$  in the one-layer case and we use that to generate the needed experiments.

Three experiments will be enough.

Fitted parameters can have these values:

$$\epsilon_{ry} = -25.261 - i6.1408 \quad (4.3.5)$$

$$C_y = 2701.88 \quad (4.3.6)$$

that were obtained with a maximum error in the fitting points of 1%.

This model is more accurate than the *series capacitive* and *parallel capacitive* models whose maximum errors, when proceeding same way, are worse.

Other verifications are given in sec. 4.4. This new model is consistent with region and bounds definition given by Milton in [77].

### 4.3.4 Circuitual Representation of the Oblique Incidence Model

The *oblique incidence* model, whose formulation is eq. 4.3.1, can be related to a capacitive elements representation through a parallel plate (electrodes)

configuration context. To achieve this we first multiply the effective permittivity expression by a constant ( $S/L$ ) given by the considered geometry box as the universal set.  $S$  for transversal section and  $L$  for total length. Then rearranging we arrive to these following equivalent circuit as a capacitors network expression:

$$C_{\text{eff}} = (C_1 // C_{r-1}) // (C_2 // C_{r-2}) + C_{r-\text{eff}} \quad (4.3.7)$$

where for  $i = 1, 2$ :

$$C_{r-i} = \epsilon_i A e^{Fy} \left( \frac{\epsilon_i}{\epsilon_r} - 1 \right) \quad (4.3.8)$$

and where:

$$C_{r-\text{eff}} = A \epsilon_r \quad (4.3.9)$$

$$C_1 = \epsilon_1 \frac{A}{e^{-Fy}} \quad (4.3.10)$$

$$C_2 = \epsilon_2 \frac{A}{(1 - e^{-Fy})} \quad (4.3.11)$$

$$A = S/L \quad (4.3.12)$$

The exponential comes from the exponential behavior of the volume fractions and  $A$ ,  $F$  and  $\epsilon_r$  are considered empirical parameters of the model.

The expression is shown in a circuit diagram in figure 4.3.2. We observe that the model's form coincides with the expectation given by the circuit models shown in figure ( 5.2.1).

We can rearrange that expression to give an empirical model of the effective capacitance with the same empirical parameters:

$$C_{\text{eff}} = A \left( \epsilon_2 + \frac{\epsilon_1 \epsilon_2 - \epsilon_2^2 - \epsilon_1 \epsilon_r + \epsilon_2 \epsilon_r}{e^{Fy} (\epsilon_1 - \epsilon_r) + (\epsilon_2 - \epsilon_1)} \right) \quad (4.3.13)$$

where  $\mathbf{A} = \frac{C_{\text{eff}}}{\epsilon}$  for  $\epsilon_M = \epsilon_0 = \epsilon$  that represents the single layer case condition and where for  $0 < y < \infty$  :

$$Fy + G = \text{Log} \left[ \frac{\epsilon_1 - \epsilon_2}{C_{\text{eff}} - A \epsilon_2} \right] \quad (4.3.14)$$

$$G = -\text{Log} \left[ A + \frac{A \epsilon_1 - C_{\text{eff}}}{(\epsilon_r - \epsilon_1)} \right] \quad (4.3.15)$$

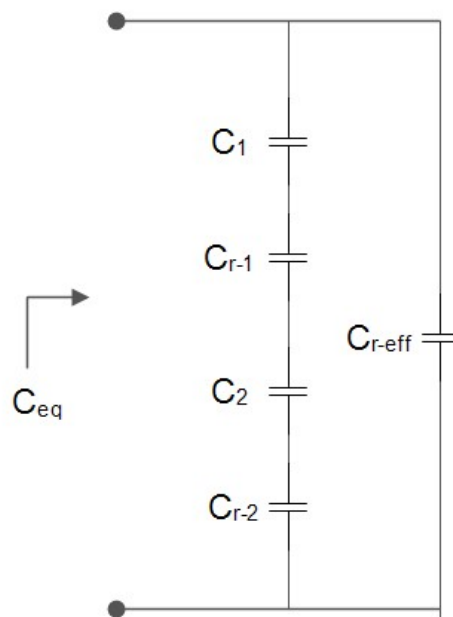


**Figure 4.3.2:** Diagram of the equivalent circuit for the two layered case with general incidence as a capacitors network.

As a test to verify the connection with the extreme cases we see that for  $\epsilon_r \rightarrow 0$  results the *series capacitors* model:

$$C_{\text{eff}} = \frac{A}{\frac{1-e^{-Fy}}{\epsilon_2} + \frac{e^{-Fy}}{\epsilon_1}} \quad (4.3.16)$$

And that for  $\epsilon_r \rightarrow \infty$  results the *parallel capacitors* model:

$$C_{\text{eff}} = A (\epsilon_1 e^{-Fy} + (1 - e^{-Fy}) \epsilon_2) \quad (4.3.17)$$

### 4.3.5 General multilayer model

In a multilayer model, each layer is geometrically characterized by its thickness, since its transversal section is assumed to be infinitely extended. This allow to use a linear approximation of the Effective Medium Theory for relating their constitutive phases with the effective value measured in a quasi-static regime (thicknesses in play much smaller than minimal wavelength). This approximation is based on a linear interpolation between the constituent parameters.

The general form of these approximations, for a material composed of N phases takes the form of a normalized weighted average function as follows:

$$\epsilon_e^{-1} = \sum_{j=0}^{N-1} \epsilon_j^{-1} \xi_j \quad (4.3.18)$$

where  $\xi_j$  is the volume fraction of the j-constituent and where also must be satisfied the following condition:

$$\sum_{j=0}^{N-1} \xi_j = 1 \quad (4.3.19)$$

An expression that relates the volume fraction to the thickness of each phase is as follows:

$$\xi_0 = \exp \left( - \sum_{i=1}^{N-1} v_i C_{v_i} \right) \quad (4.3.20)$$

$$\xi_j = (1 - \exp(v_j (-C_{v_j}))) \exp \left( - \sum_{k=1}^{j-1} v_k C_{v_k} \right) \text{ for } j = 1, 2, \dots, (N-1) \quad (4.3.21)$$

where  $v_j$  is the thickness corresponding to the  $j$ th-constituent and  $C_{v_j}$  is a model parameter. Observe that the unitary volume constraint is satisfied. Then:

$$\epsilon_e(v)^{-1} = \epsilon_0^{-1}\xi_0(v) + \sum_{j=1}^{N-1} \epsilon_j^{-1}\xi_j(v) \text{ for } v = v_1, v_2, \dots, v_{N-1} \quad (4.3.22)$$

Since the model is a linear system, its parameters can be calculated using the superposition principle:

$$C_{V_1} = -\frac{1}{v_1(0)} \log \left( \frac{\epsilon_e(v_1(0))^{-1} - \epsilon_1^{-1}}{\epsilon_0^{-1} - \epsilon_1^{-1}} \right) \quad (4.3.23)$$

$$C_{V_2} = -\frac{1}{v_2(0)} \log \left( \frac{\epsilon_e(v_2(0))^{-1} - \epsilon_1^{-1}}{\epsilon_0^{-1} - \epsilon_1^{-1}} \right) \quad (4.3.24)$$

$$C_{V_3} = -\frac{1}{v_2(0)} \log \left( \frac{\epsilon_e(v_3(0))^{-1} - \epsilon_1^{-1}}{\epsilon_0^{-1} - \epsilon_1^{-1}} \right) \quad (4.3.25)$$

where  $V_j(0)$  represents any value for  $V_j$ .

A summary of the effective dielectric model for general incidence in multilayer materials is shown in figure 4.3.3.

### 4.3.6 Consideration about finite-wavelength effects

The above quasi-static limits are derived by assuming that the wavelength is infinite. A work describing this finite-wavelength effect for composite materials is done by Aspnes in [78, 79]. Since  $\epsilon$  is itself constrained to lie somewhere "between"  $\epsilon_a$  and  $\epsilon_b$  it follows that propagation will be evanescent in the less dense phase and that the wave energy will tend to focus on the phase, with the larger value of real part of permittivity ( $Re(\epsilon)$ ). This wave-guiding or focusing mechanism skews  $\epsilon$  at finite frequencies toward the larger permittivity constituent. In striking contrast, it is the constituent with the smaller permittivity that always dominates in the quasi-static case simply because the more polarizable fraction develops more boundary charge and screens itself more effectively from the external field.

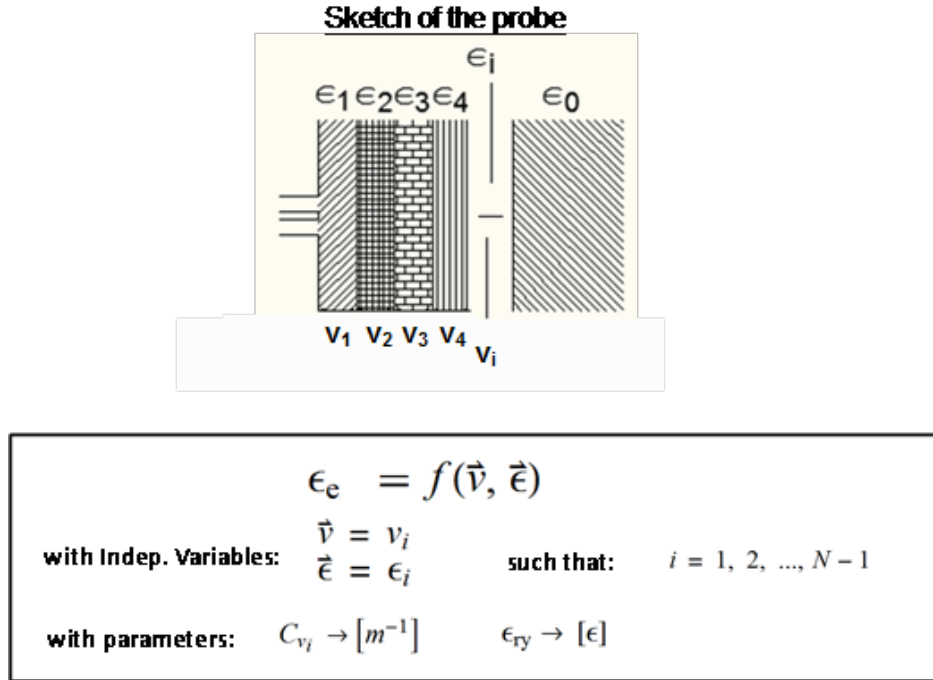


**Figure 4.3.3:** Summary of the effective dielectric model for general incidence in multilayer materials.

This mechanism can explain how the bounds derived from the quasi-static limit are relaxed at finite frequencies.

The high-order wave modes in the aperture that can be excited are mostly TM modes.

Following the Aspnes approach for the finite-wavelength effect study we were expecting that the trend would be as the one shown in fig. 2 of [79]. The frequency range of interest in our work and the structure dimensions will keep us inside of the quasi-static limit. Some studies, made in an air-bulk two-layers cases along the frequency interval of interest, that include the permittivity extraction from simulations and from Bakhtiari's model evaluation show that the changes in the effective dielectric were given mostly by the inaccuracies of the model and by the frequency dispersion of the constituents than by the waveguide mechanism explained by Aspnes, demonstrating to be inside the quasi-static limit.

We notice that the elliptical region shown in figure (4.3.4) agrees with the results shown in [74, fig.2]. That region is shown in the boxed magnified curve for the  $10\mu m$  case. Figure 2 of that article shows that, for thicknesses from  $0.1$  to  $0.01mm$  in an air-backed-by-alumina system, the changing dielectric constant response describes a curl (makes a circle) while increasing the frequency from  $4$  to  $8$  GHz. This effect was also seen in the effective dielectric response of the case depicted in figure (4.3.4) when making the projection of the curves traced in frequency to the real axis ( $Re(\epsilon)$ ).

The tendency of wave energy to concentrate in the more dense constituent will clearly also occur for more complex structures. The quasi-static limit should remain a good approximation for thicknesses smaller than  $0.1\lambda$ , but for larger ratios the more dense columnar material should dominate.

This waveguide mechanism allows to understand also why effective-medium models can describe rough surfaces: the impinging wave front is refracted into the more dense medium as the TE and TM components realize local boundary conditions and preserve a common phase factor. But the distortion will be small, and the quasistatic limit is a good approximation if the structural dimensions are small compared to  $\lambda$ .

## 4.4 Validation and applications

### 4.4.1 Introduction

Before presenting the validation, a glance at the applications of this model will be given.

Some applications are:

- Emulsion layers backed by air. This may fulfill several industrial measurement needs. Emulsions like milk, butter, water-oil, sun-screening lotions, lubricants, etc. can be included.
- Minimization of surface roughness effect by estimating an air layer equivalent to the average roughness of the material or by establishing

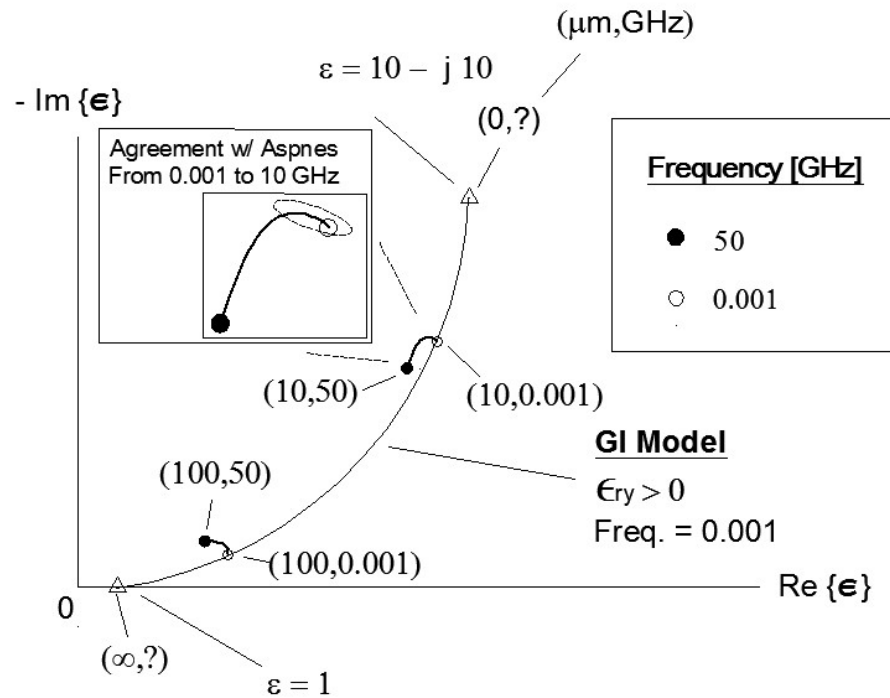


**Figure 4.3.4:** Diagram of the geometrical locus showing the frequency effect for some points

an air layer between the probe and the MUT (probe in lift-off).

- Stratified films or composite materials.
- Biological or Mineral materials like the composition of a plant's parts (trunks, leaves) or of rocks and soils. Biological materials are usually layered structure of biological tissues, such as skin and hypoderm.
- Near-field microscope scanning
- Thin water layers for phantoms of biological tissues that can be approximated by this model.
- In liquid measurements a first protective layer may be useful for preventing liquid infiltration inside the probe and surface corrosion. Two

or more layers models are required.

From all these applications, the one that represents a problem that was more intensively analyzed during the Ph.D. course is the minimization of the surface roughness effect or its characterization. This is mainly a problem in solids. The effective dielectric model developed and described in this thesis can describe this type of problem. The fact that this works is explained by the finite-wavelength effect. If the characteristic dimensions of the microstructure are small compared with  $\lambda$ , the corresponding distortions of the wavefront required to satisfy the boundary conditions will not be important. Then the material can be described as a composite medium as it was suggested by Baker-Jarvis *et al.* in [51], where the imperfectness problem is afforded by a lift-off approach, i.e. a model of two-layers material.

Another important application is in on-line system. As it was described in chapter 3, this is a dielectric effective model and it can help to include any type of N-layers problems in an easier way than the traditional N-layers full-wave models available in literature. N-layers problems include all the applications that were mentioned previously in this same section.

#### 4.4.2 Performance of the effective dielectric models for model optimization usage

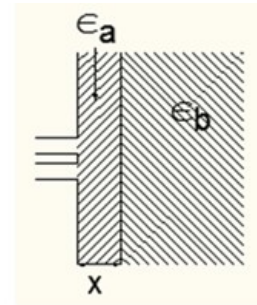
##### Introduction

In the validation we made use of the two-layers case for testing the series, parallel and general models. Several combinations of materials were employed and they also were confronted with literature data showing good agreements. We employed combination of different materials as teflon, silicon, methanol, air, FR-4, etc. modeled as lossless or lossy, and with small and large probes in some cases.

The small probes have typically an outer radius of 2 mm and the large probe for 10 mm in our work.

**Employed combinations of materials in the validation:**

- 1) Teflon backed by Air Case (small probe, lossless)
- 2) Silicon backed by Air Case (small probe, lossless)
- 3) Methanol backed by Teflon Case (small probe, lossy)
- 4) Air backed by FR-4 Case (small probe, lossless)
- 5) Air backed by Methanol Case (small probe, lossy)
- 6) Different fictitious cases



**“Fictitious” Effective Dielectric Data  
“Analytical Data”**



**Bakhtiari's model.**

**Tested models:**

- Parallel
- Series
- General

**Testing methods**

- R2 statistic test
- Graphical comparison

**Testing Objective**

- Goodness of optimized model to Analytical Data

**Figure 4.4.1:** Summary sketch of the validation of the series, parallel and general effective dielectric models.

For analyzing the effective dielectric response, we needed fictitious effective dielectric data. We got that using the Bakhtiaris model in its two-layers and single-layer fundamental-mode form.

The robust extraction scheme was employed in this following way: *We generated fictitious measured data (aperture admittance data) with the two-layers model of Bakhtiari and then with them I applied the optimization of the permittivity using a single-layer model of Bakhtiari to estimate the permittivity. The permittivity thus obtained is an effective permittivity, i.e. the fictitious effective dielectric data.*

These fictitious measured data are also called *Analytical Data*.

For testing them we use a graphical representation and a statistic test, the R2 statistic test. This test gives an evaluation from 0 to 1 according to the goodness of the model. The nearer the R2 value is to 1 the better is the models fitting capability.

We tested the best fitting they can achieve with the Analytical Data.

In figure 4.4.1 we show a summary sketch of the principal points of the validation. In the following the most illuminating case studies are presented. They are illuminating in the sense that they represent the main contributions for the posterior conclusions.

### Air-backed material and material-backed air case study

In figure 4.4.2 the results of an air backed by a lossy material and of a lossy material backed by air with those values shown in the picture are presented. The marked points in the curves correspond to specific thicknesses conditions of the material. For the  $\epsilon_1$  backed by  $\epsilon_2$  the locus start at  $\epsilon_2$  and while the thickness of the first layer (layer 1) increases, we move along the locus described by the three curves (*series* curve, *parallel* curve and *general* or *oblique* curve) following the increase direction of  $x$  shown in the plot. For  $\epsilon_2$  backed by  $\epsilon_1$  the locus start at  $\epsilon_1$  and the opposite behavior is observed.

What comes immediately to light is that in the first case, the *general* model, that follows very well the analytical data, behaves very similar to the *parallel* model. For the second case the opposite is true. This pushes us to think that if the difference in permittivity is big, one of the extreme cases approximate well the analytical data together with the *general* model.

If now we pay attention to an air-backed-by-FR4 case as the one depicted in figure 4.4.3 we can observe that also one of the extreme case, together with the *general* model fit also well.

In this last case, we can appreciate from the picture also the result of the statistic test showing that the *series* and the *general* models fit better the data than the *parallel* model as is indicated by the R2 value (the nearer to 1 the better).

**Air backed by a lossy material**

$\epsilon_1 = 1$

$\epsilon_2 = 4.65 - i 33.20$

" $\epsilon_1$  backed by  $\epsilon_2$ "

" $\epsilon_2$  backed by  $\epsilon_1$ "

References:

- - Parallel
- - Series
- ◆ - General
- ▼ - Analytical Data

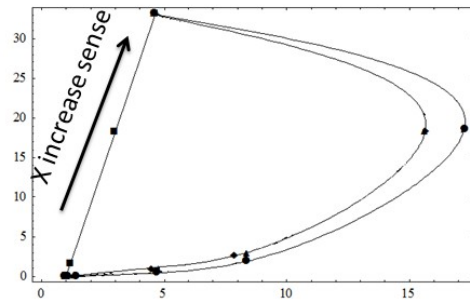
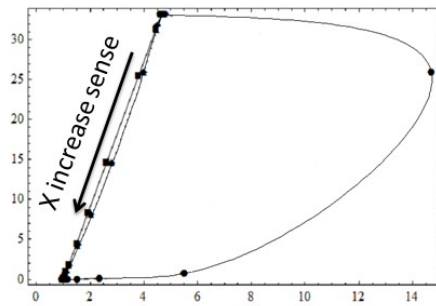
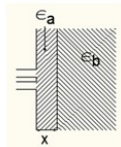


**Figure 4.4.2:** Results of the case study for air backed by a lossy material, at left, and lossy material backed by air, at right.

**Air Backed by FR4-similar**



**Parallel Model:**

R2 statistic test: 0.996875

Fitted Parameter:  $Cy \rightarrow 9501.11$

**Series Model:**

R2 statistic test: 0.999969

Fitted Parameter:  $Cy \rightarrow 2956.95$

**General Model:**

R2 statistic test: 0.999963

Fitted Parameter:  $Cy \rightarrow 2731.29, \epsilon r \rightarrow 0.122577$

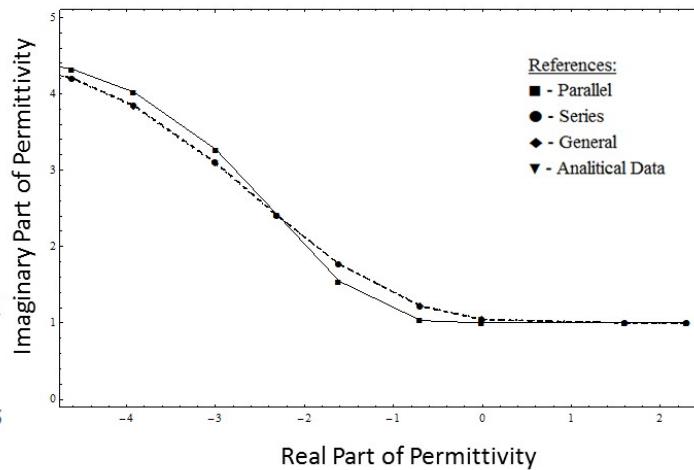


**Figure 4.4.3:** Results of the case study for air backed by an FR-4 similar material (lossless).

### Methanol backed by air case study

Now we pay attention to a methanol-backed-by-teflon case as the one depicted in figure 4.4.4 for a small probe and a frequency of 1GHz.<sup>8</sup> It is possible to observe again one of the extreme models, together with the *general* model fitting well again, but this time it is the *parallel* model which fits better than the *series*, as also shown by the R2 statistic test.

This last case, methanol backed by teflon, is a typical application of measurement of thin liquids and emulsions.

This last case was for a small probe at 1 GHz, for a large probe at same frequency we refer to figure 4.4.5. The fit is best for the *general* model, followed by the *parallel* model.

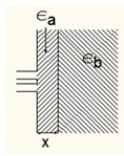
There is a disagreement only with the *analytical data* near the Methanol point (enclosed with red circle), then for very large thicknesses. Considering that the probe is large, we hypothesize that this is due to a break in the quasistatic condition for those cases with large thicknesses. Since this is not happening for the small probe case at same frequency, we suppose that the size of the probe in some way can influence the dielectric model's behavior, but this needs further analysis that has not been carried out in this work..

Again methanol backed by teflon but this time at 10 GHz with a small probe. In figure 4.4.6 it is observed a notorious diminution in the fitting goodness of the models. This is because of the higher frequency considered. We notice that the best performance was given by the *general* model, but yet not the best. This is because at such a frequency some of the considered thicknesses are surpassing the quasi-static limit and the model's validity breaks for those. Since they are considered, all, in the fitting process (Model optimization), these wrong points will worsen the overall model's response as can be seen from the curve and the R2 statistic test.

---

<sup>8</sup>In the previous cases the materials were not dispersive, here methanol is considered as a dispersive material. It was elaborated for 1 GHz and 10 GHz using the Cole-Cole parameters for the dispersion model in [73]. In addition two different sizes for the section of the probe (small and large) were considered.

### Methanol Backed by Teflon with Small Probe at 1GHz



#### Parallel Model:

R2 statistic test: 0.999482

Fitted Parameter:  $Cy \rightarrow 1667.93$

#### Series Model:

R2 statistic test: 0.867222

Fitted Parameter:  $Cy \rightarrow 5950.61$

#### General Model:

R2 statistic test: 0.998728

Fitted Parameter:  $Cy \rightarrow 1817.85, \epsilon_r \rightarrow -247.183 + i 30.9947$

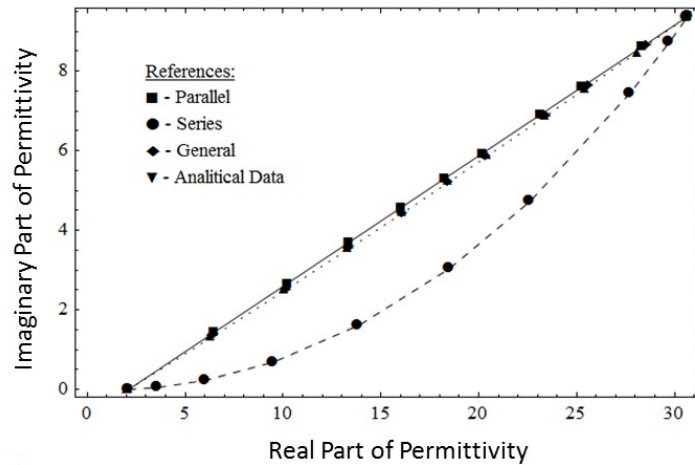
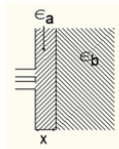


**Figure 4.4.4:** Results of the case study for methanol backed by teflon for a small probe at 1 GHz.

### Methanol Backed by Teflon with Large Probe at 1 GHz



#### Parallel Model:

R2 statistic test: 0.999392

Fitted Parameter:  $Cy \rightarrow 690.664$

#### Series Model:

R2 statistic test: 0.914107

Fitted Parameter:  $Cy \rightarrow 3058.17$

#### General Model:

R2 statistic test: 0.999819

Fitted Parameter:  $Cy \rightarrow 754.638, \epsilon_r \rightarrow -246.96$

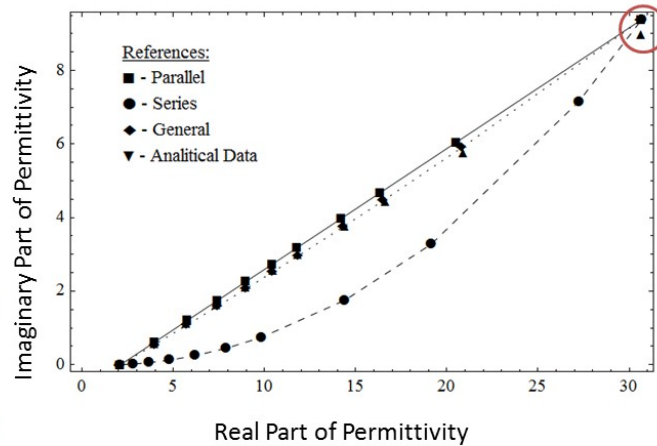


**Figure 4.4.5:** Results of the case study for methanol backed by teflon for a large probe at 1 GHz.

### Methanol Backed by Teflon with Small Probe at 10 GHz

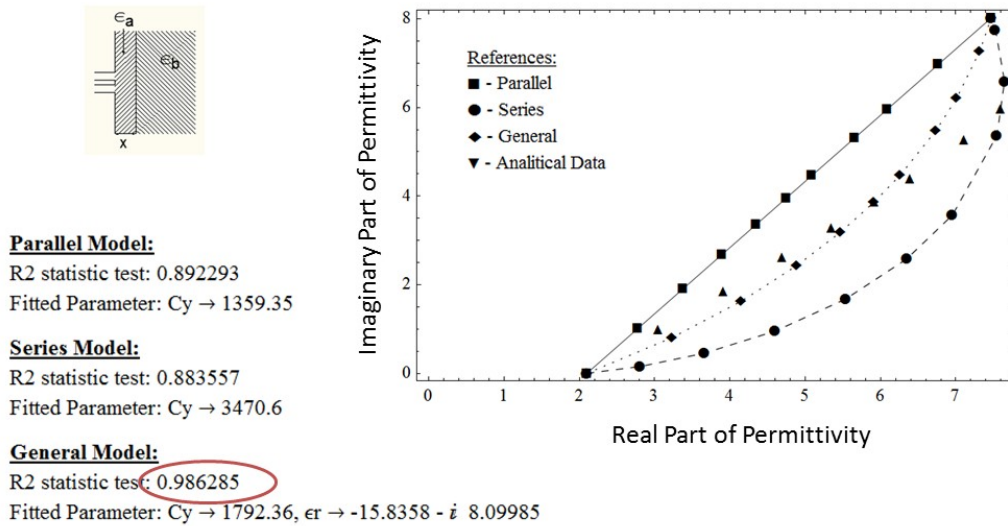


**Figure 4.4.6:** Results of the case study for methanol backed by teflon for a small probe at 10 GHz.

### Material-backed material case study

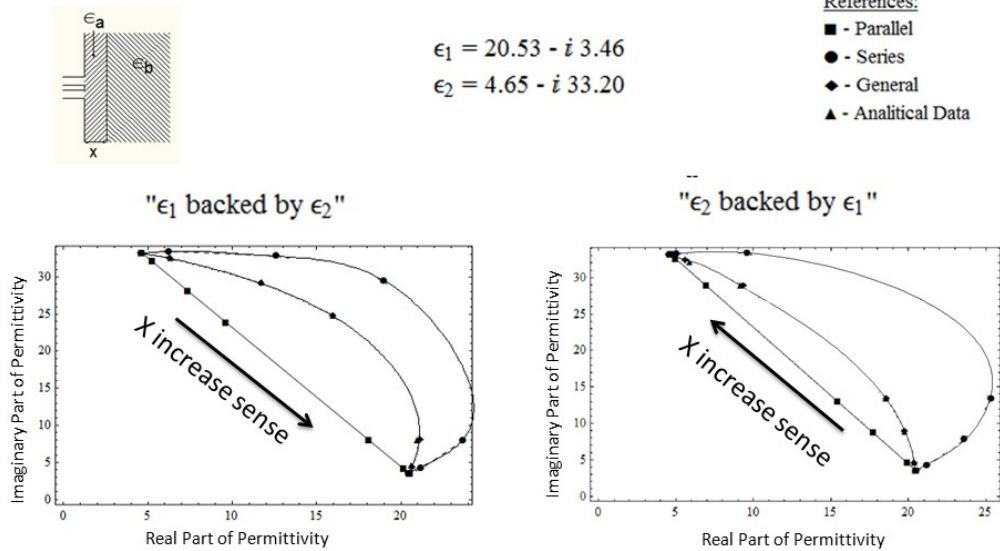
In figure 4.4.7 another case is shown that introduce a situation where only the general model gives a good fit.

We can see the tendency to the *parallel* model from the *general* model in the  $\epsilon_2$  backed by  $\epsilon_1$  in contrast with the tendency to the *series* model for the  $\epsilon_1$  backed by  $\epsilon_2$ . Which also agrees with the results in the previous cases. This suggests that the goodness of the *parallel* or *series* model depends on the magnitude of the permittivities of both layers and on its position.

### 4.4.3 Conclusions

In this section the principal conclusions are these:

- The coefficient of the argument of the exponential, ( $C_y$ ), for the best fit and best model seems to be between  $b^{-1} + a^{-1}$  and  $a^{-1}$ . This was

**Two-layered lossy case**

**Figure 4.4.7:** Results of the case study for any lossy material combination.

observed for all the analyzed cases and is of certain importance for relating the coefficient of the exponential behavior to the geometry of the probe.

- The maximum dimension of the laminar compound has not to be superior to the sensibility depth of the probe that is approx.  $4(b + a)$ .<sup>9</sup>
- The general model is the best model of all three for all the cases.
- The parallel model performs well for  $\epsilon_a > \epsilon_b$ . As for examples emulsions.
- The series model performs well for  $\epsilon_a < \epsilon_b$ . As for example when con-

<sup>9</sup>The sensibility depth definition was given in a *parallel* effective dielectric model context. In this regard, following the exponential behavior of the volume fractions we concluded that the argument of the exponential ( $C_{yy}$ ) should be  $3.91202 (\approx 4)$ . This allows a redefinition of the *sensibility depth* expression given in eq. 2.3.3 to account for the thickness of the sample required to consider the material infinitely extended. This also agrees with what reported by Bakhtiari *et al.* in [68, sec. III].

sidering the imperfectness of the contact or a protective layer for the probe.

## 4.5 Conclusions

An empirical effective dielectric model for the open-ended coaxial probe in contact with an n-phase composite material is presented. The model, here simply called *general*, takes into account all the possible values for the effective dielectric response according to the effective incidence of the field in every interface between two constituents of the composite.

The accuracy of the model is improved with respect to the previous models presented in literature.

It allows application in on-line system and can afford most of the multilayer problems that usually are boarded by other multilayer model, like imperfect contact problem boarded by lift-off approach or by effective roughness layer in rough surface materials. It can also be extended to multilayer films provided that the quasi-static condition be satisfied.

The non-euclidean geometry approach can also be included in further works for extension of the effective dielectric response to other kind of composite's structures to different frequency's ranges since it was helpful for the derivation of the *oblique incidence* model.

Further investigations are also needed to understand how the changing dielectric response with frequency can be used for incorporating the frequency behavior in the model.

# Chapter 5

## The imperfectness of the contact in open-ended coaxial probes

### 5.1 Introduction

In order to limit the uncertainty in the measurement with an appropriate probe for any of the probe models, it is extremely important, mostly in solids, that both the probe and sample surfaces be flat. Extreme care must be taken to avoid minute air gaps that might exist between the probe and the sample [75]. This is particularly critical for dielectric constant samples larger than the air. Since in many cases the imperfectness of the contact is considerable and inevitable, special attention should be given, in order to model the imperfect contact to take account of its effect. Previous works have been focused mostly in the use of the probe testing on perfect contact and on imperfect contact as lift-off contact, and convex and concave contacts [55, 76, 81, 82]. Regarding the lift-off case, where there is an air layer in between, a two-layers Air-MUT mixture model is found in the literature in its two permittivity and admittance models. Arai in [76] presents a permittivity model from series capacitive phenomena considerations into a two layer

case. The admittance model can be found instead as an application of the multilayer admittance model as in [15, 67].

Not a general study of the imperfect contact has been found performed yet in the bibliography. By general we mean one that introduces critical area identification and analysis of the effect of the air presence in the probe-MUT interface. During the Ph.D course the efforts were addressed with a simulation-aided study to this purpose. A small section probe is considered with the following characteristics: outer radius of inner conductor (“a”) of 0.4 mm, inner radius of outer conductor (“b”) of 1.14 mm, coaxial dielectric filler is the necessary to ensure a characteristic impedance of 50 ohms, the flange extension are the necessary to consider them as infinite and not producing influence. The MUT considered is methanol whose dispersion behavior is described with a Cole-Cole relaxation model following these parameters:  $\epsilon_s = 34,72$ ,  $\epsilon_\infty = 5,41$ ,  $\tau [ns] = 5,74 \times 10^{-2}$ ,  $\alpha = 0,057$  [73]. The study performed for different cases of air presences (Lift-off, Grid and an air element changing dimension and position) is presented in the following sections together to discussion and results.

## 5.2 The electric field at the aperture and the imperfect contact problem

The electric field line distribution, inside and outside the probe, between the inner and outer electrodes (terminations), is shown, approximately depicted, in figures (a) and (b) in 5.2.1. The depicted section corresponds, because of radial symmetry, to that close to the interface between the dielectric filling the probe and the MUT. Figure (a) shows the case where the probe is in direct contact with air. Figure (b), the case where a MUT is placed to be in contact with the probe and an air gap distribution is given to the interface between them as an illustration of what can be the problem. In this figure four of the five cases in which the electric field line can flow between the

electrodes of the probe are shown enclosed by dashed rectangles (I, II, III, and IV). The five cases are then illustrated from figures (c) to (g) with their respective equivalent circuits and are:

- Case I: Electric field line goes only through MUT.
- Case II: Electric field line goes through MUT and air gap.
- Case III: Electric field line goes through coaxial filler and air gap.
- Case IV: Electric field line goes through coaxial filler, air gap and MUT.
- Case V: Electric field line goes through coaxial filler and MUT

In case of perfect contact between probe and MUT only cases I and V are presents (figures (c) and (g) in 5.2.1). The probe in this case could be modeled, following a quasi-static approach, by two *parallel capacitors* circuit as depicted in figure (a) in 5.2.2.  $C_f$  accounts for the electric field concentration inside the dielectric-filled part of the coaxial line.  $C_{OUT}$ , for the perfect contact case, accounts for the fringing electric field concentration in the MUT that includes the I and V cases (figure (b) in 5.2.2). The "Ideal Open" load accounts for the ideal representation of an open load that is an infinite impedance and it is shown in the picture for didactic purpose only. In case of a non perfect contact between probe and MUT, there will be supposed an interference gap that will undesirably modify the probe response. In that situation, that gap, i.e. air gap, will interpose in the electric field line in the modes illustrated by cases II, III and IV, resulting in changes in the probe response in a very unpredictable way because of the random distribution of air. Such changes will depend on how the electric field is concentrated and distributed between the involved materials and on how is the incidence of the field in each one of the interfaces between materials (principally Air/MUT and AIR/CoaxFiller). Such changes were advised as, principally, two mechanisms by Olmi *et al.* in [83], each of them seen as the effect of an air gap between:

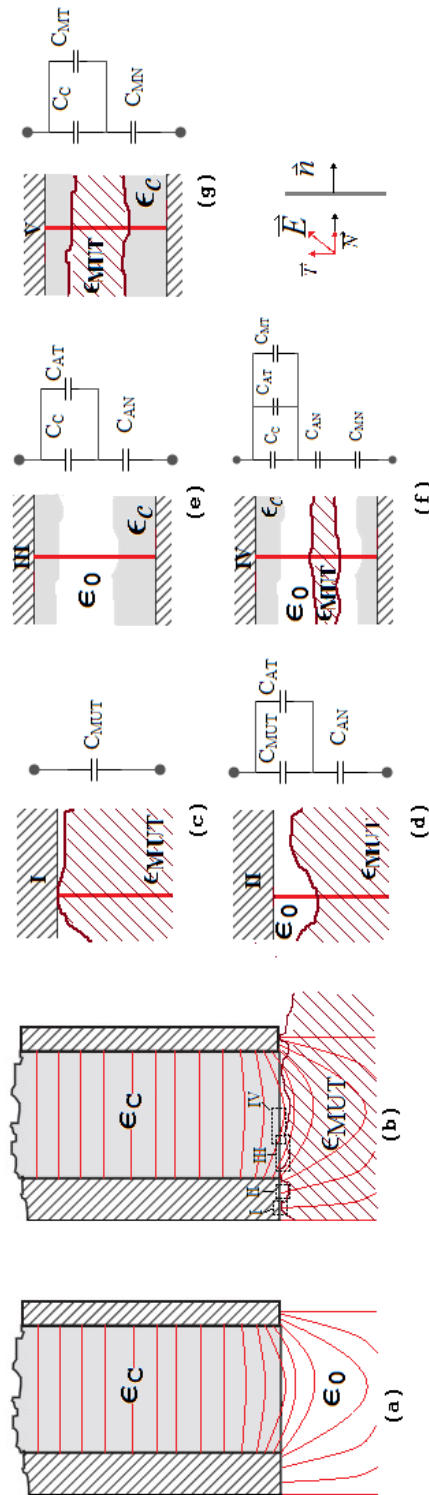


**Figure 5.2.1:** Electric field distribution in the OECC probe and air-gap problem illustration

1. a conductor of the probe and the MUT (Case II).
2. the dielectric filling the probe and the MUT (Case III and IV).

Figures (d), (e) and (f) in 5.2.1 show the electric field line (red) flowing through Air/MUT and Air/CoaxFiller interfaces through the cases II, III and IV. Each one of those cases results in a combination of a series and a parallel concentrations of the electric field according to the incidence of the electric field to the involved interfaces as depicted in their respective equivalent circuits. Normal incidence corresponds to a series combination and tangential incidence to parallel combination ([84, fig.1.b]). Because of that,  $C_{MUT}$  will be affected by a series-parallel combination that will be in some how related to the distribution of normal and tangential incidence in the involved interfaces and to the volumes of the involved materials in a complete way.

Since air has the lowest possible permittivity, its associated capacitance would be the smallest compared to the other involved materials with similar involved geometries. Because of that the most serious effects would be credited to the series combinations. A physical explanation of this phenomena is that in an interface between lossless dielectrics the boundary condition settles the continuity of both the normal components of the electric displacement field ( $\vec{D}$ ) and of the tangential components of the electric field ( $\vec{E}$ ). The normal electric field will be consequently scaled by the absolute ratio of the permittivity of each one of the two involved layers, while the tangential component will remain unchanged. That means that in the air region the electric field will be stronger than in the MUT (or Coaxial Filler) region in a proportion of  $\epsilon_{MUT}/\epsilon_0$  for the normal components while it will be the same for the tangential components.

In addition, for probes whose Coaxial Filler permittivity is chosen to be as low as to be comparable with the air permittivity, the air effect related to the Air/CoaxFiller interfaces could be consequently neglected (cases III and IV). In such a case the problem is consequently reduced to study the Air/MUT interface in cases II and IV.

Because of the structure of the probe, its electric field distribution makes

that the normal incidence be predominant in the central and flange areas. In summary, the most important aspects of the imperfect contact in an open-ended coaxial probe to be considered are:

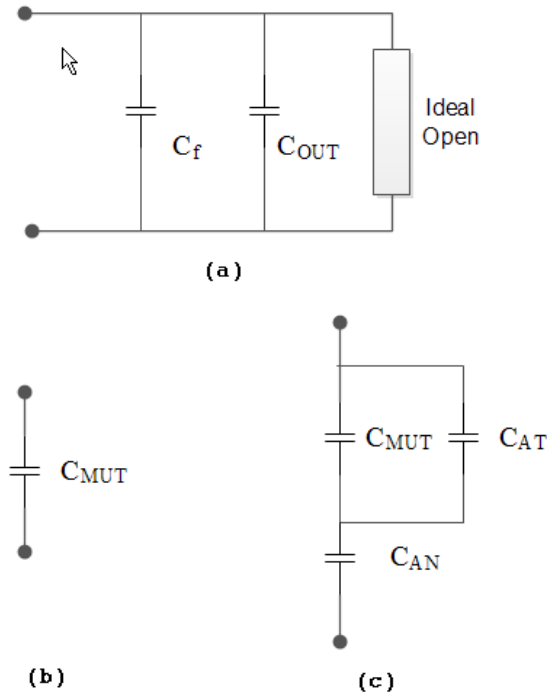
- The normal incidence predominance of the electric field to decide for a series or a series-parallel combination of the circuit model.
- The volume distribution between the phases air and MUT to decide the participation of each phase in the total response.
- The greatness in the permittivity of the MUT with respect to the one of the air. to decide the participation of each phase in the total response.

Figure (c) in 5.2.2 accounts for the series and parallel combination effect affecting  $C_{MUT}$  as an equivalent circuit for  $C_{OUT}$ . There,  $C_{AN}$  and  $C_{AT}$  accounts for the normal and parallel incidences effects previously described, respectively, and are dependent on the volume's fractions so that for a negligible fraction of air-gap results in predominance of  $C_{MUT}$  and in the opposite case of  $C_{Air}$ .

These model is equivalent to the model presented in chapter 4 when introducing the multilayer general model for the effective dielectric approach.

### 5.3 Discussion and assumptions on the surface profile nature

The probe is easier to control than the MUT. It can be protected and kept safe to avoid getting worse surface profile from the roughness point of view. From the worst case of the standard ASME/ANSI B16.5 (2009) for RF flange facing roughness, we assume that the Contact Surface of the probe is having a roughness of 5 micrometer [85]. The worst case cited by the standard for a smooth finish profile is 6.35 micrometer (250 microinch). Then we assume the Arithmetic Average Roughness Height (AARH) to be 5 micrometer.



**Figure 5.2.2:** *Equivalent Circuits*

The MUT is not necessarily controlled. A good contact surface is not granted. Irregularities related to the nature of the material and to the process of fabrication can be presented and are unknown (unestimated). In liquids, powders and surface-adaptable solids, the preferred MUT of this technique, air bubbles or spaces can appear according to the material properties and to the manipulation procedure. In solids with flat surfaces (not curved to the probe plane) the surface profile can have many variants according to the fabrication and preparation processes. According to the standard fabrication processes, the AARH of the surface profile can range from 15 nm to 50 micrometer from Polishing to Sawing as shown in figure 2.4 in [86]. In solids with curved surfaces (convex or concave) the air space can take bigger volumes than those obtained with the flat profile [82, 81].

Consequently we assume the probe as a reference flat level for the roughness effect analysis, giving the MUT surface the role of the irregular surface profile. The air presence will be settle in the area surrounded by the MUT and the probe according to each case, but always at the MUT side. Figure 5.3.1 shows two of air-MUT profiles employed in this study, those that bring more significant results to the present work. The lift-off profile, (a) in that figure, characterized by its level, separation from the probe-MUT interface in the perfect contact case. The Air-brick profile, (b) in same figure, characterized by its squared section (in XY plane) and its depth.

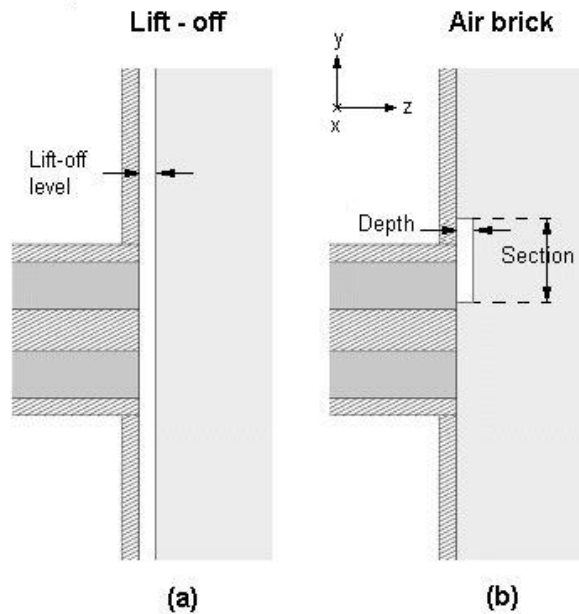


**Figure 5.3.1:** Employed Air-MUT profiles

## 5.4 Simulation role and permittivity extraction

In order to study the permittivity behavior while the measurement system is affected by air presence in the probe-MUT interface, we need to recreate the aperture admittance from a model representing in a more realistic way the considered phenomena that take into account all the principal real descriptive features of the system: probe, air presence and MUT. Consequently the extraction procedure will take place to obtain the effective permittivity with the air presence dependence.

In order to recreate the aperture admittance without appealing to measurement, the use of the environment of the commercial software CST MWS STUDIO,[52], (now CAD) and of its transient solver have been considered. Given a geometrical model of the measuring system conformed by the open-ended coaxial probe, the air element and the MUT material characteristics, and setting up the simulation specifications, the solver will provide the admittance at the aperture ( $Y_{CST}$ ) for each air presence combination.

Some of the most significant simulation specifications that were set were:

- Hexahedral meshing based on the Expert System set to previous Adaptive Mesh Refinement cases with a good refinement at high intensity electric displacement field areas.
- Frequency Range considered: 0 – 15 GHz.
- Open Boundary conditions and geometrical dimension of the problem adequate to underestimate the Perfect Matching Layer (PML) problem for dispersive media.

The lack of data of measured admittance at aperture for methanol makes it difficult to completely validate and verify the admittance provided by the CAD. There is also the fact that CST allows to use the TD and FD solvers for the validation. That goes but the grid becomes a problem. Found literature data in Ref. [61], did not give a satisfactory agreement. Figure 5.4.1

shows how CST result disagrees with measurement result provided by that reference. CST result was the best obtained by best convergence in both the solver and the meshing. This opens the discussion of whether use this CAD or not since hypothetically we must be carrying an error by using it. Anyway, this error must be constant if we keep a good convergence criterion for both the solver and the meshing, and we can use this tool qualitatively.

As we are interested on the permittivity extraction, the error associated to

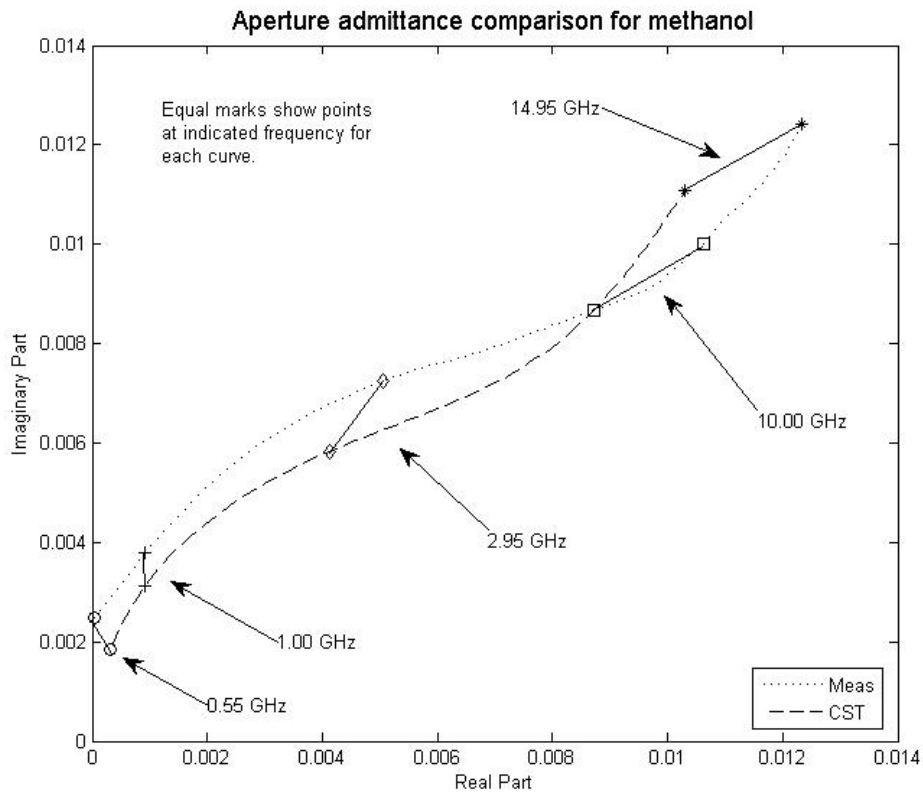


**Figure 5.4.1: CST Issue**

the CAD can be neglected. Besides of the model for the aperture admittance recreation, another admittance model for the permittivity extraction is required. The parameters of this last model can be made dependent on the CAD error to compensate it on the extraction. To accomplish this compensation, we need to assure that similar convergence specifications occurs in all

the cases with the CAD to keep a similar error.

Once obtained the admittance at the aperture, to extract the permittivity we need to consider an adequate admittance model and adequate fitting experiments. We use an aperture admittance radiation model, taken from Eq 3.22 in [15], because of its simplicity to operate, its intermediately good representation of the problem and because, keeping the hypothesis of CAD error constant, it can help to eliminate this error from the permittivity value itself. Then the radiation model is:

$$Y(\varepsilon) = k_1 + k_2\varepsilon + k_3\varepsilon^{\frac{5}{2}} \quad (5.4.1)$$

$$k_1 = j \cdot \omega \cdot C_f \quad (5.4.2)$$

$$k_2 = j \cdot \omega \cdot C_0 \quad (5.4.3)$$

$$k_3 = G(\omega, \epsilon_0) \quad (5.4.4)$$

where  $\epsilon$  is the complex permittivity of the MUT,  $C_f$  is related to the capacitance determined only by the coaxial structure,  $C_0$  is related to the capacitance of an air capacitor and  $G$  is related to the air radiation conductance, frequency-dependent, of the coaxial aperture in air.

For completing the extraction we need to pass through a fitting process (model optimization) and an inversion process (permittivity optimization), i.e, a soft extraction scheme. The first is for the model parameters. The second is for the own extraction. The model parameters are obtained from the extreme cases: (1) full air contact case and (2) full MUT contact case, where  $\epsilon$  and  $Y$  are known. With the first case we manage to calculate the  $k_3$  parameter since the real part of the admittance coincides with the air radiation conductance as seen in Eq. 3.19-20 in [15]. The other two parameters are found rearranging the eq. 5.4.1 to a linear least-square (LLS) problem in  $x$ :

$$Ax = b \quad (5.4.5)$$

$$\begin{aligned}
 A &= \left[ 2 \cdot \omega_i \quad (re(\epsilon_i) + im(\epsilon_i) + 1) \cdot \omega_i \right]_{N \times 2} \\
 x &= \left[ C_f \quad C_0 \right]_{2 \times 1} \\
 b &= [im(Y_{A,i}) + re(Y_{A,i}) + im(Y_{M,i}) \\
 &\quad -c_i \cdot G_i \cdot (\cos(d_i) + \sin(d_i))]_{N \times 1} \\
 c_i &= [re(\epsilon_i)^2 + im(\epsilon_i)^2]^{\frac{5}{2}} \\
 d_i &= \frac{5}{2} \cdot \arctan(\epsilon_i)
 \end{aligned}$$

where the subscript  $i$  refers to the index pointing to all the  $N$  experiments,  $\omega$  is the angular frequency, the subscripts  $A$  and  $M$  refer to air and MUT respectively.

In order to get a good calibration or fitting, several cases of full MUT contact were considered, weighted following a meshing criterion since it was not possible to get the exact value of the admittance with a full MUT contact since it was found necessary to achieve a mesh with a very large density of elements, which was not possible with the at-hand computational resources. In addition, for the estimation of  $C_f$  and  $C_0$ , as they are frequency independent, we considered as experiments all the simulated frequencies for the problem. 400 experiments in total. Resulting then in an overdetermined LLS system with solution:

$$\begin{aligned}
 C_f &= 10,526 [fF] \\
 C_0 &= 16,045 [fF] \\
 G_{av} &= 1,3259 [\mu\Omega]
 \end{aligned}$$

These values of the model parameters seem to be reasonable according to values found in literature as for example appear in the open standard definition in table A-3 of Ref: [87].

The inversion process uses the model parameters and the admittance value in an implicit prescription of eq.5.4.1 and finds the appropriate root representing the extracted permittivity value. This value should correspond to the extreme cases if air or MUT have been used. With an air-MUT profile, the ef-

fective value is given. We can study these values on the permittivity diagram.

## 5.5 Lift-Off case: simulation results and conclusion

In the lift-off case, the probe is not in direct contact to the MUT, but there is a layer of air in between. A prevalent presence of normally incident electric field is expected. We analyze this case and its expectation on the view of usage of both the permittivity and the admittance diagrams. Figure 5.5.1

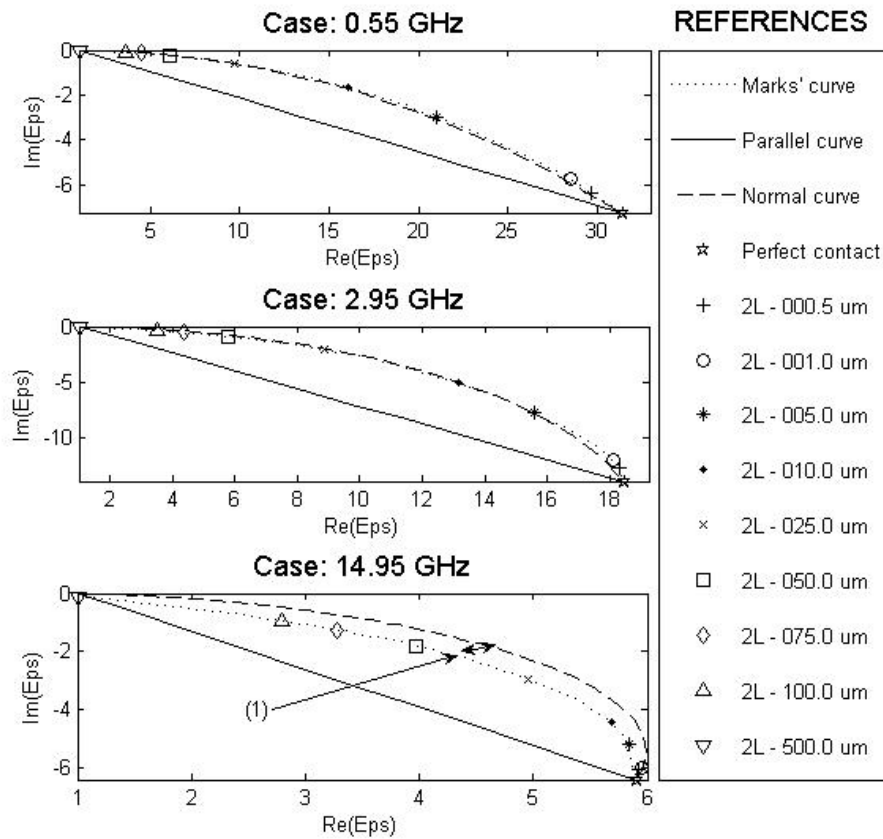


Figure 5.5.1: Permittivity Diagrams for Lift-off case

shows three permittivity diagrams for three different frequencies: 0,55 GHz, 2,95 GHz and 14,95 GHz. Marked points denote the repertory of all the effective permittivity values collected from the extraction of the admittance of the simulated lift-off cases. Lift-off of 500 micrometer to perfect contact have been considered. It can be seen that in its overall they describe a curve very similar to the normal curve (series capacitive model). But at high frequencies (14,95 GHz), see (1), it is no more coincident with the normal curve, but with an inner curve in the domain. By checking the electric field with the CAD in some points at the air-MUT interface plain of the lift-off case of 10 micrometers and computing an approximation of  $pP^1$ , we see that by increasing the frequency the  $pP$  relation decreases from 1 (predominantly normal case). For 0.55GHz,  $pP = 0.96$ , for 2.95 GHz,  $pP = 0.94$  and for 14.95 GHz,  $pP = 0.87$ . This can explain the separation (inward trend) from the normal curve.

In addition to this explanation, we must also take into consideration the errors associated to the radiation model as another reason for that trend. By using this model with the parameters adjusted in that way (fitting process), we expect an average absolute error of 0.0009064 for the admittance and of 0.9140 for the permittivity. Also is expected that while the frequency increases, both the admittance and permittivity errors increase. Consequently, we can consider the permittivity high frequency trend as due to primarily the above explained field phenomena.

In conclusion a lift-off can be described with a series capacitive model because of its normal field predominance. This model fails at high frequencies because the normal field contribution is no more the predominant one, but

---

<sup>1</sup>Totally normal incidence degree of predominance ( $pP$ ): This parameter plays the role of the degree of predominance of the totally normal incident electric field at every boundary in the interface between one layer and other layer in the composite material. For setting this parameter we evaluate the ratio of the summation of the normal component of each incident field at every boundary to the summation of both components of each incident field at every boundary.  $pP$  will vary from 0 to 1 as from parallel to normal component predominance.

parallel field contribution at the interface begins to be important too. All those facts are also justifying the utility of the permittivity domain and its parameters associated to the air presence. And the use of a *general* model.

## 5.6 Air brick case: simulation and conclusion

We now propose to study the effect of an air brick on the probe-MUT interface. We intend to witness the effect of its position and dimensions (Frontal size and depth) from the effective permittivity point of view. The brick's frontal size, the one in touch with the probe-MUT interface, will be varied from 0 to infinite and its position moved from the center toward infinite along the X (or Y) axis. This case of study will contribute to verify that air elements can not be modeled by a totally normal model since a participation of the parallel component is also expected making to the utility of the *general* model. Figure 5.6.1 shows six permittivity diagrams at 0.55 GHz which differentiate each other on the variation of the depth and of the position. A collection of marked (AirHole) points is presented in each diagram representing different brick's sizes (hole's size) and describing a line (behavior curve). This line connects the perfect contact (PC) case to the lift-off (2L) case corresponding to the same depth.

## 5.7 Conclusions

The idea of non considering the flange area in the imperfect contact study between the material under test (MUT) and the open-ended coaxial probe was emphasized in this chapter. The attention should be given to the spatial area surrounding the coaxial section aperture, principally the central conductor where the intensity of the normal electrical field is undesirably high to weight up the air phase transition effect from the MUT phase transition

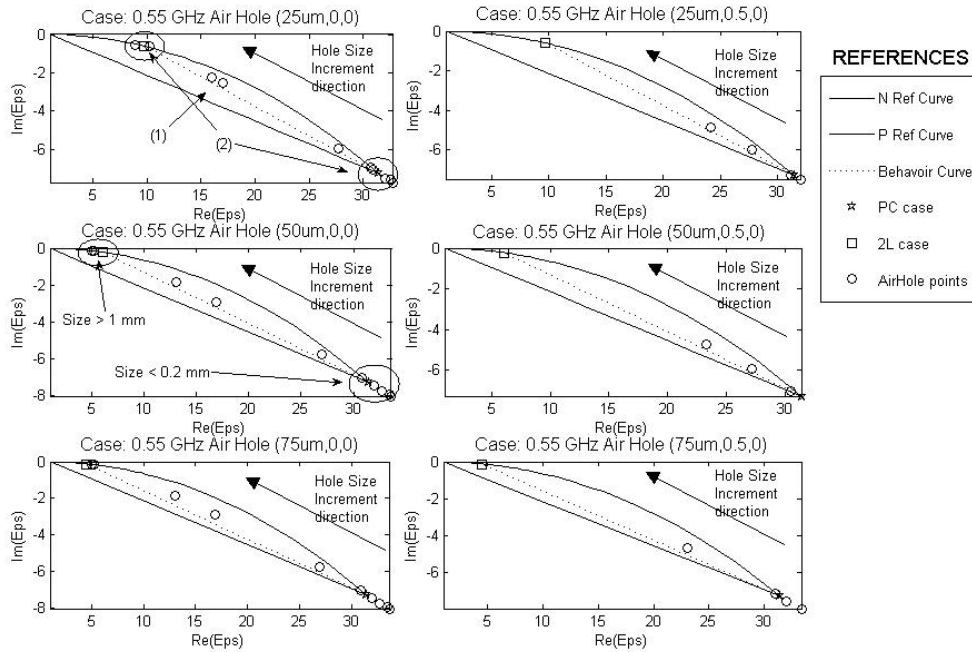


Figure 5.6.1: Permittivity Diagrams for Air Brick cases

effect. Such spatial region, is proposed to be cylindrical, with a radius of at least 3 times the radius of the central conductor of the coaxial probe. Air elements within this spatial region with contact surface section of less than a quarter of the squared radius of the central conductor of the probe and with depths less than few micrometers can be neglected.

The use of effective magnitude domain diagrams for the complex permittivity have been found useful to study this kind of problem and can also be extended to other measurement probe problems. This approach gives a global view of the behavior of these two magnitudes against the operating frequency and the air presence or the imperfectness of the contact. This scores also as a tool for analyzing and validating: complex permittivity homogenization or effective dielectric models representing the complexity of the deficient contact for further corrections on the parameter extraction, and reflection coefficient models for detecting and quantifying air or second phase element presence on any kind of diagnostic process.

---

Lift-off contact situations can be modeled with the parallel plate *series capacitive* model or the *general* model. At frequencies higher than about 7 GHz the *general* model is the only one that gives a good solution.



# Bibliography

- [1] L. Solymar and D. Walsh. *Electrical Properties of Materials*. Oxford University Press, Oxford, 6th edition, 1998.
- [2] C. Kittel. *Introduction to Solid State Physics*. John Wiley & Sons, New York., 7th edition, 1997.
- [3] Arthur R. Von Hippel. *Dielectric materials and applications*. Number XII. the M.I.T. press, 1954.
- [4] P. Robert. *Electrical and Magnetic Properties of Materials*. Artech House, Norwood., 1988.
- [5] D. Jiles. *Introduction to Magnetism and Magnetic Materials*. Chapman & Hall, London., 2nd edition, 1998.
- [6] J. Smit. *Magnetic Properties of Materials*. McGraw-Hill, New York., 1971.
- [7] M. Tinkham. *Introduction to Superconductivity*. McGraw-Hill, Singapore., 1996.
- [8] M. E. Lines and A. M. Glass. *Principles and Applications of Ferroelectrics and Related Materials*. Clarendon Press, Oxford., 1977.
- [9] J. R. Ramo, S. Whinnery and T. Van Duzer. *Fields and Waves in Communication Electronics*. John Wiley & Sons, New York., 3rd edition, 1994.

- 
- [10] J. F. Knott, E. F. Shaeffer and M. T. Tuley. *Radar Cross Section*. Artech House, Boston., 2nd edition, 1993.
- [11] M. I. Montrose. *EMC and the Printed Circuit Board: Design, Theory, and Layout made Simple*. IEEE Press, New York., 1999.
- [12] J. Thuery and E. H. Grant. *Microwaves: Industrial, Scientific and Medical Applications*,. Artech House, Boston., 1992.
- [13] R. Zoughi. *Microwave Non-Destructive Testing and Evaluation*. Kluwer Academic Publishers, Dordrecht., 2000.
- [14] E. Nyfors and P. Vainikainen. *Industrial Microwave Sensors*. Artech House, Norwood., 1989.
- [15] L. F. Chen, C. K. Ong, C. P. Neo, V. V. Varadan, and V. K. Varadan. *Microwave Electronics - Measurement and Materials Characterization*. John Wiley I& Sons, July 2004.
- [16] Encyclopdia Britannica. Encyclopdia Britannica Online. Encyclopdia Britannica Inc. Britanica. "Dielectric [Physics]". Website, Feb 2012.
- [17] Max Born and Emil Wolf. *Principles of Optics*. Cambridge: Cambridge University Press., 1999. ISBN 0521642221.
- [18] S. Puliafito. *Propagacion y radiacion de ondas electromagneticas: El campo electromagnetico (Parte I)*, volume I. Editorial IDEARIUM, Universidad de Mendoza, Mendoza, Argentina, 1985.
- [19] S. Havriliak and S. Negami. A complex plane representation of dielectric and mechanical relaxation processes in some polymers. *Polymer*, 8:161210, 1967.
- [20] J. A. Kong. *Electromagnetic Wave Theory*,. John Wiley & Sons, New York., 2nd edition, 1990.

- 
- [21] S. Van Damme, A. Franchois, D. De Zutter, and L. Taerwe. Nondestructive determination of the steel fiber content in concrete slabs with an open-ended coaxial probe. *IEEE T Geosci Remote*, 42(11):2511–2521, 2004.
- [22] C. L. Pournaropoulos and D. Misra. A study on the coaxial aperture electromagnetic sensor and its application in material characterization. *IEEE T Instrum Meas*, 43(2):111–115, 1994.
- [23] M.D.A. Rosen, P.J. Scheno, and M.A. Lizza. Conformal tip for coaxial test probe for non-destructive testing of dielectric/magnetic materials. United state patent, 1996.
- [24] W. R. Tinga. Mixture laws and microwave-material interactions. *Progress in Electromagnetics Research (PIER)*, (6):1–40, 1992.
- [25] G. Banhegyi. *Characterization of Composite Materials*, chapter Dielectric spectroscopy. Ed., Butterworth-Heinemann, Boston., 1994.
- [26] T. C. Choy. *Effective Medium Theory: Principles and Applications*. Oxford University Press, New York., 1999.
- [27] Henrik Kettunen, Jiaran Qi, Wallen, and Ari Sihvola. Homogenization of Dielectric Composites with Finite Thickness. In *26th Annual Review of Progress in Applied Computational Electromagnetics (ACES)*, pages 490–495(6), 2010.
- [28] G. Tompkins Harland and A. Irene Eugene. *Handbook of ellipsometry*. William Andrew, 2005.
- [29] V. K. Varadan and V. V. Varadan. *Acoustic, Electromagnetic and Elastic Wave Scattering Focus on the T-matrix Approach*,. Pergamon Press, New York., 1979.

- [30] V. Brongi and V. Varadan. Average dielectric properties of discrete random media using multiple scattering theory. *IEEE T Antenn Propag*, 31(2):371–375, 1983.
- [31] V. Varadan and Y. Ma. Anisotropic dielectric properties of media containing aligned nonspherical scatterers. *IEEE T Antenn Propag*, 33(8):886–890, 1985.
- [32] V. V. Varadan and V. K Varadan. *Multiple Scattering of Waves in Random Media and Random Rough Surfaces*. Pennsylvania State University Press, Pennsylvania., 1985.
- [33] M. F. Iskander and J. B. DuBow. Time- and Frequency-Domain Techniques for Measuring the Dielectric Properties of Rocks: A Review. *Journal of Microwave Power*, 18(1):55–74, 1983.
- [34] A. Rajendran and P. Neelamegam. Dielectric Constant Measurement Using an Artificial Neural Network. *Instrumentation Science & Technology*, 32(4):413–422, 2004.
- [35] Charles A. Schmuttenmaer. Exploring Dynamics in the Far-Infrared with Terahertz Spectroscopy. In *Chemical Reviews*, volume 104 of *Chemical Reviews Series*, pages 1759–1776. American Chemical Society, 2004.
- [36] Stanislaw S. Stuchly, Maria A. Stuchly, and Benito Carraro. Permittivity Measurements in a Resonator Terminated by an Infinite Sample. *IEEE T Instrum Meas*, 27(4):436–439, 1978.
- [37] Maria A. Stuchly and Stanislaw S. Stuchly. Coaxial Line Reflection Methods for Measuring Dielectric Properties of Biological Substances at Radio and Microwave Frequencies-A Review. *Instrumentation and Measurement, IEEE Transactions on*, 29(3):176–183, 1980.
- [38] Baiqiang Tian and W. R. Tinga. A microwave oscillation loop for dielectric constant measurement. *IEEE T Microw Theory*, 42(2):169–176, 1994.

- [39] A. Franchois, Y. Pineiro, and R. H. Lang. Microwave permittivity measurements of two conifers. *IEEE T Geosci Remote*, 36(5):1384–1395, 1998.
- [40] J.M. Grimm, D.P. Nyquist, M. Thorland, and D. Infante. Broadband material characterization using microstrip/stripline field applicator. In *Antennas and Propagation Society International Symposium, 1992. AP-S. 1992 Digest. Held in Conjunction with: URSI Radio Science Meeting and Nuclear EMP Meeting., IEEE*, pages 1202 –1205 vol.2, jul 1992.
- [41] Iñigo Cuiñas and Manuel García Sánchez. Permittivity and Conductivity Measurements of Building Materials at 5.8 GHz and 41.5 GHz. *Wirel. Pers. Commun.*, 20:93–100, January 2002.
- [42] G. Kent. A new method for measuring the properties of dielectric substrate. In *Microwave Symposium Digest, 1988., IEEE MTT-S International*, pages 751 –754 vol.2, may 1988.
- [43] A. A. Pistolcors. Theory of the Circular Diffraction Antenna. *Proceedings of the IRE*, 36(1):56–60, 1948.
- [44] Harold Levine and Charles H. Papas. Theory of the Circular Diffraction Antenna. *Journal of Applied Physics*, 22(1):29–43, 01 1951.
- [45] Nathan Marcuvitz. *Waveguide handbook*. McGraw-Hill, 10 radiation laboratory series of massachusetts institute of technology edition, 1951.
- [46] G. Gajda, M.A. Stuchly, and S.S. Stuchly. Mapping of the near-field pattern in simulated biological tissues. *Electron Lett*, 15(4):120–121, 1979. cited By (since 1996) 4.
- [47] G.B. Gajda. A method for measurement of permittivity at radio and microwave frequencies. In *Conference digest - International electrical, electronics conference and exposition*, Toronto, Ont, Can, Oct 1979.

- [48] E. C. Burdette, F. L. Cain, and J. Seals. In Vivo Probe Measurement Technique for Determining Dielectric Properties at VHF through Microwave Frequencies. *IEEE T Microw Theory*, 28(4):414–427, 1980.
- [49] M. M. Brady, S. A. Symons, and S. S. Stuchly. Dielectric Behavior of Selected Animal Tissues in Vitro at Frequencies from 2 to 4 GHz. *Biomedical Engineering, IEEE Transactions on*, BME-28(3):305–307, 1981.
- [50] J.R. Mosig, J. Besson, M. Gex-Fabry, and F. Gardiol. Reflection of an Open-Ended Coaxial Line and Application to Nondestructive Measurement of Materials. *IEEE Transactions on Instrumentation and Measurement*, IM-30(1):46–51 (6), March 1981.
- [51] J Baker-Jarvis and et al. *Measuring the Permittivity and Permeability of Lossy Materials: Solids, Liquids, Metals, Building Materials, and Negative-Index Materials*. US Department of Commerce - National Institute of Standards and Technology (NIST), Boulder, CO, USA, technical note 1536 edition, February 2005.
- [52] CST Microwave Studio. CST - Computer Simulation Technology, Wellesley Hills, MA, USA,, 2011. [www.cst.com](http://www.cst.com).
- [53] G.B. Gajda and S.S. Stuchly. Numerical Analysis of Open-Ended Coaxial Lines. *Microwave Theory and Techniques, IEEE Transactions on*, 31(5):380–384, may 1983.
- [54] G. P. Otto and W. C. Chew. Improved calibration of a large open-ended coaxial probe for dielectric measurements. *IEEE T Instrum Meas*, 40(4):742–746, 1991.
- [55] J. Baker-Jarvis, M. D. Janezic, P. D. Domich, and R. G. Geyer. Analysis of an open-ended coaxial probe with lift-off for nondestructive testing. *IEEE T Instrum Meas*, 43(5):711–718, 1994.

- [56] Kjetil Folger and Tore Tjomsland. Permittivity measurement of thin liquid layers using open-ended coaxial probes. *Measurement Science and Technology*, 7(8):1164, 1996.
- [57] Lily S. Anderson, Gregory B. Gajda, and Stanislaw S. Stuchly. Analysis of an open-ended coaxial line sensor in layered dielectrics. *IEEE Transactions on Instrumentation and Measurement*, IM-35(1):13–18, 1986. cited By (since 1996) 14.
- [58] S. Fan, K. Staebell, and D. Misra. Static analysis of an open-ended coaxial line terminated by layered media. *Instrumentation and Measurement, IEEE Transactions on*, 39(2):435–437, April 1990.
- [59] F. M. Ghannouchi and R. G. Bosisio. Measurement of microwave permittivity using a six-port reflectometer with an open-ended coaxial line. *IEEE T Instrum Meas*, 38(2):505–508, 1989.
- [60] T. W. Athey, M. A. Stuchly, and S. S. Stuchly. Measurement of Radio Frequency Permittivity of Biological Tissues with an Open-Ended Coaxial Line: Part I. *IEEE T Microw Theory*, 30(1):82–86, 1982.
- [61] D. Misra, M. Chhabra, B. R. Epstein, M. Microtznik, and K. R. Foster. Noninvasive electrical characterization of materials at microwave frequencies using an open-ended coaxial line: test of an improved calibration technique. *IEEE T Microw Theory*, 38(1):8–14, 1990.
- [62] Gregory B. Gajda. *Numerical Analysis of In-Vivo Dielectric Sensors*. M.a.sc. thesis, Graduate Studies and Research of the University of Ottawa as partial fulfillment of the requirements for the M.A.Sc. degree in Electrical Engineering, Ottawa, Ontario, 1982.
- [63] Gregory Gajda and Stanislaw S. Stuchly. An Equivalent Circuit of an Open-Ended Coaxial Line. *Instrumentation and Measurement, IEEE Transactions on*, 32(4):506–508, 1983.

- [64] D. K. Misra. A Quasi-Static Analysis of Open-Ended Coaxial Lines (Short Paper). *IEEE T Microw Theory*, 35(10):925–928, 1987.
- [65] G. Chen, Kang Li, and Zhong Ji. Bilayered dielectric measurement with an open-ended coaxial probe. *IEEE T Microw Theory*, 42(6):966–971, 1994.
- [66] LL Li, NH Ismail, LS Taylor, and CC. Davis. Flanged coaxial microwave probes for measuring thin moisture layers. *IEEE Trans Biomed Eng.*, 39(1):49–57, Jan 1992.
- [67] P. De Langhe, K. Blomme, L. Martens, and D. De Zutter. Measurement of low-permittivity materials based on a spectral-domain analysis for the open-ended coaxial probe. *IEEE T Instrum Meas*, 42(5):879–886, 1993.
- [68] S. Bakhtiari, S. I. Ganchev, and R. Zoughi. Analysis of radiation from an open-ended coaxial line into stratified dielectrics. *IEEE T Microw Theory*, 42(7):1261–1267, 1994.
- [69] Dictionaries Oxford. Oxford Dictionaries. Internet, April 2010.
- [70] Richard C. Aster, Brian Borchers, and Clifford Thurber. *Parameter Estimation and Inverse Problems*. c 2002-2004, aster, borchers, and thurber edition, June 2004.
- [71] Sean Luke. *Essentials of Metaheuristics*. Lulu, 2009. Available for free at <http://cs.gmu.edu/~sean/book/metaheuristics/>.
- [72] U. Reggiani L. Sandrolini M. Artioli, M.D. Perez. Particle Swarm Optimization Method for Complex Permittivity Extraction of Dispersive Materials. In *Proceedings of the Asia-Pacific Symposium on Electromagnetic Compatibility, Beijing, China.,* 2010.
- [73] U. Reggiani L. Sandrolini M. Artioli, M.D. Perez. Extraction of the Complex Permittivity of Dispersive Materials with a Stochastic Op-

- timization Technique. In *26th Annual Review of Progress in Applied Computational Electromagnetics (ACES)*, pages 18–23 (6), April 26-29 2010.
- [74] G. Q. Jiang, W. H. Wong, E. Y. Raskovich, W. G. Clark, W. A. Hines, and J. Sanny. Measurement of the microwave dielectric constant for low-loss samples with finite thickness using open-ended coaxial-line probes. *Rev. Sci. Instrum.*, 64(6):1622–1626, 1993.
- [75] G. Q. Jiang, W. H. Wong, E. Y. Raskovich, W. G. Clark, W. A. Hines, and J. Sanny. Open-ended coaxial-line technique for the measurement of the microwave dielectric constant for low-loss solids and liquids. *Rev. Sci. Instrum.*, 64(6):1614–1621, jun 1993.
- [76] M. Arai, J.G.P. Binner, and T.E. Cross. Estimating errors due to sample surface roughness in microwave complex permittivity measurements obtained using a coaxial probe. *Electronics Letters*, 31(2):115–117, jan. 1995.
- [77] G. W. Milton. Bounds on the complex dielectric constant of a composite material. *Appl. Phys. Lett.*, 37:300, 1980.
- [78] D. E. Aspnes. Optical properties of thin films. *Thin Solid Films*, 89(3):249–262, 3 1982.
- [79] D. E. Aspnes. Bounds on allowed values of the effective dielectric function of two-component composites at finite frequencies. *Phys. Rev. B*, 25:1358–1361, Jan 1982.
- [80] Peter Petrik. *Characterization of polysilicon thin films using in situ and ex situ spectroscopic ellipsometry*. PhD thesis, Department of Experimental Physics of the Technical University of Budapest, 1999.
- [81] Abdul-Kadum A. Hassan, Deming Xu, Ling Zhan, and Maode Niu. Modeling and analysis of finite-flange open-ended coaxial probe for planar

- and convex surface coating material testing by fdtd method. *Microwave and Optical Technology Letters*, 24(2):117–120(4), January, 20 2000.
- [82] A.-K. A. Hassan, Deming Xu, Lin Zhang, Maode Niu, and YuJian Zhang. A modified open-ended coaxial probe for concave surface coating materials testing. In *Proc. Microwave Symp. Digest. 2000 IEEE MTT-S Int*, volume 3, pages 1867–1870, 2000.
- [83] R Olmi, M Bini, A Ignesti, and C Riminesi. Non-destructive permittivity measurement of solid materials. *Measurement Science and Technology*, 11(11):1623, 2000.
- [84] J Fleig and J Maier. The Influence of Laterally Inhomogeneous Contacts on the Impedance of Solid Materials: A Three-Dimensional Finite-Element Study. *Journal of Electroceramics*, 1:73–89, 1997. 10.1023/A:1009902532596.
- [85] Pipe Flanges and Flanged Fittings: NPS 1/2 Through NPS 24 Metric/Inch Standard, 2009.
- [86] T.V. Vorburger and J. Raja. *Surface Finish Metrology Tutorial*. US Department of Commerce - National Institute of Standards and Technology (NIST), Gaithersburg, MD, June 1990.
- [87] Stanislaw S. Stuchly, Gregory Gajda, Lily Anderson, and Andrzej Kraszewski. New sensor for dielectric measurements. *IEEE Transactions on Instrumentation and Measurement*, IM-35(2):138–141, 1986. cited By (since 1996) 2.